Separation and Purification Technology 274 (2021) 118959

Contents lists available at ScienceDirect

Separation and Purification Technology

journal homepage: www.elsevier.com/locate/seppur

# Advanced configurations for post-combustion $CO_2$ capture processes using an aqueous ammonia solution as absorbent

José-Francisco Pérez-Calvo [a], Daniel Sutter [a,1], Matteo Gazzani [b], Marco Mazzotti [a,*]

[a] Institute of Energy and Process Engineering, ETH Zurich, 8092 Zurich, Switzerland
[b] Copernicus Institute of Sustainable Development, Utrecht University, 3584 CB Utrecht, The Netherlands

ARTICLE INFO

*Keywords:*
$CO_2$ capture with aqueous ammonia
Advanced configurations
$NH_3$ abatement
Integration of units
Energy consumption minimization
Excess heat utilization

ABSTRACT

In this work, we have developed advanced process configurations for solvent-based $CO_2$ capture processes that use aqueous ammonia as absorbent. In total, ten different advanced configuration concepts have been optimized and analysed, aiming at: (i) achieving in spec $NH_3$ emissions in a controlled way; (ii) minimizing capital costs by avoiding redundant process components; (iii) minimizing the energy demand of the capture process by minimizing the requirements of high temperature steam and by maximizing the possibilities for the use of excess heat from the $CO_2$ point source. As a result, we propose a new benchmark configuration for $NH_3$-based capture processes that, with proper tuning of the process operating conditions, allows to minimize the specific energy consumption while enhancing the flexibility of the capture process with respect to the type and to the features of the electricity and steam available at the $CO_2$ point source, at the minimum consumption of chemicals and process water. This new benchmark configuration for $NH_3$-based capture processes is built upon the Chilled Ammonia Process, avoids the formation of solids and includes: (i) a multi-pressure desorber with recycled vapour compression that is able to decrease the high temperature steam requirements for solvent regeneration, i.e. at ca. 140–160 °C, to values as low as 1.1 $MJ_{th}\ kg^{-1}_{CO_2 captured}$, (ii) a vacuum integrated stripper for the recuperation of the solvent that is able to use low temperature steam instead, i.e. below 100 °C, and (iii) a flue gas water-wash column that is able to reduce the $NH_3$ concentration in the $CO_2$-depleted flue gas to values below 10 $ppm_v$ without the need of an acid-wash column before the stack.

## 1. Introduction: critical review of the state of the art in ammonia-based $CO_2$ capture processes

Aqueous ammonia-based capture processes are among the most promising technologies for post-combustion $CO_2$ capture. In addition to show a very competitive energetic performance compared to amine-based processes, aqueous $NH_3$ presents advantages with respect to aqueous amine solutions [1–4], i.e.: (i) it is stable in the presence of impurities and does not thermally degrade or oxidize, (ii) it has better

*Abbreviations:* AFS, Advanced Flash Stripper; ANA, Advanced $NH_3$ Absorber; BAT, Best Available Technology; CAP, Chilled Ammonia Process; CCS, Carbon Capture and Storage; CHP, Combined Heat and Power; $CO_2$-WW, $CO_2$ Water-Wash; CRSP, Cold Rich Solvent Preheating; CSIRO, Commonwealth Scientific and Industrial Research Organisation; DCC, Direct Contact Cooler; DCCh, Direct Contact Chiller; DCH, Direct Contact Heater; ECRA, European Cement Research Academy; EU, European Union; FG, Flue Gas; FG-WW, Flue Gas Water-Wash; IHD, Inter-heated Desorber; IS, Integrated Stripper; KIER, Korea Institute of Energy Research; LHV, Low Heating Value; LVC, Lean Vapour Compression; LVC(3), Lean vapour compression with expansion of the hot $CO_2$-lean stream to the inlet pressure of the second-to-last stage of the multi-stage compressor; LVC(4), Lean vapour compression with expansion of the hot $CO_2$-lean stream to the inlet pressure of the last stage of the multi-stage compressor; LVC(4,3), Lean vapour compression where the hot $CO_2$-lean stream is expanded in two steps, first to the inlet pressure of the last stage of the multi-stage compressor, and then to the inlet pressure of the second-to-last compression stage; LVC(4,3,2), Lean vapour compression where the hot $CO_2$-lean stream is expanded in three steps, first to the inlet pressure of the last stage of the multi-stage compressor, then to the inlet pressure of the second-to-last compression stage, and finally to the second stage of the multi-stage compressor; MEA, Monoethanolamine; MED, Multi-effect Desorber; MPD, Multi-pressure Desorber; NAW, $NH_3$ Absorber with Water-wash section; NG, Natural Gas; PC-SAFT, Perturbed-Chain Statistical Associating Fluid Theory; PFD, Process Flow Diagram; RecVC, Recycled Vapour Compression; RG, Refinery Gas; RIST, Research Institute of Industrial Science and Technology; RSS, Rich Solvent Splitting; RVC, Rich Vapour Compression; SNA, Standard $NH_3$ Absorber; SOC, Stripper Overhead Compression; SPECCA, Specific Primary Energy Consumption per $CO_2$ Avoided; SQP, Successive Quadratic Programming; VIS, Vacuum Integrated Stripper

* Corresponding author.
*E-mail address:* marco.mazzotti@ipe.mavt.ethz.ch (M. Mazzotti).
[1] Current address: Climeworks AG, Birchstrasse 155, 8050 Zurich, Switzerland.

https://doi.org/10.1016/j.seppur.2021.118959
Received 11 March 2021; Received in revised form 5 May 2021; Accepted 10 May 2021
Available online 13 May 2021

global availability, lower environmental footprint and lower cost, and (iii) it is less corrosive and has viscosities similar to water [5] thus allowing for broad ranges of pressures for solvent regeneration and of solvent concentration in the liquid phase. However, high $NH_3$ volatility is the main disadvantage that $NH_3$-based capture technologies present with respect to the best performing amine solutions [6]. Consequently, measures are implemented to control the $NH_3$ slip to the $CO_2$-depleted Flue Gas (FG) and to the $CO_2$ product stream, and to limit solvent losses in order to minimize fresh $NH_3$ make-up requirements.

In $NH_3$-based $CO_2$ capture processes, $NH_3$ can reach concentrations between 4,500 and 31,000 ppm in the FG exiting the $CO_2$ absorber [7]. Nevertheless, the maximum $NH_3$ concentration recommended by the US National Institute of Occupational Safety and Health is 25 $ppm_v$ [8], and emission limits at the stack of existing ammonia production facilities in the European Union (EU) do not exceed concentrations higher than 10 to 40 $ppm_v$, depending on the specific national legislation [9]. $NH_3$ concentration in the FG leaving the $CO_2$ absorber can be limited by lowering the temperature, by decreasing the $NH_3$ concentration and by increasing the $CO_2$ content of the solvent [3]. To this aim, the Chilled Ammonia Process (CAP) patented by Alstom [10] uses aqueous $NH_3$ solutions at temperatures between 0 and 20 °C to limit the $NH_3$ slip to the FG, which requires additional energy for solvent refrigeration. The original CAP concept suggests the formation of solids in the absorber tower as a way to limit the energy consumption in the $CO_2$ desorber. Nevertheless, clogging of the tower packing and difficulties in operating the system have prompted the CAP towards a solid-free operating mode [11,12]. Accordingly, the current CAP implementations avoid solid formation by limiting the solvent $NH_3$ and $CO_2$ concentration in the absorber [13,14]. Although the energy consumption of the CAP, including the solvent chilling demand, can be minimized by proper selection of the operating conditions throughout process optimization [3,14], the FG exiting the $CO_2$ absorber still requires further treatment to limit the $NH_3$ concentration at the stack to values below 10 $ppm_v$. Scrubbing technologies are broadly used in the chemical industry to limit the emission of harmful compounds to the atmosphere [6]. Among them, water washing and further acid washing using aqueous sulphuric acid ($H_2SO_4$) solutions are implemented in the CAP for the post-treatment of the FG [3,14–16]. In order to minimize $NH_3$ losses and fresh $NH_3$ make-up, the washing water is regenerated and $NH_3$ is recuperated by means of thermal energy using steam, which increases the energy consumption of the capture process. Water washing of the $CO_2$-depleted FG and solvent recuperation by thermal regeneration are also implemented in mild-temperature $NH_3$-based capture processes such as the Korea Institute of Energy Research (KIER) process and the Research Institute of Industrial Science and Technology (RIST) process [17]. However, the higher temperature of such processes leads to higher $NH_3$ concentrations in the FG exiting the $CO_2$ absorber, which requires thermal energy demands for $NH_3$ recuperation comparable to the thermal energy needed for the regeneration of the solvent used for $CO_2$ capture [18]. Aiming at decreasing the energy consumption while meeting environmental limits regarding $NH_3$ emissions, the mild-temperature $NH_3$-based capture process developed by the Commonwealth Scientific and Industrial Research Organisation (CSIRO) proposes to couple the water washing of the $CO_2$-depleted FG with the FG pre-treatment column placed upstream of the $CO_2$ absorber [19]: in addition to cooling down the FG, the $NH_3$-rich stream obtained in the water-wash column removes $SO_2$ from the inlet FG, while the heat contained in the inlet gas should be able to strip-off the $NH_3$ from the solvent; $NH_3$ is recycled to the $CO_2$ absorber within the FG and the regenerated $NH_3$-lean solution, after undergoing chilling, is used to capture $NH_3$ from the $CO_2$-depleted FG exiting the $CO_2$ absorber. Nevertheless, the temperature of the FG at the stack is below ambient [19], which penalizes the dispersion of the gas plume. Subsequently, CSIRO has updated the process by including the removal of $NO_x$ from the inlet gas, thus leading to the so-called advanced, $NH_3$-based combined $NO_x/SO_x/CO_2$ emission control process [20]: firstly, NO is oxidized to $NO_2$ and $SO_2$ is removed from the FG using a $NaClO_2$ aqueous solution; secondly, the $NO_2$ is removed from the FG by means of the $NH_3$-rich solution generated out of the water-wash column that eliminates $NH_3$ from the FG exiting the $CO_2$ absorber; finally, further $NH_3$ removal from the $CO_2$-depleted FG is achieved by means of acid washing using the solution generated out of the $SO_2$ removal and NO oxidation stage. Although the advanced CSIRO's process allows to reach higher FG temperatures at the stack, i.e. around 50 °C, the thermal energy requirements for the regeneration of the $NH_3$-lean stream are not avoided in this case and depend strongly on the $NH_3$ concentration in the $CO_2$-depleted FG thus on the $CO_2$ absorber operating conditions [21]. Therefore, not only the process operability and controllability are hindered as a consequence of the greater process complexity and interdependency among different process sections, but neither the stripper to regenerate the lean-$NH_3$ solution nor the associated energy requirements are avoided. On the other hand, the water and acid washing considered in the CAP is a simpler configuration that has been shown to have minor contribution to the overall energy requirements of the full capture process [3,14]. However, the implications on the size of the water-wash scrubber still have to be thoroughly determined. At this regard, although Jilvero et al. [16] carried out an analysis of the operating costs for different $NH_3$ abatement configurations combining water and acid washing units, the implications on the equipment size were not taken into consideration and the water-wash column considered in their study was as tall as the $CO_2$ absorber.

As a consequence of the high volatility of $NH_3$, $NH_3$-based $CO_2$ capture processes are usually criticized in the literature due to their complexity [6,7,17,22]. Indeed, they require specific units not only related to the $NH_3$ abatement from the $CO_2$-depleted FG, but also associated with the removal of $NH_3$ from the $CO_2$ gas stream and with the minimization of aqueous $NH_3$ solution make-up. As a consequence of the FG post-treatment, the temperature of the FG exiting the $NH_3$ absorber is generally lower than the temperature of the FG entering the $CO_2$ absorber. Therefore, a purge stream is required to avoid water building up within the solvent circulating in the $CO_2$ capture loop. $NH_3$ and $CO_2$ contained in the purge stream are recuperated using thermal energy in a solvent recovery section and recycled to the capture process in order to minimize the $CO_2$ losses and the $NH_3$ make-up [14]. In any case, a small $NH_3$ make-up is always required to maintain the $NH_3$ concentration in the solvent circulating in the $CO_2$ capture loop in order to counteract the $NH_3$ losses in the vented FG and in the $CO_2$ stream. Such $NH_3$ make-up is introduced by means of a fresh aqueous $NH_3$ solution whose water content also affects the water balance in the process. Therefore, the solvent recovery section is not only required in the CAP, where low temperature is used as one of the strategies for $NH_3$ abatement [14], but also in mild-temperature $NH_3$-based capture processes, specially if the temperature of the gas stream is not controlled properly. An example of the latter situation is the advanced, $NH_3$-based combined $NO_x/SO_x/CO_2$ emission control process mentioned above [20], where the temperature of the vented gas sent for $NH_3$ removal is lower than the temperature of the FG entering the absorber. Another example is the mild-temperature $NH_3$-based capture process developed at the Tunghai University, where the water accumulation in the solvent can be calculated from mass balances around the battery limits of the capture process using the data of the reported stream tables [23,24]. Therefore, even mild-temperature $NH_3$-based capture processes require to purge a fraction of liquid solvent, thus should include a process section for $NH_3$ (and $CO_2$) recuperation in order to achieve stable process operation and to minimize the $NH_3$ make-up. Alternatively, the aforementioned CSIRO's mild-temperature $NH_3$-based capture process [2] includes a water recovery section that does not only consist of a solvent recovery unit, but also includes a cooling tower. The cooling tower decreases the temperature of the FG that enters the $CO_2$ absorber to values similar to those of the FG exiting

the $CO_2$ capture section in order to avoid the accumulation of water in the solvent.

Furthermore, the $NH_3$ concentration in the $CO_2$ gas stream generated in the $CO_2$ desorber has to be limited, aiming at: (i) avoiding solid formation in the condensate streams generated downstream, i.e. either in the condenser of the $CO_2$ desorber [13,25], or during $CO_2$ compression [13]; and, (ii) limiting pipeline corrosion during $CO_2$ transportation [26]. The introduction of the Rich Solvent Splitting (RSS), i.e. a split of the cold $CO_2$-rich stream that bypasses the rich/lean heat exchanger and that is fed to the top of the $CO_2$ desorber, has been found to be an efficient and cost effective solution that: (i) improves the energetic performance of $NH_3$-based capture processes, (ii) limits the $NH_3$ slip in the $CO_2$ gas stream, and (iii) avoids the use of a condenser in the $CO_2$ desorber, thus avoiding the formation of solids in the resulting condensate [4,14,27]. $NH_3$ is normally further removed from the $CO_2$ gas stream by scrubbing, using water as washing medium [3,14,18,28], in order to meet the concentration limits of impurities for $CO_2$ transportation.

Additionally, despite the fact that $NH_3$-based capture processes may reach specific reboiler energy demands as low as 2.1 $MJ_{th}\,kg^{-1}_{CO_2captured}$ for solvent regeneration, the energetic optimization of the CAP that avoids solid formation applied to coal-fired power plants and to cement plants has shown that approximately 2/3 of the overall energy demand of the process, expressed as specific equivalent work, is associated with the heat requirements in the reboiler of the $CO_2$ desorber [14]. The remaining 1/3 is provided by means of electrical power. Aiming at decreasing the energy required for the regeneration of the solvent, advanced process configurations originally developed for capture technologies using aqueous amine solvents [29,30] have been implemented in $NH_3$-based capture processes. Among them, the RSS, whose implementation has minor effect on the capital costs and operability of the process, has been proven to decrease significantly the energy requirements of $NH_3$-based capture processes when the split fraction of cold $CO_2$-rich stream bypassing the rich/lean heat exchanger is optimized together with the pressure of the $CO_2$ desorber and with the feed stage of the hot $CO_2$-rich stream to the $CO_2$ desorber [14, 27]. Li et al. assessed the performance of the Inter-heated Desorber (IHD) [2] and of the Cold Rich Solvent Preheating (CRSP) [31], alone and in combination with the RSS, thus obtaining specific reboiler duties above 2.4 $MJ_{th}\,kg^{-1}_{CO_2captured}$ in all cases. Liu [23] assessed the performance of the IHD in mild-temperature $NH_3$-based capture processes and obtained energy savings of almost 22% with respect to the simplest absorber-desorber configuration. Nevertheless, the IHD achieves negligible energy savings when implemented together with the RSS at optimal conditions [27]. Jiang et al. [4,21] evaluated the performance of the Advanced Flash Stripper (AFS), originally developed by Rochelle [32] for $CO_2$ capture with aqueous piperazine, in combination with the RSS, which led to specific reboiler duties for the regeneration of the $CO_2$-lean $NH_3$ solvent as low as 1.9 $MJ_{th}\,kg^{-1}_{CO_2captured}$. Although very competitive in terms of reboiler duties, the results obtained by Jiang et al. [21] can be questioned because their simulations: (i) neglected the additional energy requirements associated with the solvent recovery from the solvent stream purged to avoid water accumulation, (ii) did not constrain the $NH_3$ concentration in the $CO_2$ stream to avoid corrosion in pipelines and equipment during $CO_2$ compression and transportation [33], and (iii) modelled the counter-current rich/lean heat exchanger by setting the cold side temperature approach to 3 °C and neglecting the internal vaporization of the hot $CO_2$-rich solution, which does not allow to detect infeasible pinch point temperatures within the rich/lean heat exchanger below 3 °C or even temperature crossovers [14]. As a result, the heat recovered in the rich/lean heat exchanger is overestimated and the reboiler duty underestimated. In addition, the AFS was only assessed in combination with the RSS so that the stand-alone effect of the feed stage of the hot $CO_2$-rich stream to the $CO_2$ desorber cannot be determined; on the contrary, independent investigations have found stage 7 out of 10—including the reboiler—from the top of the column as the optimal feed stage for the hot $CO_2$-rich stream to the $CO_2$ desorber, which minimizes the energy consumption required for solvent regeneration [14,27]. Finally, Ullah et al. [34] assessed the performance of the Lean Vapour Compression (LVC) and of the Rich Vapour Compression (RVC), and reported energetic savings of 15% and 3%, respectively, with respect to the simplest absorber-desorber configuration in $NH_3$-based capture processes. Similarly, Nguyen et al. [35] reported more than 43% energy savings for the LVC. Nevertheless, when implemented together with the RSS at optimal conditions, Liu et al. [27] reported negligible energy savings for the LVC and even negative values for the RVC, with respect to the process with the RSS. The LVC and the RVC decrease the energy required for solvent regeneration at the cost of increasing electrical demand for vapour re-compression. Therefore, their performance depends strongly on the features of the electricity accessible in the environment in which the capture plant is available, i.e. cost and associated $CO_2$ emissions. In addition, other authors have investigated other advanced process configurations specific to $NH_3$-based capture processes that aim at improving the energy consumption by decreasing the reboiler duty of the $CO_2$ desorber. Namely, Liu [36] proposed to compress the vapour exiting the top of the $NH_3$ desorber and inject it to the bottom of the $CO_2$ desorber, in combination with the LVC.

Nevertheless, all the aforementioned advanced configurations of the $CO_2$ desorber have been analysed in the literature by means of single-variable sensitivity analyses that do not take into account the interdependencies among different process variables, and have been compared to reference processes whose configuration and operating conditions have not been optimized previously, thus hindering comprehensive assessments and conclusive results.

As far as the source of heat required for solvent regeneration is concerned, the most cost efficient strategy is the use of saturated steam whose temperature must be above—at least by 10 °C—the reboiler temperature of the $CO_2$ desorber. In the case of $NH_3$-based capture processes, the optimal regeneration of the aqueous $NH_3$ solution that allows for the minimal energy consumption takes place at pressures around 20 bar and temperatures between 140 and 150 °C [14]. Similar steam temperatures are required by other amine-based capture processes, where the reboiler temperature in the $CO_2$ desorber ranges between ca. 120 °C, when using aqueous monoethanolamine (MEA) solutions as absorbent [37], and 150 °C, for aqueous piperazine [38]. When applied to power plants, the steam required for the $CO_2$ capture process is extracted from the low pressure turbine of the electricity generation island. Increasing reboiler duties and temperatures penalize the electricity throughput thus worsening the energetic performance of the capture process. In the case of applying the capture process to a steelworks facility, the steam required for solvent regeneration can also be extracted from the existing power island. While the electricity required can be imported from the grid if there does not exist a power plant in the vicinity, the need of steam hinders the application of solvent-based $CO_2$ capture processes to other industrial $CO_2$ intensive point sources where the steam required might not be available, for example in the case of cement plants, thus leading to additional capital costs related to on-site steam production [39]. In such cases, importing steam from a neighbouring Combined Heat and Power (CHP) plant has been found to decrease, between 10% and 20%, the cost of $CO_2$ avoided in cement plants when using solvent-based post-combustion technologies for $CO_2$ capture [40]. Unfortunately, the vast majority of existing cement plants are not located in the vicinity of a power plant [39], i.e. less than 10% of the existing European cement plants [33]. The competitiveness of solvent-based $CO_2$ capture processes can also be favoured by the possibility of integrating the excess heat available in the $CO_2$ point source. In the case of a typical European cement plant using the Best Available Technology (BAT), it has been reported that approximately between 5 and 10% of the steam required for solvent regeneration could be generated at limited cost and complexity using the excess heat of the clinker cooler exhaust air [39,40]. Norcem Brevik

is an extreme, still rare, case of a cement plant where up to 50% of the steam required for solvent regeneration in the capture plant could be generated by the excess heat available in the cement plant [41]. Other $CO_2$ intensive industries such as refineries and iron and steel plants also have process streams whose excess heat can be used for solvent regeneration. The amount of excess heat that can be integrated with the capture plant increases for lower solvent regeneration temperatures: On the one hand, the number of process streams whose heat cannot be used internally increases and, on the other hand, the pinch point temperature with respect to the capture process increases [42,43]. In fact, a solvent regeneration temperature around 90 °C or below has been reported to increase significantly the use of excess heat in the iron and steel industry [43]. Arasto et al. [44] simulated a hypothetical solvent with regeneration temperature of 70 °C for $CO_2$ capture in an iron and steel plant in order to show how low solvent regeneration temperatures enable the application of solvent-based capture processes even for relatively high solvent regeneration duties. In case of application to the power sector, the condenser of the power plant might supply heat for solvent regeneration at temperatures around 50 °C or below [3]. Therefore, the performance of the advanced configurations that affect the energy needs of the capture plant and the comparison among them depend not only on the steam and electricity requirements, but also on: (i) the temperature of the steam required, thus on the solvent regeneration temperature, (ii) the features of the available electricity and steam, i.e. the primary energy source and the associated $CO_2$ emissions, and (iii) the amount and temperature of the excess heat that can be recuperated from the $CO_2$ point source and used for solvent regeneration.

In this work, we have developed and analysed advanced configurations for $NH_3$-based $CO_2$ capture processes that aim at: (i) meeting $NH_3$ emission limits with the lowest impact on energy consumption, equipment size, process complexity and consumption of chemicals; (ii) simplifying the process by decreasing the required number of units, without affecting negatively either the process energetic performance or the fulfilment of process specifications and constraints; (iii) improving the energetic performance of the capture process by minimizing the steam requirements as well as by increasing its versatility regarding the type of energy that can be used and the integration of waste, low temperature heat available in the industrial $CO_2$ point source to which capture is applied. The CAP has been considered as standard benchmark configuration among $NH_3$-based capture processes since: (i) it has been extensively validated and demonstrated at different scales [11,12,45,46]; and (ii) it shows a very competitive techno-economic performance with respect to other post-combustion $CO_2$ capture technologies [39,40]. Process simulations of the $NH_3$-based capture process have been carried out using Aspen Plus, Version 8.6. Furthermore, the performance of the different advanced configurations depends on the process operating conditions [47]. Therefore, the advanced configurations here studied have been implemented on the CAP configuration presented and optimized earlier [14], and the performance assessments and comparison among different configurations have been carried out at three different optimal sets of operating conditions of the $CO_2$ absorber. Additional operating parameters have been optimized when relevant for a specific advanced configuration, in order to enable for proper performance assessment and comparison. In the following, the $NH_3$-based capture process used as reference configuration is described in Section 2, and the inputs, specifications and constraints of the process simulations, along with the performance indicators selected for the assessment of the advanced configurations are presented in Section 3. Then, the advanced configurations are introduced and classified depending on their objective in Section 4, followed by the detailed description of the process and of the optimization strategy of each advanced configuration, as well as by the results obtained in each case. Finally, conclusions of the work and recommendations for the application of the advanced configurations here developed are provided.

## 2. State-of-the-art process flow scheme

The Process Flow Diagram (PFD) considered as benchmark state-of-the-art configuration for $NH_3$-based capture processes and used in this work as basic scheme for the implementation of advanced configurations is shown in Fig. 1. The description of the process and the purposes of each process section and unit operation have been detailed elsewhere [14]. Such process flow scheme is the result of implementing the patents related to the CAP [10,48–51], including process sections that allow for the control of $NH_3$ emissions and for the recuperation of $NH_3$, as well as simple process modifications broadly applied in solvent-based capture processes that allow to decrease the overall energy consumption with minor impact on the process complexity and operability, e.g. the RSS. More specifically and most relevant to this work, the benchmark PFD considers:

- The absorber pumparound (within the $CO_2$ absorption section (F) in Fig. 1), a slip stream of the cold $CO_2$-rich stream that is cooled, chilled and sent to the top of the $CO_2$ absorber in order to minimize the $NH_3$ slip to the gas.
- The FG post-conditioning section (A), which is able to further decrease the $NH_3$ concentration in the $CO_2$-depleted FG to values that meet the regulatory limits at the stack. It consists of a Flue Gas Water-Wash (FG-WW) column that is an $NH_3$ absorber, followed by an acid-wash scrubber using an aqueous solution of $H_2SO_4$.
- The $CO_2$ Water-Wash ($CO_2$-WW) section (B), which is used to minimize gaseous $NH_3$ losses from the $CO_2$ desorber, consists of a Direct Contact Cooler (DCC) that uses water to remove $NH_3$ from the $CO_2$ gas stream produced in the $CO_2$ desorber.
- The solvent recovery section (C), whose goal is to minimize the $NH_3$ make-up requirements, is composed of two different distillation columns, namely: (i) the $NH_3$ desorber, whose purpose is the recuperation of $NH_3$ (and $CO_2$) from the $NH_3$-rich solution exiting the $NH_3$ absorber; and, (ii) the appendix stripper, which recovers $NH_3$ (and $CO_2$) from the solvent stream purged from the $CO_2$ absorber/$CO_2$ desorber loop and from the liquid stream purged from the $CO_2$-WW section. Both the $NH_3$ desorber and the appendix stripper operate at atmospheric pressure and generate an almost pure water stream at the bottom of the column, requiring ca. 100 °C at the reboiler.
- The RSS (within the $CO_2$ desorber section (E)), a split of the cold $CO_2$-rich stream that bypasses the rich/lean heat exchanger and that is directly sent to the top of the $CO_2$ desorber instead. In addition to control the temperature in the $CO_2$ desorber thus the $NH_3$ slip to the $CO_2$ stream, its optimization, together with the pressure in the $CO_2$ desorber, allows minimizing the energy demand while avoiding solid formation downstream in the process [14].
- The solvent is regenerated and $CO_2$ is stripped-off in the $CO_2$ desorber (E), which operates at pressures between 7.5 and 30.0 bar and that reaches temperatures in the reboiler between 115 and 150 °C.

The operating variables that govern the overall performance of the benchmark state-of-the-art CAP are indicated in Fig. 1 [14]. They are enumerated below, and arranged according to the capture process section to which they belong:

- $CO_2$ absorber (F) decision variables, i.e. the apparent $NH_3$ concentration in the $CO_2$-lean stream, $\hat{c}_{NH_3}$ [$mol_{NH_3}\,kg_{H_2O}^{-1}$], the $CO_2$ loading of the $CO_2$-lean stream considering apparent species, $l_{lean}$ [$mol_{CO_2}\,mol_{NH_3}^{-1}$], the liquid-to-gas flowrate ratio for the $CO_2$-lean liquid and inlet gas streams entering the $CO_2$ absorber, $L^{lean}/G^{in}$ [$kg\,kg^{-1}$], the temperature of the pumparound stream, $T_{pa}$ [°C], and the pumparound split fraction, $f_s$ [-].

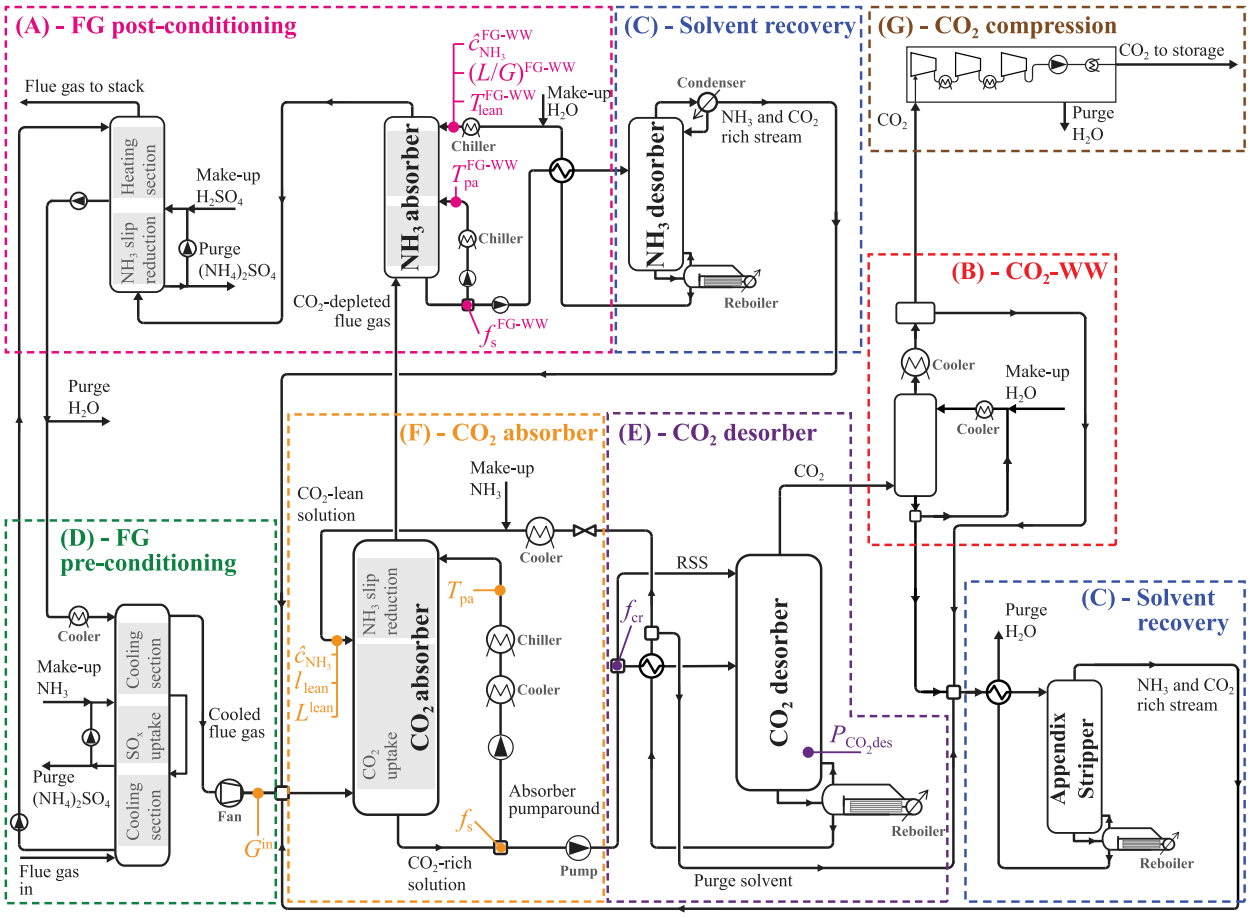


**Fig. 1.** Benchmark state-of-the-art flow scheme of the CAP used as reference configuration of $NH_3$-based capture processes. Boxes with dashed lines are introduced for the identification of the different sections of the process, i.e. A to G. Labels provide the name of the process section or, if within a unit operation, the equipment or equipment section identification. The operating variables whose value govern the performance of the process are indicated in the flow scheme and have been colour-coded according to the process section to which they belong, i.e. orange for $CO_2$ absorber operating variables, violet for $CO_2$ desorber operating variables and magenta for FG-WW column operating variables. (For interpretation of the references to colour in this figure caption, the reader is referred to the web version of this article.)

- $CO_2$ desorber (E) decision variables, i.e. the pressure in the $CO_2$ desorber, $P_{CO_2des}$ [bar], and the cold-rich bypass split fraction, $f_{cr}$ [-].
- FG-WW column (A) decision variables, i.e. the apparent $NH_3$ concentration in the $NH_3$-lean stream, $\hat{c}_{NH_3}^{FG-WW}$ [$mol_{NH_3}\ kg_{H_2O}^{-1}$], the liquid-to-gas flowrate ratio for the $NH_3$-lean liquid and the $CO_2$-depleted FG entering the $NH_3$ absorber, $(L/G)^{FG-WW}$ [$kg\ kg^{-1}$], the temperature of the $NH_3$-lean stream, $T_{lean}^{FG-WW}$ [°C], the temperature of the pumparound stream, $T_{pa}^{FG-WW}$ [°C], and the pumparound split fraction, $f_s^{FG-WW}$ [-].

**Table 1**
Inlet FG characteristics.

| Variable | Units | Value |
|---|---|---|
| Total flowrate | [kg/s] | 107 |
| Temperature | [°C] | 110 |
| Pressure | [bar] | 1.1 |
| Composition | [mole frac.] | |
| $y_{air}$ | | 0.730 |
| $y_{CO_2}$ | | 0.180 |
| $y_{H_2O}$ | | 0.090 |

## 3. Process simulation and performance assessment

Advanced process configurations have been assessed for inlet FG conditions corresponding to a typical European cement plant using the Best Available Technology (BAT), as defined for the EU-H2020 project CEMCAP with the collaboration of the European Cement Research Academy (ECRA) [33]. The inlet FG conditions are provided in Table 1. For the sake of simplicity, only species derived from $CO_2$, $NH_3$ and $H_2O$ have been considered in the process simulations. On the one hand, $NO_x$ has been assumed to enter the capture process in the form of NO, which is not soluble in the solvent [52], while $SO_2$ has been considered to be removed completely in the FG pre-conditioning section [19,51]. On the other hand, full removal of $NH_3$ by acid washing has been assumed in the FG post-conditioning section [6,51]. Consequently, the FG pre-conditioning section and the last column before the stack in the FG post-conditioning section have been simulated as a DCC and as a Direct Contact Heater (DCH), respectively, still accounting rigorously for the heat integration and cooling needs. The flowrate of aqueous $NH_3$ (or caustic) make-up, of aqueous $H_2SO_4$ make-up and of pure solid ammonium sulphate ($(NH_4)_2SO_4$) can still be computed from simple straightforward mass balances.

Simulations have been performed in Aspen Plus, Version 8.6, using the rate-based model described, implemented and validated earlier [14]. Equilibrium-based simulations of the full capture process have been combined with rate-based simulations of the $CO_2$ absorber and of the FG-WW column. Only those simulations leading to results meeting the specifications and constraints indicated in Table 2 were considered as representative of feasible process operation hence used for the assessment of the advanced configurations. The $CO_2$ capture efficiency is fixed to 0.9 in all cases in order to allow for a fair comparison among different process configurations. Additionally, all advanced configurations are designed to avoid the formation of solids in the process. The

**Table 2**
Specifications and constraints considered in all process simulations of $NH_3$-based capture processes.

| | |
|---|---|
| **Overall $CO_2$ capture process** | |
| $CO_2$ capture efficiency ($\psi$) [-] | 0.9 |
| Formation of solids | Avoided |
| $NH_3$ concentration in the FG at the stack [$ppm_v$] | ≤ 10 |
| Apparent $NH_3$ concentration in purge liquid streams [$ppm_{wt}$] | ≤ 150 |
| $CO_2$ gas stream for transport by pipeline to storage | |
| Pressure [bar] | 110 |
| Temperature [°C] | 28 |
| Temperature of aqueous $NH_3$ liquid streams [°C] | <150 |
| **$CO_2$-WW section** | |
| $CO_2$ gas stream to compression | |
| Temperature [°C] | 35 |
| $NH_3$ concentration ($y_{NH_3}^{CO_2comp,in}$) [$ppm_v$] | <50 |
| $CO_2$ purity [vol%] | >99 |

specifications of the $CO_2$ gas stream at the battery limits of the capture plant have been set to those defined for transport by pipeline [26,33,39]. The $CO_2$ compression section is also simulated in Aspen Plus, Version 8.6, by means of the configuration provided by Manzolini et al. [53] and using the Perturbed-Chain Statistical Associating Fluid Theory (PC-SAFT) as thermodynamic model, which enables reliable results at supercritical conditions but does not include $NH_3$ as one of the components of the thermodynamic package. Therefore, components in the $CO_2$ gas stream other than $CO_2$ and $H_2O$, i.e. $NH_3$, have been neglected, so as specifications and constraints regarding temperature, composition and avoidance of solid formation are applied to the $CO_2$ gas stream entering the $CO_2$ compression section, which warrants their fulfilment downstream. The maximum $NH_3$ concentration allowable in the liquid streams purged from the process, i.e. 150 $ppm_{wt}$, has been selected as an intermediate value from maximum values for European ammonia production facilities using the BAT, where it ranges between 80 and 175 $ppm_{wt}$ [54]. Such limited pollution with biodegradable $NH_3$ allows for simple sewage water treatment that can be used to produce the process water make-up required in the capture process. In addition, the temperature of aqueous $NH_3$ liquid streams has been limited to 150 °C or below in order to assure the lack of any corrosion on typical materials used in the construction of the capture process units, i.e. stainless steel.

The performance assessment of the advanced configurations and the comparison among different PFD's have been carried out with reference to the following process performance indicators:

- Energy consumption is considered as an indicator of the operating costs of the capture process. The **specific equivalent work**, $\omega$ [$MJ\,kg^{-1}_{CO_2captured}$], considers the steam demand in the reboilers of the process as well as the electricity required for chilling, cooling, pumping and compression. The conversion of each energy consumer to specific equivalent work has been detailed in our previous work [14]. In addition, the specific equivalent work associated with the $NH_3$ capture loop defined by the FG-WW column and the $NH_3$ desorber, $\omega_{FG-WW}^{NH_3}$ [$MJ\,kg^{-1}_{NH_3captured}$], has also been used as energetic performance indicator of those configurations aiming at controlling $NH_3$ emissions in the $CO_2$-depleted FG, and it has been computed as follows:

$$\omega_{FG-WW}^{NH_3} = \omega_{FG-WW}\left(\frac{\dot{m}_{CO_2}^{storage}}{\dot{m}_{NH_3}^{FG-WW,in} - \dot{m}_{NH_3}^{FG-WW,out}}\right) \quad (1)$$

where $\omega_{FG-WW}$ [$MJ\,kg^{-1}_{CO_2captured}$] is the equivalent work per unit of mass of $CO_2$ captured associated with the energy consumers of the FG-WW column and of the $NH_3$ desorber, $\dot{m}_{CO_2}^{storage}$ [$kg_{CO_2}\,s^{-1}$] is the mass flowrate of $CO_2$ captured and sent to storage, and $\dot{m}_{NH_3}^{FG-WW,in}$ and $\dot{m}_{NH_3}^{FG-WW,out}$ [$kg_{NH_3}\,s^{-1}$] are the mass flowrates of $NH_3$ in the FG stream entering and leaving, respectively, the FG-WW column.

Furthermore, the **type of energy** required is analysed, when relevant, by means of the breakdown of steam required in the reboilers of the $CO_2$ desorber, $q_{reb,CO_2}$, the appendix stripper, $q_{reb,app}$, and the $NH_3$ desorber, $q_{reb,NH_3}$ [$MJ_{th}\,kg^{-1}_{CO_2captured}$], vs. the electricity requirements—assumed to be equal to the specific equivalent work—for chilling, cooling, pumping and $CO_2$ compression, $e$ [$MJ_{el}\,kg^{-1}_{CO_2captured}$].

Besides the two types of energy requirements, the **Specific Primary Energy Consumption per $CO_2$ Avoided (SPECCA)** index, $\zeta$ [$MJ_{LHV}\,kg^{-1}_{CO_2avoided}$], is used as energy performance indicator to assess advanced configurations aiming at improving the energetic performance of $NH_3$-based capture processes. As pointed out in our previous research [14], $\zeta$ is preferred as energy performance indicator when the capture process is applied to a specific $CO_2$ point source, which might not have access to the electricity and steam produced in a power plant and where low temperature excess heat might be available for generation of (part of) the steam required in the capture plant. If the capture plant is an end-of-pipe technology that avoids modifications of the manufacturing process carried out in the $CO_2$ point source, as done in this work, $\zeta$ can be computed as follows:

$$\zeta = \frac{q_{CCS}}{\epsilon_{ref} - \epsilon_{CCS}} \quad (2)$$

where $q_{CCS}$ is the primary energy consumption of the Carbon Capture and Storage (CCS) plant, considering the Low Heating Value (LHV) of the fuel consumed, [$MJ_{LHV}$], and $\epsilon_{ref}$ and $\epsilon_{CCS}$ are the $CO_2$ emissions of the point source without and with CCS plant, respectively, [$kg_{CO_2avoided}$].

- The **productivity** depends on the volume of the pieces of equipment, which can be used as an indication of the trends of capital costs of the capture process. The cost of the $CO_2$ absorber has been reported as a major contributor to the investment costs associated with a solvent-based capture plant [55]. However, in this work we have added the productivity of the FG-WW column, $Pr_{FG-WW}$, to that of the $CO_2$ absorber, $Pr_{CO_2abs}$, in both cases referenced to the flowrate of $CO_2$ captured, i.e. [$kg_{CO_2captured}\,m^{-3}\,h^{-1}$], in order to assess and compare advanced $NH_3$ abatement configurations. Therefore, the overall process productivity, Pr, is calculated as follows:

$$Pr = \frac{1}{\frac{1}{Pr_{CO_2abs}} + \frac{1}{Pr_{FG-WW}}} = \frac{\dot{m}_{CO_2}^{storage}}{V_{CO_2abs} + V_{FG-WW}} \quad (3)$$

where $V_{CO_2abs}$ and $V_{FG-WW}$ are the volumes of packing required in the $CO_2$ absorber and in the $NH_3$ absorber, respectively, which are calculated considering: (i) cylindrical shape, (ii) a hydraulic load at the bottom of each column at 70% of flooding [56], and (iii) a random packing of 25-mm Pall rings with a specific surface area of 207 $m^2\,m^{-3}$ used in the pilot tests reported by Yu et al. [52] and further detailed by Qi et al. [57] whose results were used to validate the rate-based model [14] used in this work. Additionally, another productivity related to the removal of $NH_3$ in the FG-WW column, $Pr_{FG-WW}^{NH_3}$ [$kg_{NH_3captured}\,m^{-3}\,h^{-1}$], has been defined:

$$Pr_{FG-WW}^{NH_3} = \frac{\dot{m}_{NH_3}^{FG-WW,in} - \dot{m}_{NH_3}^{FG-WW,out}}{V_{FG-WW}} \quad (4)$$

- The **consumption of water** and the **consumption of chemicals in aqueous solution**, $F_{H_2O}^{in}$ and $F_{chem,i}^{in}$, respectively, [$kg\,t^{-1}_{CO_2captured}$], with $i$ referring to $NH_3$ or to $H_2SO_4$, do not only contribute to the operating costs but can also be considered as an indication of process sustainability—in the case of aqueous $NH_3$ solution (25 wt%) and water—or as an indicator for the capture process retrofitability if chemicals that require stringent safety considerations are required for the capture process—in the case of aqueous $H_2SO_4$ solution (98 wt%).

**Table 3**
Process operating conditions that minimizes the specific equivalent work of the benchmark state-of-the-art CAP configuration shown in Fig. 1, aiming at 0.9 $CO_2$ capture efficiency, when fixing the apparent $NH_3$ concentration in the $CO_2$-lean stream to 5 (low $\hat{c}_{NH_3}$), to 7 (mid $\hat{c}_{NH_3}$) and to 9 (high $\hat{c}_{NH_3}$) $mol_{NH_3}\ kg^{-1}_{H_2O}$, reported in the *Supplementary Material* of our previous optimization work [14]. The $NH_3$ slip in the $CO_2$-depleted FG stream leaving the $CO_2$ absorber, $y^{FG-WW,in}_{NH_3}$, and in the $CO_2$ gas stream exiting the $CO_2$ desorber, $y^{CO_2-WW,in}_{NH_3}$, are also reported for each set of operating conditions, along with the corresponding values of the process performance indicators.

| | Variable | Units | Simulation case | | |
|---|---|---|---|---|---|
| | | | low $\hat{c}_{NH_3}$ | mid $\hat{c}_{NH_3}$ | high $\hat{c}_{NH_3}$ |
| $CO_2$ absorber parameters | $\hat{c}_{NH_3}$ | $[mol_{NH_3}\ kg^{-1}_{H_2O}]$ | 5.0 | 7.0 | 9.0 |
| | $l_{lean}$ | $[mol_{CO_2}\ mol^{-1}_{NH_3}]$ | 0.33 | 0.35 | 0.38 |
| | $L^{lean}/G^{in}$ | $[kg\ kg^{-1}]$ | 5.5 | 5.0 | 5.5 |
| | $f_s$ | [-] | 0.21 | 0.25 | 0.25 |
| | $T_{pa}$ | [°C] | 11 | 12 | 12 |
| $CO_2$ desorber parameters | $P_{CO_2des}$ | [bar] | 17.5 | 22.5 | 22.5 |
| | $f_{cr}$ | [-] | 0.0500 | 0.0475 | 0.0450 |
| FG-WW column parameters | $\hat{c}^{FG-WW}_{NH_3}$ | $[mol_{NH_3}\ kg^{-1}_{H_2O}]$ | 0.05 | 0.05 | 0.05 |
| | $(L/G)^{FG-WW}$ | $[kg\ kg^{-1}]$ | 0.1 | 0.1 | 0.1 |
| | $T^{FG-WW}_{lean}$ | [°C] | 1.5 | 1.5 | 1.5 |
| | $T^{FG-WW}_{pa}$ | [°C] | 1.5 | 1.5 | 1.5 |
| | $f^{FG-WW}_s$ | [-] | 0.001 | 0.001 | 0.001 |
| Internal $NH_3$ slip | $y^{FG-WW,in}_{NH_3}$ | $[ppm_v]$ | 3110 | 4780 | 7880 |
| | $y^{CO_2-WW,in}_{NH_3}$ | $[ppm_v]$ | 610 | 1410 | 2050 |
| Performance indicators | $\omega$ | $[MJ\ kg^{-1}_{CO_2captured}]$ | 1.057 | 1.043 | 1.078 |
| | $\omega_{FG-WW}$ | $[MJ\ kg^{-1}_{CO_2captured}]$ | 0.031 | 0.037 | 0.045 |
| | $\omega^{NH_3}_{FG-WW}$ | $[MJ\ kg^{-1}_{NH_3captured}]$ | 5.932 | 4.414 | 3.218 |
| | $q_{reb,CO_2}$ | $[MJ_{th}\ kg^{-1}_{CO_2captured}]$ | 2.22 | 2.16 | 2.23 |
| | $T_{reb,CO_2}$ | [°C] | 145 | 147 | 143 |
| | $q_{reb,app}$ | $[MJ_{th}\ kg^{-1}_{CO_2captured}]$ | 0.06 | 0.08 | 0.10 |
| | $T_{reb,app}$ | [°C] | 105 | 105 | 105 |
| | $q_{reb,NH_3}$ | $[MJ_{th}\ kg^{-1}_{CO_2captured}]$ | 0.11 | 0.14 | 0.17 |
| | $T_{reb,NH_3}$ | [°C] | 99 | 99 | 99 |
| | $e$ | $[MJ_{el}\ kg^{-1}_{CO_2captured}]$ | 0.287 | 0.277 | 0.290 |
| | Pr | $[kg_{CO_2captured}\ m^{-3}\ h^{-1}]$ | 56.4 | 57.7 | 56.6 |
| | $Pr_{CO_2abs}$ | $[kg_{CO_2captured}\ m^{-3}\ h^{-1}]$ | 72.9 | 85.4 | 113.7 |
| | $Pr_{FG-WW}$ | $[kg_{CO_2captured}\ m^{-3}\ h^{-1}]$ | 249.2 | 178.0 | 112.6 |
| | $Pr^{NH_3}_{FG-WW}$ | $[kg_{NH_3captured}\ m^{-3}\ h^{-1}]$ | 1.314 | 1.476 | 1.574 |
| | $F^{in}_{H_2O}$ | $[kg\ t^{-1}_{CO_2captured}]$ | 7.04 | 14.26 | 27.52 |
| | $F^{in}_{chem,NH_3}$ | $[kg\ t^{-1}_{CO_2captured}]$ | 1.47 | 1.48 | 1.49 |
| | $F^{in}_{chem,H_2SO_4}$ | $[kg\ t^{-1}_{CO_2captured}]$ | 1.06 | 1.06 | 1.07 |

Furthermore, the comparison among different advanced configurations has been performed at different $\hat{c}_{NH_3}$ values. Namely, 5, 7 and 9 $mol_{NH_3}\ kg^{-1}_{H_2O}$ have been selected as representative of a low, a mid and a high typical concentration of solvent in $NH_3$-based capture processes [3,14,52]. The values of the remaining operating conditions for each $\hat{c}_{NH_3}$ value have been extracted from the optimization results obtained in our previous work [14] on the benchmark state-of-the-art CAP configuration shown in Fig. 1. The operating conditions have been selected aiming at minimizing the specific equivalent work for $CO_2$ capture efficiency equal to 0.9. These optimal values are indicated in Table 3, along with their corresponding process performance indicators.

The minimal specific equivalent work was obtained for the mid $\hat{c}_{NH_3}$ case, although the low $\hat{c}_{NH_3}$ case and the high $\hat{c}_{NH_3}$ case also performed very competitively in terms of energy consumption. On the one hand, increasing apparent $NH_3$ concentration in the solvent increases the $NH_3$ slip both in the $CO_2$-depleted FG leaving the $CO_2$ absorber, $y^{FG-WW,in}_{NH_3}$, and in the $CO_2$ gas stream exiting the $CO_2$ desorber, $y^{CO_2-WW,in}_{NH_3}$. As a result, there is an increase of the specific reboiler duties of the $NH_3$ desorber, $q_{reb,NH_3}$, and of the appendix stripper, $q_{reb,app}$, required for the recuperation of $NH_3$ from the vapour streams in the solvent recovery sections. Nevertheless, the main energy consumer of the process is the reboiler of the $CO_2$ desorber, $q_{reb,CO_2}$, regardless of the $NH_3$ content of the solvent. On the other hand, operating the capture process at higher $\hat{c}_{NH_3}$ requires greater water make-up flowrates, $F^{in}_{H_2O}$, to recover the $NH_3$ slipped to the gas streams, while the flowrates of aqueous $NH_3$ solution make-up, $F^{in}_{chem,NH_3}$, and of aqueous $H_2SO_4$ solution make-up, $F^{in}_{chem,H_2SO_4}$, remain almost unchanged. As far as the productivity of the process is concerned, increasing $\hat{c}_{NH_3}$ allows for greater $CO_2$ absorber productivity, $Pr_{CO_2abs}$, as pointed out earlier [14], while it has the opposite effect on the productivity of the FG-WW column, $Pr_{FG-WW}$. As a result, the overall process productivity, Pr, finds a maximum for the mid $\hat{c}_{NH_3}$ case, although the low $\hat{c}_{NH_3}$ case and the high $\hat{c}_{NH_3}$ also allowed for very competitive results. Notwithstanding that the selection of the optimal set of operating conditions that optimizes the capture process can be only determined by means of cost calculations, which is out of the scope of this work, the different effect of the three sets of operating conditions provided in Table 3 on the energy demand, on the absorbers' size and on the $NH_3$ slip of each process section seems to make them ideal to carry out a general performance assessment and fair comparison of the advanced configurations proposed in this work.

Unless mentioned otherwise, other assumptions regarding equipment specifications and utilities, required for process simulation and for the computation of the performance indicators, can be found in our previous work [14].

## 4. Advanced process configurations

In this work, different advanced process configurations have been implemented on the benchmark state-of-the-art CAP shown in Fig. 1, referred to as reference configuration (or simply "Ref" in figures and tables) hereinafter. Most of them are novel configurations that have been developed specifically for $NH_3$-based capture processes. In addition, some promising advanced configurations for amine-based capture processes reported in literature have been considered in this study, either to analyse their performance when using aqueous $NH_3$ as a solvent,

**Table 4**
Advanced configuration concepts of $NH_3$-based capture processes implemented in this work classified depending on their objective (in **bold**).

| |
|---|
| **Control of $NH_3$ emissions—No $H_2SO_4$(aq) requirements** |
| Standard $NH_3$ Absorber (SNA) |
| $NH_3$ Absorber with Water-wash section (NAW) |
| Advanced $NH_3$ Absorber (ANA) |
| **Simplification of the PFD—CAPEX reduction** |
| No $CO_2$-WW column |
| No appendix stripper |
| Integrated Stripper (IS) |
| **Improvement of the energetic performance—OPEX reduction** |
| Recycled Vapour Compression (RecVC) |
| Lean Vapour Compression (LVC) |
| Multi-pressure Desorber (MPD) |
| Vacuum Integrated Stripper (VIS) |

or to determine possible synergies when combined with novel advanced configurations specific of $NH_3$-based capture processes. In total, ten different advanced configuration concepts, and several combinations among them, have been implemented, analysed and compared in this work. Table 4 classifies the different advanced configuration concepts according to their objective.

In the following, the advanced configurations are described in the order introduced in Table 4, grouped in different sub-sections according to their ultimate goal and labelled depending on the process section of the reference configuration that is modified. In addition to the process description, the operating variables that determine the performance of each configuration and the process optimization strategy designed in each case are also detailed, as well as the results obtained.

### 4.1. Advanced configurations for the control of $NH_3$ emissions

#### 4.1.1. Process description and optimization strategy

Power plants and most of the $CO_2$ emitting industrial sectors, e.g. cement and steelwork plants, do not use strong acidic (or basic) solutions within their manufacturing process. Therefore, the advanced configurations for the control of $NH_3$ emissions aim at avoiding the requirement of acid washing thus the handling and consumption of aqueous $H_2SO_4$ solutions. As a result, three different advanced configurations for the control of $NH_3$ emissions have been proposed, as shown in Fig. 2. All of them modify the FG post-conditioning section of the reference configuration (process section A in Fig. 1) by introducing operating and/or design modifications into the FG-WW column, which enable the removal of the acid washing. Further details are provided below for each advanced configuration of the FG-WW column.

**Configuration A1 with the SNA**, which still considers the FG-WW column configuration of the reference CAP but allows for the removal of the acid-wash column by tuning the operating conditions of the SNA. The SNA consists of two sections: (i) a lower section whose goal is the removal of the bulk amount of $NH_3$ contained in the $CO_2$-depleted FG coming from the $CO_2$ absorber, and (ii) an upper section in which the $NH_3$ concentration in the FG is further decreased to values in the order of magnitude of tens to hundreds of $ppm_v$. While the upper section of the $NH_3$-absorber in the reference CAP configuration decreases the $NH_3$ content in the FG, $y_{NH_3}^{FG-WW,out}$ in Fig. 2, to values around 200 $ppm_v$, the removal of the acid-wash column downstream requires to reach concentrations below 10 $ppm_v$ instead, in order to meet the $NH_3$ emissions limits at the stack. The $NH_3$-lean solution regenerated in the $NH_3$ desorber is chilled before entering the top of the $NH_3$ absorber. While flowing down along the column, the aqueous $NH_3$ solution captures $NH_3$ and $CO_2$ from the FG flowing upwards in counter-current, increasing both its $NH_3$ and its $CO_2$ concentration. The $NH_3$-rich stream obtained at the bottom of the $NH_3$ absorber is sent back to the $NH_3$ desorber, where $NH_3$ and $CO_2$ are stripped off from the liquid solution, regenerating the $NH_3$-lean stream to be used again in the $NH_3$ absorber. A fraction of the $NH_3$-rich solution leaving the bottom of the $NH_3$ absorber is recycled to an intermediate stage of the column after being chilled. The goals of this pumparound stream are: (i) to approach the $NH_3$ concentration in the FG leaving the lower section of the $NH_3$ absorber to the $NH_3$ partial pressure in equilibrium with the pumparound stream using high enough a liquid-to-gas flowrate ratio, and (ii) to maximize the $NH_3$ removal in the lower section of the $NH_3$ absorber by decreasing the temperature of the liquid solution.

In order to assess the performance of the process configuration when removing the acid-wash column using the SNA, a multi-objective optimization problem of the FG-WW section has been solved for each $\hat{c}_{NH_3}$ case (thus for different $NH_3$ concentration values in the $CO_2$-depleted FG entering the column, $y_{NH_3}^{FG-WW,in}$). As a result, the optimal set of operating conditions and the SNA design are obtained, aiming at minimizing the specific equivalent work associated with the FG-WW section, $\omega_{FG-WW}$, and at maximizing the productivity of the $NH_3$ absorber, $Pr_{FG-WW}$. In practice, such multi-objective optimization problem is run as a series of single-objective rigorous optimization problems based on Successive Quadratic Programming (SQP) whereby the minimum $\omega_{FG-WW}$ is found when varying the FG-WW column height, $H_{FG-WW}$ [m]. The decision variables of the optimization problem, which are shown in Fig. 2, are the FG-WW column decision variables introduced in Section 2, i.e. $\hat{c}_{NH_3}^{FG-WW}$, $T_{lean}^{FG-WW}$, $(L/G)^{FG-WW}$, $f_s^{FG-WW}$ and $T_{pa}^{FG-WW}$, along with the relative height at which the pumparound stream enters the packing of the $NH_3$ absorber, $h_{pa}^{FG-WW}$ [-], defined as:

$$h_{pa}^{FG-WW} = \frac{H_{pa}^{FG-WW}}{H_{FG-WW}} \tag{5}$$

where $H_{pa}^{FG-WW}$ [m] is the height of the packing of the FG-WW column at which the pumparound stream is fed. Additionally, the liquid-to-gas flowrate ratio for the bottom section of the SNA, $(L^{bot}/G)^{FG-WW}$ [$kg\,kg^{-1}$], can be computed from $f_s^{FG-WW}$ and $(L/G)^{FG-WW}$ in order to provide a parameter that facilitates the understanding of the operation within the SNA, as follows:

$$(L^{bot}/G)^{FG-WW} = \frac{(L/G)^{FG-WW}}{1 - f_s^{FG-WW}} \tag{6}$$

Besides the specification of $y_{NH_3}^{FG-WW,out}$, constraints to the optimization problem are that: (i) the $NH_3$ content in the stream purged from the FG post-conditioning section (see Fig. 2), $w_{NH_3}^{purge}$, is below 150 $ppm_{wt}$, which effectively constrains the value of $\hat{c}_{NH_3}^{FG-WW}$ unless there is no purge stream, i.e. $F_{purge}^{FG-WW} = 0\,kg\,s^{-1}$, and (ii) $T_{lean}^{FG-WW}$ and $T_{pa}^{FG-WW}$ are, on the one hand, lower than the temperature of the streams entering their corresponding chillers but, on the other, higher than 1.5 °C in order to enable the use of simple industrial refrigeration systems.

**Configuration A2 with the NAW**. The NAW consists of three sections: (i) a lower section where the bulk of $NH_3$ contained in the $CO_2$-depleted FG is removed from the gas, as for the SNA, (ii) an intermediate section in which the $NH_3$ concentration in the FG is further decreased to values of a few tens of $ppm_v$, and (iii) an upper section where the $NH_3$ concentration is decreased to values below 10 $ppm_v$. With this aim, in this configuration the acid-wash packing section included in the FG post-conditioning section of the reference configuration is exchanged for a water-wash packing section, which is added to the top of the $NH_3$ absorber. A water make-up stream at ambient temperature enters the top of the column and captures $NH_3$ from the FG flowing upwards in counter-current. As a consequence of the increase in $NH_3$ concentration, the liquid is expected to capture also some $CO_2$ from the FG. The polluted water exiting the bottom of the water-wash section of the FG-WW column is then fed to the top of the intermediate packing section, together with the $NH_3$-lean stream. As for the rest of the column, the NAW is similar to the SNA.

In order to assess the performance of the NAW, a multi-objective optimization of the FG-WW section has been carried out following the same strategy and approach detailed above for the SNA. As far as the

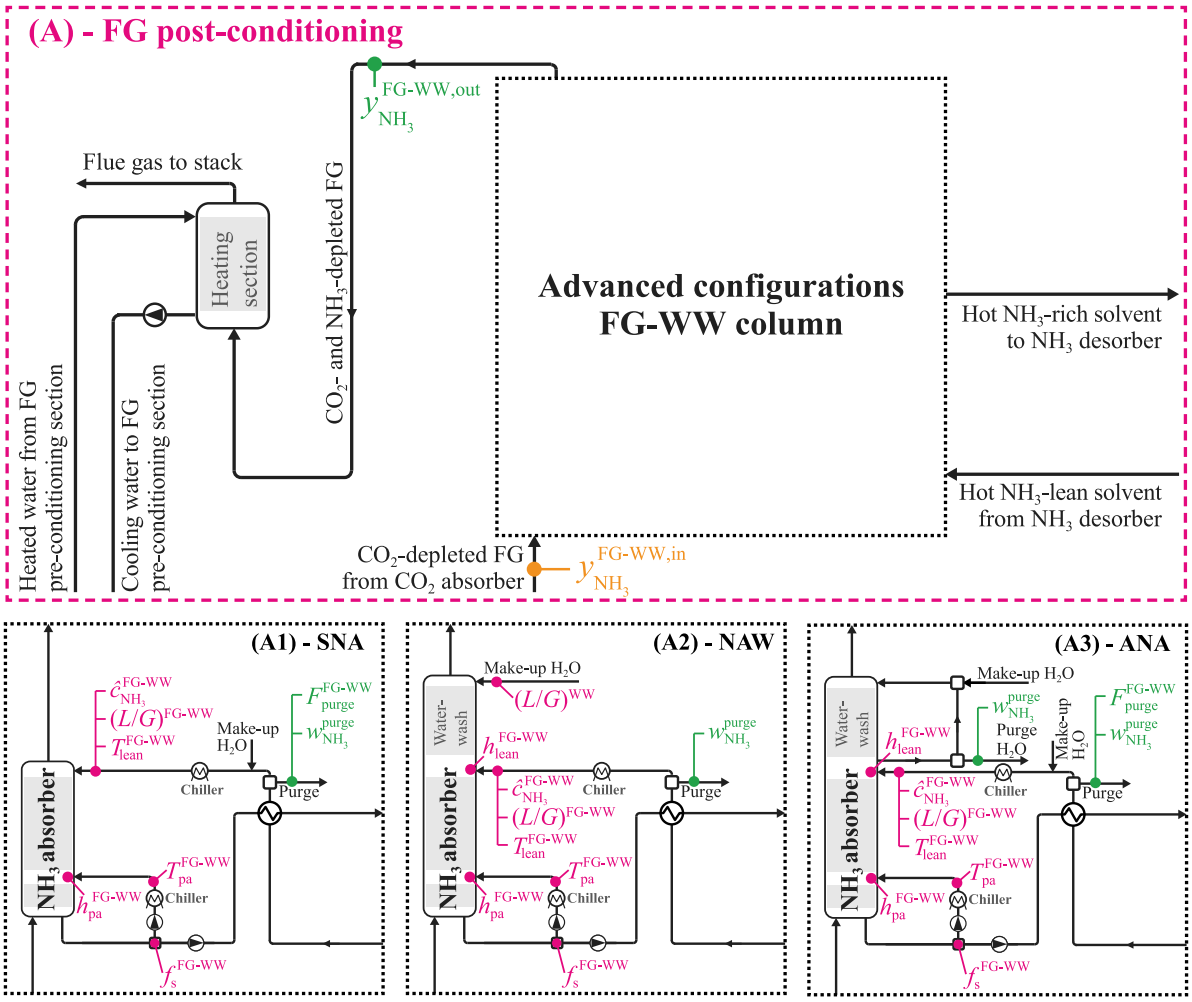


**Fig. 2.** Flow diagram of the FG post-conditioning section of the CAP without acid-wash column using different configurations of the FG-WW column with respect to the reference process. The operating variables that govern the performance of the configuration, i.e. the decision variables of the optimization problem, the process specifications and constraints, and the input variables have been colour-coded in magenta, green and orange, respectively. (For interpretation of the references to colour in this figure caption, the reader is referred to the web version of this article.)

decision variables are concerned, we consider eight in total, which are shown in Fig. 2; in addition to those considered for the optimization of the SNA, we have included the following operating variables of the NAW: (i) the liquid-to-gas flowrate ratio for the make-up water stream entering at the top of the water-wash section and the $CO_2$-depleted FG entering at the bottom of the FG-WW column, $(L/G)^{WW}$ [kg kg$^{-1}$], and (ii) the relative height at which the $NH_3$-lean stream enters the packing of the FG-WW column, $h_{lean}^{FG-WW}$ [-], defined as:

$$h_{lean}^{FG-WW} = \frac{H_{lean}^{FG-WW}}{H_{FG-WW}} \tag{7}$$

where $H_{lean}^{FG-WW}$ [m] is the height of the packing of the FG-WW column at which the $NH_3$-lean stream enters the packing of the NAW. Regarding constraints to the optimization problem, $w_{NH_3}^{purge}$ is limited to values below 150 $ppm_{wt}$ in all cases for this process configuration, since a purge stream is always required. This effectively limits $\hat{c}_{NH_3}^{FG-WW}$ to values below 0.01 $mol_{NH_3}\ kg_{H_2O}^{-1}$.

**Configuration A3 with the ANA**, which is a slight variation of the NAW. The FG-WW column consists of the same three sections, but the polluted water leaving the bottom of the water-wash section is withdrawn from the column instead of being mixed with the $NH_3$-lean stream entering the $NH_3$ absorber. Instead, the polluted water stream is partly recycled to the top of the column, partly purged from the process to avoid the accumulation of $NH_3$ and $CO_2$ in the liquid flowing through the water-wash section of the ANA. Therefore, a water make-up stream is required at the top of the FG-WW column to maintain the liquid-to-gas flowrate ratio in the water-wash section. While in the case of the NAW polluted water is mixed with the $NH_3$-lean stream thus cleaned in the $NH_3$ desorber, the ANA aims at avoiding the additional steam required by the NAW for water cleaning. Consequently, the amount of $NH_3$ captured from the gas in the water-wash section of the ANA is limited by the maximum $NH_3$ concentration allowed in liquid streams purged from the process, i.e. below 150 $ppm_{wt}$. In practice, the ANA consists of two different sections that operate independently, i.e. a SNA (Configuration A1) followed by a water-wash section, which improves its operability and controllability with respect to the NAW configuration.

As far as the performance assessment of the configuration including the ANA is concerned, a multi-objective optimization of the FG-WW column has been carried out following the same strategy and approach as for the SNA and for the NAW. In this case, seven decision variables have been considered in the optimization problem, as shown in Fig. 2. These are the same decision variables used for the optimization of the configuration with the NAW, except for $(L/G)^{WW}$. While increasing $(L/G)^{WW}$ is penalized in the NAW configuration by a greater reboiler duty in the $NH_3$ desorber, it does not have any direct effect on the specific equivalent work of the ANA configuration. Therefore, including $(L/G)^{WW}$ as decision variable for the optimization of the ANA configuration would lead to values enabling the capture of all gaseous $NH_3$

in the water-wash packing section of the ANA. As a consequence, no energy consumption would be required in the $NH_3$ desorber, at the cost of uncontrolled water make-up requirements. On the contrary, if the flowrate of water make-up is constrained, the process optimization would lead to the maximum allowable $(L/G)^{WW}$ value. Therefore, $(L/G)^{WW}$ has been considered as a parameter instead of as a decision variable in the case of the ANA optimization. This implies that the multi-objective optimization of the process configuration including the ANA has been carried out for different values of $(L/G)^{WW}$, covering the process water consumption typical of amine-based post-combustion $CO_2$ capture processes, i.e. $\approx 500\,kg\,t^{-1}_{CO_2 captured}$ for aqueous MEA applied to the same inlet FG composition considered in this study [39]. As for the process constraints, these are the same defined for the SNA configuration, along with the $NH_3$ concentration limit in the purge stream from the water-wash section of the FG-WW column.

#### 4.1.2. Results and discussion

The reference CAP configuration shown in Fig. 1 was optimized in our previous work considering the energy consumption associated both with the FG-WW column and with the $NH_3$ desorber [14], while the productivity of the $NH_3$ absorber was not considered in the optimization problem. Nevertheless, the volume of the $NH_3$ absorber may be significant in comparison with the size of the $CO_2$ absorber, specially for increasing $NH_3$ concentrations in the solvent circulating between the $CO_2$ absorber and the $CO_2$ desorber, as shown in Table 3. Therefore, here we have carried out the multi-objective optimization of the FG-WW column of the reference CAP configuration following the same approach described in Section 4.1.1 for Configuration A1, since both consist of the SNA, specifying a $y^{FG-WW,out}_{NH_3}$ value of 200 $ppm_v$ instead. The results of such optimization problem are illustrated in Fig. 3, which shows the results in the specific equivalent work-productivity plane, providing a pareto front for each $\hat{c}_{NH_3}$ value; this defines a frontier where the productivity can only be increased at the cost of a higher minimum specific equivalent work. Despite not belonging to the pareto fronts, the performance of the reference configuration operating at the base conditions of the FG-WW column provided in Table 3 are plotted in Fig. 3 for comparison purposes.

Fig. 3(a) shows the optimization results considering only the performance of the FG-WW column and of the $NH_3$ desorber, in the plane $\omega_{FG-WW}$-$Pr_{FG-WW}$: Greater $NH_3$ concentration in the solvent circulating within the $CO_2$ capture section, thus higher $NH_3$ concentration in the $CO_2$-depleted FG entering the $NH_3$ absorber, increases the requirements of the FG post-conditioning section, in terms of both energy consumption and size of the FG-WW column.

The results provided in Fig. 3(b) show that the performance of the FG post-conditioning section (and of the $NH_3$ desorber) has a significant impact on the performance of the full $CO_2$ capture process: While Pr can be increased by more than 50% with respect to the base operating conditions of the FG-WW column, this would be achieved at the cost of increasing $\omega$ up to 10%. Nevertheless, Pr can still be significantly increased with respect to the base operating conditions of the FG-WW column at a low energy cost, regardless of the $\hat{c}_{NH_3}$ level. As far as the comparison among different $\hat{c}_{NH_3}$ cases is concerned, the optimization of the reference configuration of the FG post-conditioning section improved the most its performance for higher $NH_3$ concentration levels in the process with respect to the base set of operating conditions. As a result, while the mid $\hat{c}_{NH_3}$ case performed the best at the base set of operating conditions of the FG-WW column in terms of specific equivalent work and productivity, the high $\hat{c}_{NH_3}$ case with optimized FG-WW column conditions outperformed the rest in terms of Pr, approaching the $Pr_{CO_2 abs}$ value reported in Table 3.

On the contrary, the high $\hat{c}_{NH_3}$ case outperforms the lower $NH_3$ concentration cases in terms of both productivity and specific equivalent work associated with the FG post-conditioning, if referred to the amount of $NH_3$ captured in the FG-WW column, as shown in Fig. 3(c). That implies that the removal of $NH_3$ in the SNA is still efficient when the $NH_3$ concentration in the $CO_2$-depleted FG is as high as 8,000 $ppm_v$ and hence, that $\hat{c}_{NH_3}$ values above 9 $mol_{NH_3}\,kg^{-1}_{H_2O}$ might further increase Pr with an acceptable increase of $\omega$ if the FG-WW column of the reference CAP configuration is optimized as in this work—our previous optimization work showed that increasing $\hat{c}_{NH_3}$ improves the productivity of the $CO_2$ absorber with a small increment of energy demand [14].

In addition, the optimal values for each FG-WW column decision variable along the pareto fronts shown in Fig. 3 are plotted in the *Supplementary Material*. Although the effect of the FG-WW column decision variables on the process performance is subject to complex interdependencies, qualitative trends of the optimal conditions can be inferred:

- Each decision variable shows similar trends when comparing among different $\hat{c}_{NH_3}$ cases.
- Decision variables reach their optimal values within the studied ranges, except for $(L/G)^{FG-WW}$, which stays at the lower bound for lower productivity values; values of $(L/G)^{FG-WW}$ below $0.1\,kg\,kg^{-1}$ have not been considered in order to avoid operational issues at industrial scale associated with liquid maldistribution.
- In general, we can move towards higher productivity values while minimizing the increase in energy requirements by simultaneously decreasing $\hat{c}^{FG-WW}_{NH_3}$, increasing $(L/G)^{FG-WW}$, decreasing $T^{FG-WW}_{lean}$, increasing $(L^{bot}/G)^{FG-WW}$ and decreasing $T^{FG-WW}_{pa}$. These trends increase the capacity of the solvent to absorb $NH_3$ from the FG. On the other hand, the relative height at which the pumparound stream enters the FG-WW column, $h^{FG-WW}_{pa}$, reaches a maximum and then decreases for increasing Pr values.
- However, the former trends suffer from discontinuities at intermediate Pr values, which stem from the change of operation regime of the FG-WW column. As mentioned above, higher Pr values can only be achieved by decreasing the pumparound and lean stream temperatures and by increasing the liquid-to-gas flowrate ratio along the $NH_3$ absorber, which decreases the temperature of the FG exiting the column. Therefore, a purge stream to avoid water accumulating in the FG-WW column-$NH_3$ desorber loop is required at high Pr values, which constraints the $NH_3$ concentration in the $NH_3$-lean stream entering the top of the SNA. On the contrary, no purge stream to control the water balance is required at low Pr values, which allows for the selection of the optimal $\hat{c}^{FG-WW}_{NH_3}$ value; as soon as the constraint on the $NH_3$ concentration of the $NH_3$-lean stream becomes active, a step or discontinuity is noticed in the trends of the optimal values of the remaining decision variables.

As far as the advanced configurations of the FG-WW column without acid washing are concerned, Fig. 4 shows the performance of the SNA, of the NAW and of the ANA, resulting from the multi-objective optimizations described in Section 4.1.1. The performance of the ANA is studied as a function of the liquid-to-gas flowrate ratio for the inlet water and inlet gas streams entering the top and the bottom of the FG-WW column, respectively. For comparison purposes, Fig. 4 also shows the performance of the reference configuration. In all cases, the performances of the advanced configurations of the FG-WW column are shown for the high $\hat{c}_{NH_3}$ case, where the higher $NH_3$ concentration in the FG entering the FG post-conditioning section makes the differences among configurations more noticeable.

Fig. 4(a) shows the resulting pareto fronts in the specific equivalent work-productivity plane, associated with the energetic consumers of the FG-WW column and the $NH_3$ desorber, and with the FG-WW column, respectively, for each configuration of the FG post-conditioning section. For a given specific equivalent work value associated with the FG-WW column and the $NH_3$ desorber, higher FG-WW column productivity values can be achieved if moving from the NAW, to the SNA and, eventually, to the ANA configuration. For the latter,

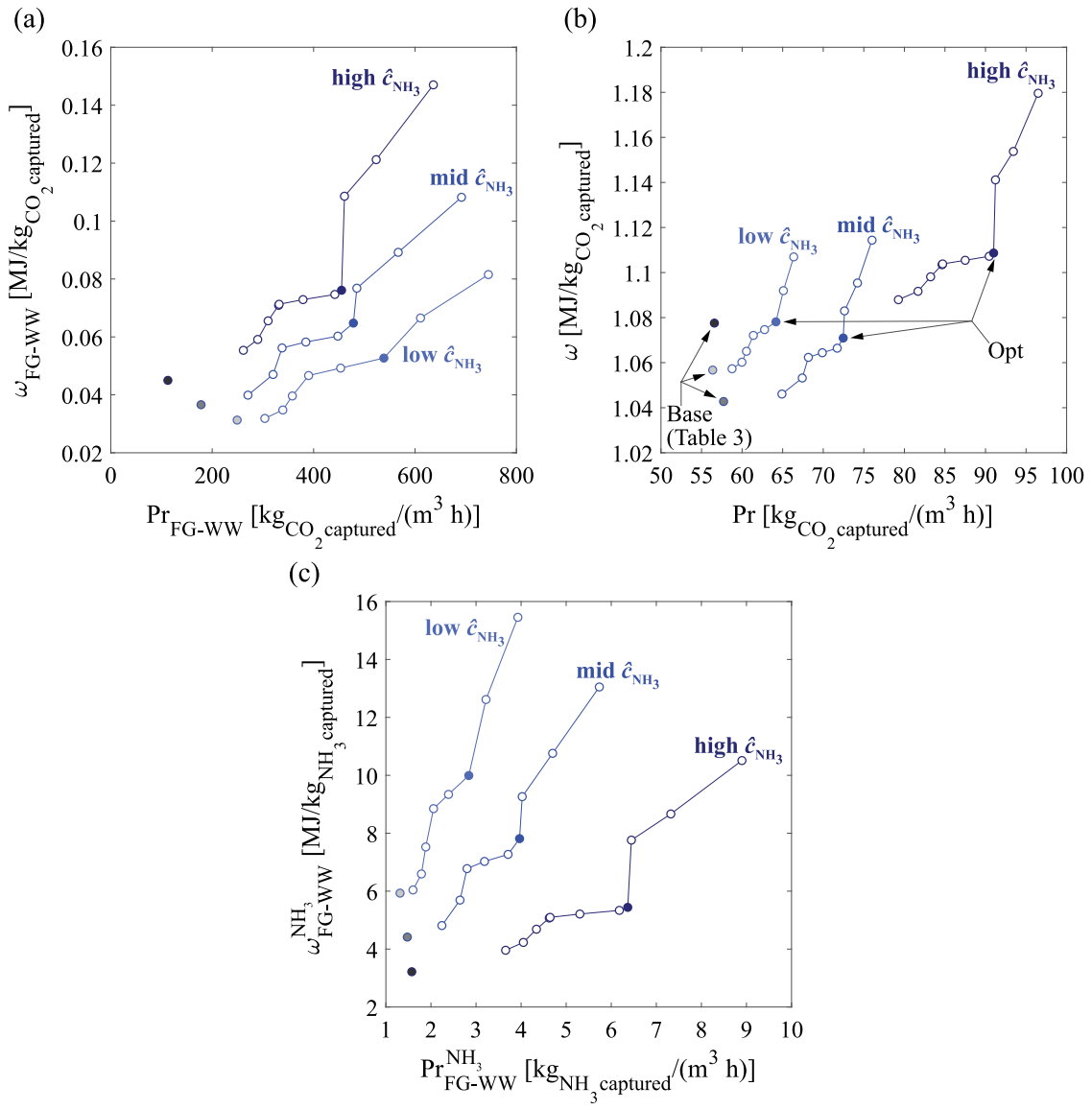


**Fig. 3.** Resulting pareto fronts of the optimization of the FG-WW column belonging to the state-of-the-art benchmark configuration for different apparent $NH_3$ concentration values in the solvent circulating in the $CO_2$ absorber-$CO_2$ desorber loop, i.e. low $\hat{c}_{NH_3}$ (light blue), mid $\hat{c}_{NH_3}$ (blue) and high $\hat{c}_{NH_3}$ (dark blue), in the plane: (a) specific equivalent work associated with the FG post-conditioning section and the $NH_3$ desorber vs. productivity of the $NH_3$ absorber; (b) total specific equivalent work vs. total productivity; and, (c) as of (a) but referenced to the $NH_3$ captured in the FG-WW column. The performance at the operating conditions of the FG-WW column provided in Table 3 (hereinafter referred to as "Base" operating conditions for the reference configuration) is shown by means of the circles filled in grey at low productivity values. The optimal performances of the FG-WW column in the state-of-the-art benchmark configuration for each solvent concentration are shown as filled circles. Such optimal performances have been selected qualitatively as the last pareto point where the process productivity is still significantly increased with a minor increase of the specific energy consumption. (For interpretation of the references to colour in this figure caption, the reader is referred to the web version of this article.)

greater $(L/G)^{WW}$ allows for increases in $Pr_{FG-WW}$ at the same minimum energy demand, as expected. In all cases, $Pr_{FG-WW}$ can be increased significantly at the cost of a very small increment of the energy demand for low productivity values. For increasing $Pr_{FG-WW}$ values, a step in the pareto front is found in all cases, from where steeper increases of $\omega_{FG-WW}$ are obtained for increasing $Pr_{FG-WW}$. In addition, the NAW requires significantly greater energy demand than the other advanced configurations for low productivity values, as a result of the greater liquid flowrate entering the $NH_3$ desorber, which requires greater reboiler duty for the regeneration of the $NH_3$-lean stream. While the optimal $L/G^{WW}$ value that minimizes the energy requirements of the configuration with the NAW for given FG-WW column productivity is always at its lower boundary, i.e. $0.1\,kg\,kg^{-1}$, $L/G^{WW}$ is parametrized for the ANA configuration, as explained in Section 4.1.1, between 0.1 and $0.2\,kg\,kg^{-1}$. The shape of the pareto fronts shown in Fig. 4(a) is similar, for each configuration, to the shape of the curves plotted in Fig. 4(b), where the specific reboiler duty of the $NH_3$ desorber for the pareto points of Fig. 4(a) is represented as a function of $Pr_{FG-WW}$. In fact, the specific equivalent work associated with the steam required in the reboiler of the $NH_3$ desorber contributes in all cases more than 75% to the specific equivalent work associated with the control of $NH_3$ emissions in the $CO_2$-depleted FG, while the other main energetic demand stems from the refrigeration requirements for the chilling of the pumparound stream and of the $NH_3$-lean stream entering the FG-WW column.

Although the reference configuration outperforms the advanced configurations in terms of energy demand and productivity, the size of the acid-wash column has not been considered in the productivity computation. Furthermore, the reference configuration not only requires the consumption of aqueous $H_2SO_4$, but also demands greater flowrate of fresh aqueous $NH_3$ as make-up to replace the greater amount of $NH_3$ exiting the FG-WW column, as shown in Fig. 4(c), which provides the

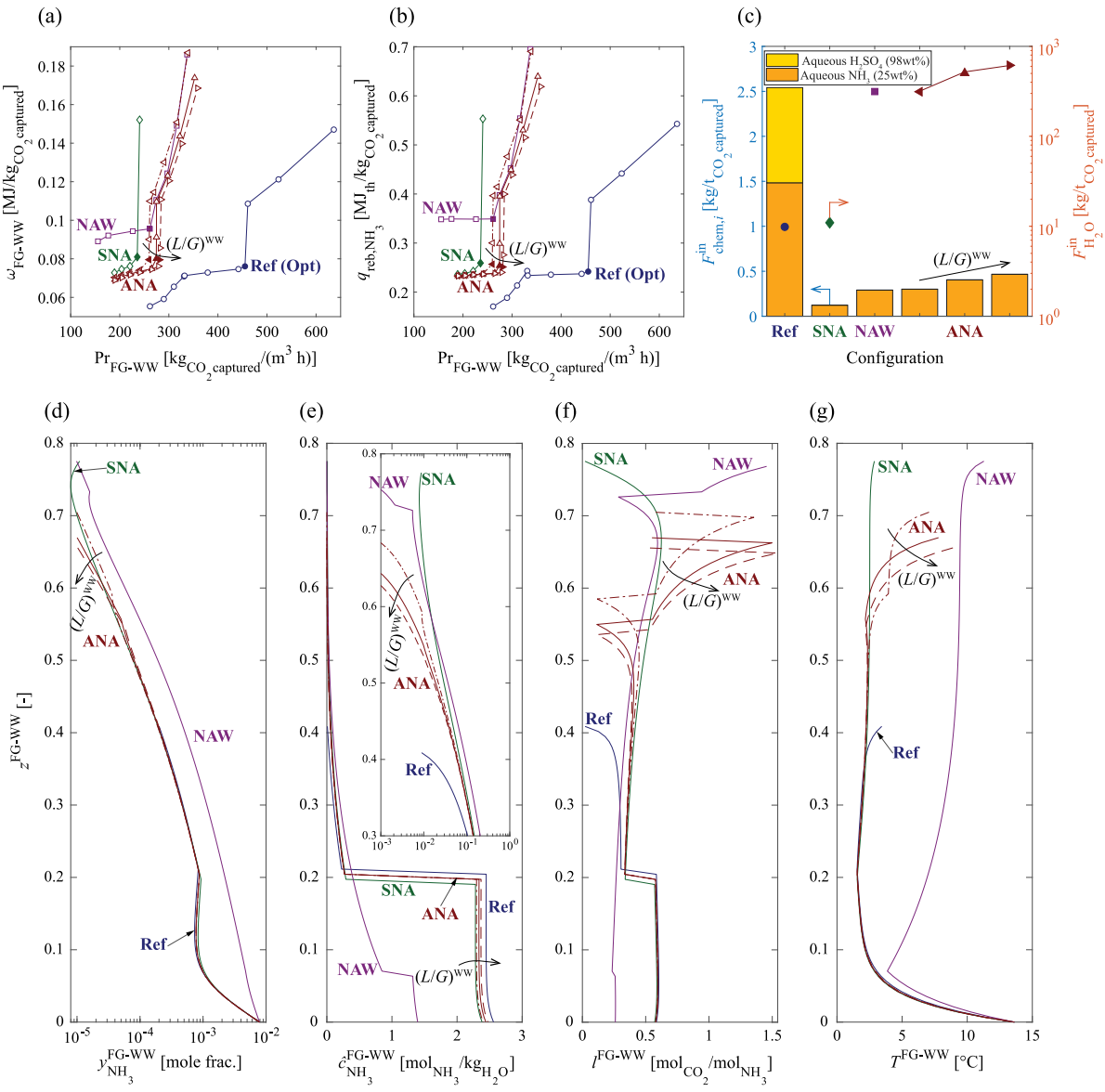


**Fig. 4.** (a) Pareto fronts resulting from the optimization of the advanced configurations of the FG post-conditioning section in the plane specific equivalent work of the FG-WW column plus $NH_3$ desorber-productivity of the FG-WW column, for the reference configuration (○) and for the advanced configurations using the SNA (◇), the NAW (□) and the ANA with $(L/G)^{WW} = 0.100\,kg\,kg^{-1}$ (◁), $(L/G)^{WW} = 0.163\,kg\,kg^{-1}$ (△) and $(L/G)^{WW} = 0.200\,kg\,kg^{-1}$ (▷), considering the composition of the $CO_2$-depleted FG resulting from the high $\hat{c}_{NH_3}$ case (see Table 3); (b) associated values of the reboiler duty of the $NH_3$ desorber that minimizes the specific equivalent work of the FG-WW column plus $NH_3$ desorber as a function of the FG-WW column productivity; (c) consumption of chemicals and water demand associated with each configuration corresponding to the filled points in (a) (and (b)); and profiles along the FG-WW column, i.e. (d) $NH_3$ concentration in the vapour phase, (e) apparent $NH_3$ concentration in the liquid phase, (f) apparent $CO_2$ loading in the liquid phase, and (g) temperature, representative of each configuration corresponding to the filled points in (a) (and (b)), as a function of the relative height of the FG-WW column with respect to the height of the $CO_2$ absorber in the high $\hat{c}_{NH_3}$ case reported in Table 3. (For interpretation of the references to colour in this figure caption and legend, the reader is referred to the web version of this article.)

consumption of chemical solutions and process water corresponding to the filled points plotted in Fig. 4(a) (and (b)). On the contrary, the advanced configuration of the FG post-conditioning section using the SNA requires the lowest $NH_3$ make-up flowrate. Slightly higher $NH_3$ make-up flowrates are needed for the NAW and for the ANA configurations, since part of the $NH_3$ captured from the FG leaves the FG-WW column within the water purged. As far as the consumption of process water is concerned, the reference configuration and the advanced configuration of the FG post-conditioning section using the SNA require similar flowrates, while the water needs for the NAW and for the ANA configurations depend on the $L/G^{WW}$ value; the greater the water flowrate is, the more $NH_3$ that leaves within the stream purged. Consequently, increasing $L/G^{WW}$ values lead to greater consumption of fresh aqueous $NH_3$ solution for the ANA configuration, although the ratio fresh aqueous $NH_3$ solution flowrate-to-fresh water flowrate decreases for increasing $L/G^{WW}$ within the range of values studied.

The operation and $NH_3$ capture process in each FG-WW column configuration can be understood by analysing Figs. 4(d)–(g), where the profiles along the FG-WW column are shown for the conditions corresponding to the filled points plotted in Fig. 4(a) (and (b)). The FG-WW column profiles belonging to the reference configuration are also included. The vertical axis shows the relative height of the packing in the FG-WW column with respect to the height of the packing in the $CO_2$ absorber, setting the origin at the bottom. The height of the FG-WW columns belonging to the advanced configurations of the FG post-conditioning section require around 70% of the height of the $CO_2$ absorber packing for the high $\hat{c}_{NH_3}$ case; lower $NH_3$ concentration levels in the $CO_2$ capture solvent will require lower relative heights for the FG-WW column, since taller $CO_2$ absorbers are required (see $Pr_{CO_2abs}$

values in Table 3) and shorter FG-WW columns are needed. The FG-WW column of the reference configuration only requires a packing height which is approximately 40% of the height of the $CO_2$ absorber for the optimal operating conditions of the high $\hat{c}_{NH_3}$ case, but that does not include the additional acid-wash section required. As previously introduced in Section 4.1.1, the bulk amount of $NH_3$ contained in the inlet $CO_2$-depleted FG is captured in the bottom section of the $NH_3$ absorber, where the $NH_3$ concentration in the gas is decreased to around 1,000 $ppm_v$, as it is shown in Fig. 4(d). Despite the greater apparent $NH_3$ concentration in the liquid circulating through the bottom section of the $NH_3$ absorber, as shown in Fig. 4(e), the decrease in the equilibrium partial pressure of $NH_3$ of the liquid required to capture $NH_3$ from the gas is achieved by means of a liquid with higher $CO_2$ loading, i.e. above 0.5 $mol_{CO_2}\ mol_{NH_3}^{-1}$, that decreases the temperature of the gas, as shown in Figs. 4(f) and (g), respectively. Then, $NH_3$ is further removed from the gas in the upper section of the $NH_3$ absorber due to the low apparent $NH_3$ concentration in the liquid flowing in counter-current, as shown in Fig. 4(e); while the SNA only uses a very diluted $NH_3$-lean solution to reach the $NH_3$ concentration limit in the outlet gas stream, the NAW and the ANA uses an additional water-wash section on the top of the $NH_3$ absorber to decrease the $NH_3$ concentration in the FG from a few tens of $ppm_v$ to 10 $ppm_v$. The water and the $NH_3$-lean solution not only capture $NH_3$ from the FG, but also $CO_2$, thereby increasing the $CO_2$ loading of the liquid, as shown in Fig. 4(f), thus enhancing the $NH_3$ transfer from the vapour to the liquid stream. In general, the profiles shown in Figs. 4(d)–(g) are very similar for the reference configuration with the SNA, and for the advanced configurations of the FG post-conditioning section using the SNA or the ANA, but differ for the NAW, where most of the $NH_3$ is removed from the gas stream in the intermediate section of the FG-WW column—top section of the $NH_3$ absorber—i.e. between the $NH_3$-lean stream inlet and the pumparound stream inlet.

In summary, according to the results shown in Figs. 4(a) and (c), the advanced configuration of the FG post-conditioning section using the SNA as FG-WW column is able to decrease significantly the requirements of fresh aqueous $NH_3$ solution with respect to the reference configuration, and to avoid the consumption of aqueous $H_2SO_4$ solution, while maintaining the water demand; if the same equivalent work is aimed with both configurations, the advanced configuration of the FG post-conditioning section using the SNA reaches FG-WW column productivities which are approximately 50% of those of the reference configuration. Further productivity increments for the advanced configurations of the FG post-conditioning section can be obtained by means of the ANA, FG-WW column configuration that outperforms the NAW in terms of specific energy consumption. Such productivity increment is mainly obtained at the cost of greater process water demand, reaching consumptions when $(L/G)^{WW} = 0.163\ kg\ kg^{-1}$ similar to what is expected in amine-based capture processes [39]. Therefore, the results obtained for the optimization of the advanced FG post-conditioning section using the SNA, and the ANA (with $(L/G)^{WW} = 0.163\ kg\ kg^{-1}$), are illustrateds in Fig. 5 in the total specific equivalent work-total productivity plane.

Fig. 5 provides a pareto front for each $\hat{c}_{NH_3}$ case and advanced configuration of the FG-WW column. As for the reference configuration, the mid $\hat{c}_{NH_3}$ case outperforms the low and the high $\hat{c}_{NH_3}$ cases both for the SNA and for the ANA, while the high $\hat{c}_{NH_3}$ case outperforms the lower $\hat{c}_{NH_3}$ cases in terms of total productivity achievable for both advanced configurations. In addition, the ANA outperforms the SNA in terms of energy consumption and productivity, for each $NH_3$ concentration level studied in this work. The results shown in Fig. 5 also illustrate that the performance of the FG post-conditioning section and of the $NH_3$ desorber has a significant impact on the performance of the full $CO_2$ capture process, similar to what was obtained for the reference configuration (see Fig. 3(b)).

In all pareto sets shown in Fig. 5, the productivity can be improved without increasing significantly the minimum specific equivalent work,

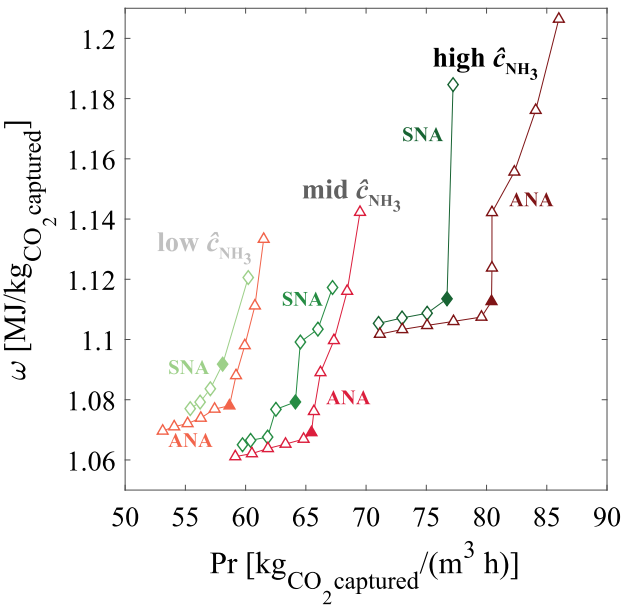


**Fig. 5.** Resulting pareto fronts of the optimization of the advanced configurations of the FG post-conditioning section using the SNA (◇), and the ANA with $(L/G)^{WW} = 0.163\ kg\ kg^{-1}$ (△), for different $NH_3$ concentration values in the solvent circulating in the $CO_2$ absorber-$CO_2$ desorber loop, i.e. low $\hat{c}_{NH_3}$, mid $\hat{c}_{NH_3}$ and high $\hat{c}_{NH_3}$ from light to dark colour, in the plane total specific equivalent work vs. total productivity. Filled circles indicate the sets of operating conditions—one per configuration and per $\hat{c}_{NH_3}$ case—with the best qualitative trade-off between energy consumption and productivity. (For interpretation of the references to colour in this figure caption, the reader is referred to the web version of this article.)

at low productivity values, while for high productivities, moving to the right along the pareto fronts would require in all cases considerable increments of the minimum energy demand. The optimum values for each FG-WW column decision variable to move along each pareto front shown in Fig. 5 are provided in the *Supplementary Material*. Although the effect of the FG-WW column decision variables on the process performance are subject to complex interdependencies among them, qualitative trends of the optimal conditions can be inferred:

- Each decision variable shows similar trends when comparing among different $\hat{c}_{NH_3}$ cases for the same configuration of the FG-WW column.
- The optimal design of the SNA and of the ANA configurations requires in all cases that a split of the $NH_3$-lean stream is purged from the FG-WW column-$NH_3$ desorber loop to avoid water accumulation. Therefore, the concentration of apparent $NH_3$ in the $NH_3$-lean stream is limited in all cases to a maximum value of 0.0088 $mol_{NH_3}\ kg_{H_2O}^{-1}$ (equivalent to 150 $ppm_{wt}$).
- The optimal performance of the FG-WW column either with the SNA or with the ANA is highly influenced by the optimal $(L/G)^{FG-WW}$ value. The optimal $(L/G)^{FG-WW}$ value stays at its lower boundary for lower productivity values, where the productivity is increased by varying the remaining FG-WW column decision variables at the cost of a small increase in the minimum specific energy demand. At higher productivity though, increasing Pr values are achieved by increasing the $(L/G)^{FG-WW}$, which leads to significant increments of the minimum specific equivalent work.
- In general, we can move towards higher productivity values while minimizing the increase in energy requirements by additionally and simultaneously: (i) decreasing $\hat{c}_{NH_3}^{FG-WW}$, only for the SNA configuration, (ii) decreasing $T_{lean}^{FG-WW}$, (iii) decreasing the relative height at which the $NH_3$-lean stream enters the ANA, which does not apply to the SNA, (iv) increasing $(L^{bot}/G)^{FG-WW}$, and

(v) decreasing $T_{pa}^{FG-WW}$. On the other hand, the relative height at which the pumparound stream enters the FG-WW column, $h_{pa}^{FG-WW}$, reaches a maximum and then decreases for increasing Pr values.

- Discontinuities and/or change of slope in the former trends of the optimal FG-WW column decision variables appear when the optimal value of the $(L/G)^{FG-WW}$ goes above the lower boundary, i.e. it is greater than 0.1 kg kg$^{-1}$.

The dimensions of the FG-WW column at optimal operating conditions for the most performing configurations of the FG post-conditioning section are provided in Table 5. The optimal set of operating conditions for each case have been selected from the qualitative assessment of the results shown in Figs. 3 and 5, aiming at the pareto point where the slope in the $\omega$ vs. Pr plots increases drastically, i.e. with the best qualitative trade-off between energy consumption and productivity. Such points have been filled in the plots of Figs. 3 and 5.

The results given in Table 5 for the height of the FG-WW column, $H_{FG-WW}$, of the reference configuration show that operating the FG-WW column at optimal operating conditions is of paramount importance for the proper assessment of a certain process configuration. Such optimization is more critical the higher the $NH_3$ slip in the $CO_2$ absorber is, i.e. at higher $NH_3$ concentrations in the solvent. In fact, the height of the FG-WW column in the FG post-conditioning section of the reference configuration decreases from 15.1 m at the base set of operating conditions to 5.0 m at the optimal set of operating conditions for the low $\hat{c}_{NH_3}$ case and from 32.4 to 5.8 m for the high $\hat{c}_{NH_3}$ case, at the cost of a very small increase of the minimum energy requirements of the process, as it can be seen in Fig. 3. Greater packing heights are required for the FG-WW column when using the SNA or the ANA, although the difference in packing requirements of the FG post-conditioning section with respect to the reference configuration decreases if the additional acid-wash packed column needed in the latter is considered. Additionally, the optimization of the process operating conditions allows for very competitive packing heights in the FG-WW column independently of the concentration of apparent $NH_3$ in the solvent used for $CO_2$ capture. In all cases, the most promising configurations of the FG-WW column operating at optimal conditions require smaller packing heights than those required in the $CO_2$ absorber, which are also reported in Table 5 for comparison purposes and that correspond to the $CO_2$ absorber operating conditions reported in Table 3.

When compared to the performance of other configurations of the FG post-conditioning section of $NH_3$-based $CO_2$ capture processes reported in the literature, the advanced configurations developed in this study perform very competitively. Jilvero et al. [16] proposes as most performing configuration a 15 m high FG-WW column that allows to decrease the $NH_3$ concentration in the FG before the stack to values around 10 ppm thus avoiding the use of an acid-wash column downstream; the worse performance when compared to our advanced configuration using the SNA stems from the fact that Jilvero et al. [16] designed their FG-WW column only considering the top section of our SNA, without pumparound stream and bottom section. Jiang et al. [21] proposed a packing of 6.4 m high for the water-wash column followed by a 3.25 m high packing for the acid-wash column as part of their most performing process configuration, which compares with the packing heights required for the FG-WW columns of the advanced configurations of the FG post-conditioning section developed in this study. Nevertheless, while the configuration of Jiang et al. [21] requires more than 0.3 $MJ_{th}\,kg^{-1}_{CO_2captured}$ for the regeneration of the $NH_3$-lean stream, the thermal energy requirements of our designs at optimal operating conditions of the FG-WW column range between 0.1 and 0.25 $MJ_{th}\,kg^{-1}_{CO_2captured}$, depending on the $NH_3$ concentration in the $CO_2$ capture solvent thus on the $NH_3$ slip in the $CO_2$ absorber. Furthermore, such designs and performances of the FG-WW column are associated with a packing height in the $CO_2$ absorber of 20 m and 24.4 m for the optimal configurations of Jilvero et al. [16] and of Jiang et al. [21], respectively, using structured packings with 250 $m^2\,m^{-3}$ of specific surface area. On the contrary, our process configurations lead to packing heights in the $CO_2$ absorber ranging between 14 and 22 m using a packing with 20% lower specific surface area, i.e. 207 $m^2\,m^{-3}$.

In addition, it is worth noting that Jiang et al. [21] simulated a simplified CAP as reference process for their study that required a packing more than 25 m high for the FG-WW column in order to decrease the $NH_3$ concentration in the FG exiting the $CO_2$ absorber from 29,000 to less than 1 $ppm_v$, and 1.4 $MJ_{th}\,kg^{-1}_{CO_2captured}$ for the regeneration of the $NH_3$-lean stream. This is a clear example of results obtained using a process configuration and operating conditions far from optimality, which lead to misleading performance assessments.

### 4.2. Advanced configurations to simplify the PFD

#### 4.2.1. Process description and optimization strategy

Advanced configurations that simplify the PFD with respect to the reference CAP configuration aim at reducing the investment costs associated with $NH_3$-based capture processes. This objective is pursued by decreasing the number of units of the capture process without affecting negatively its energetic performance and the fulfilment of the process specifications and constraints. Therefore, the different process sections and unit operations of the reference CAP configuration shown in Fig. 1 have been analysed in terms of goals, operating conditions and feed streams in order to identify pieces of equipment that: (i) either can be integrated within another unit operation, or (ii) can be removed from the capture process; in addition, both cases might require the adaptation of the boundary conditions and/or the redefinition of the constraints of certain process sections. As a result, advanced configurations of the reference CAP that do not include the $CO_2$-WW section or the appendix stripper, or that integrate the appendix stripper with the $NH_3$ desorber have been identified. Further details for each of them are provided below.

**Configuration B1 without the $CO_2$-WW column**, where the $CO_2$ stream that leaves the top of the $CO_2$ desorber is directly cooled down before being sent to compression; the condensate stream produced in the cooler of process section B is sent to the solvent recovery section as in the reference configuration shown in Fig. 1. Consequently, the operating conditions of the $CO_2$ desorber need to be adapted in order to still meet the constraints downstream in the process, i.e. $y_{NH_3}^{CO_2comp,in}$ below 50 $ppm_v$ and no solid formation in the condensate of the $CO_2$ stream before the $CO_2$ compression section, which will affect the specific reboiler duty of the $CO_2$ desorber thus the energetic performance of the capture process [14]. Therefore, the configuration without the $CO_2$-WW column is assessed by means of multi-variable sensitivity analyses whereby the influence of the $CO_2$ desorber decision variables on the process performance is studied. As a result, the optimal set of operating conditions of the $CO_2$ desorber, i.e. $P_{CO_2des}$ and $f_{cr}$, that minimize $\omega$ while meeting the process specifications and constraints provided in Table 2 are obtained for each $\hat{c}_{NH_3}$ case.

**Configuration C1 without the appendix stripper**, whose PFD is shown in Fig. 6. In addition to the removal of the appendix stripper, Configuration C1 includes an additional packing section at the top of the column in the FG pre-conditioning section that further cools down the FG to values below ambient temperature, referred to as Direct Contact Chiller (DCCh) hereinafter. The DCCh uses chilled water for cooling purposes, which can reach values as low as 1.5 °C, instead of cooling water at 21.2 °C. The purpose of the DCCh is to reach temperatures of the FG entering the $CO_2$ absorber as low as those of the $CO_2$- and $NH_3$-depleted FG exiting the FG-WW column in order to minimize water accumulating in the solvent circulating between the $CO_2$ absorber and the $CO_2$ desorber. As a consequence, the purge of solvent from the $CO_2$ absorber-$CO_2$ desorber loop is avoided, which is the source of most of the $NH_3$ and $CO_2$ recuperated in the appendix stripper. Therefore, the appendix stripper is removed and other inlet

**Table 5**
Dimensions of the FG-WW column, i.e. packing height and diameter, corresponding to the most promising configurations of the FG post-conditioning section for the FG conditions provided in Table 1. The optimal sets of operating conditions for each configuration of the FG post-conditioning section have been selected by means of the qualitative assessment of the results obtained in the plane $\omega$ vs. Pr and that have been shown as filled markers in Figs. 3 and 5. The dimensions of the FG-WW column corresponding to the reference configuration at the base sets of operating conditions of the FG-WW column provided in Table 3 have also been introduced for comparison purposes. Also for comparison purposes, we provide the dimensions of the $CO_2$ absorber corresponding to the three different sets of operating conditions of the $CO_2$ absorber section indicated in Table 3. A random packing of 25-mm Pall rings with a specific surface area of 207 $m^2\,m^{-3}$, as specified in Section 3, has been considered in both the $CO_2$ absorber and the FG-WW column. For a fair comparison, an additional packing section should be considered for the acid wash column of the reference FG post-conditioning section; Jiang et al. [21] have reported an acid-wash column with a packing height of 3.25 m to decrease the $NH_3$ concentration in the $CO_2$-depleted FG from 1000 to <1 $ppm_v$ so that a shorter packing is expected to be required in the acid-wash column of the reference FG post-conditioning section of this study, where the $NH_3$ concentration in the FG is decreased from 200 to <10 $ppm_v$.

| Variable | Units | Configuration of the FG post-conditioning section and $\hat{c}_{NH_3}$ case | | | | | | | | | | | |
|---|---|---|---|---|---|---|---|---|---|---|---|---|---|
| | | Ref | | | | | | A1 (SNA) | | | A3 (ANA) | | |
| | | Base | | | Opt | | | Opt | | | Opt | | |
| | | low | mid | high | low | mid | high | low | mid | high | low | mid | high |
| $H_{FG-WW}$ | [m] | 15.1 | 20.9 | 32.4 | 5.0 | 5.5 | 5.8 | 9.0 | 10.0 | 11.0 | 9.0 | 9.5 | 9.5 |
| $D_{FG-WW}$ | [m] | 5.6 | 5.6 | 5.7 | 6.6 | 6.7 | 6.7 | 6.7 | 6.7 | 6.7 | 6.6 | 6.6 | 6.7 |
| $H_{CO_2abs}$ | [m] | 22.3 | 19.4 | 14.2 | 22.3 | 19.4 | 14.2 | 22.3 | 19.4 | 14.2 | 22.3 | 19.4 | 14.2 |
| $D_{CO_2abs}$ | [m] | 8.5 | 8.4 | 8.5 | 8.5 | 8.4 | 8.5 | 8.5 | 8.4 | 8.5 | 8.5 | 8.4 | 8.5 |

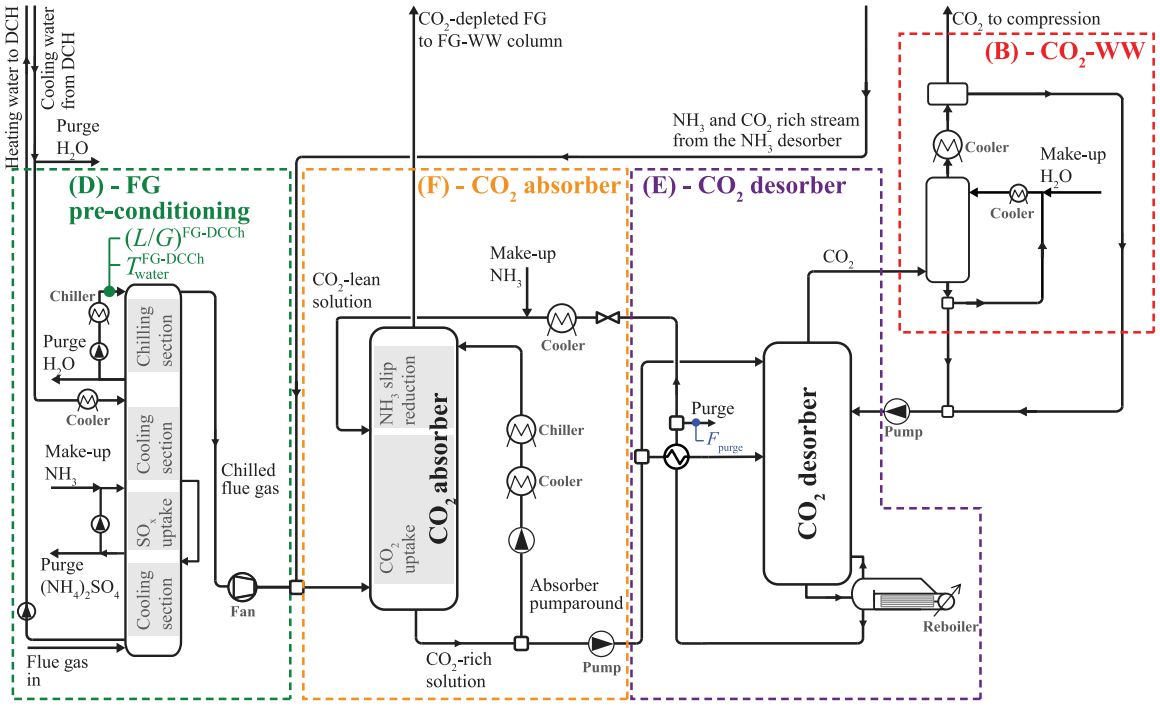


**Fig. 6.** Flow diagram of Configuration C1 without the appendix stripper and including the DCCh at the top of the DCC in the FG pre-conditioning section for the chilling of the FG before entering the $CO_2$ absorber. The remaining process sections, i.e. (A) the FG post-conditioning section, (C) the solvent recovery section with the $NH_3$ desorber, and (G) the $CO_2$ compression section, are omitted for the sake of visuality but are those included in the reference CAP configuration shown in Fig. 1. The variables that govern the performance of the configuration, i.e. the process parameters that are varied in the sensitivity analysis, and the process constraints have been colour-coded in green and blue, respectively. (For interpretation of the references to colour in this figure caption, the reader is referred to the web version of this article.)

streams with minor content of $NH_3$ (and $CO_2$), i.e. the purge stream from the $CO_2$-WW column and the condensate of the $CO_2$ stream before compression, are fed to the $CO_2$ desorber instead. Since the flowrates of the latter streams are two and three orders of magnitude smaller than the flowrate of the cold-rich bypass, respectively, their feed stage to the $CO_2$ desorber has a minor/negligible effect on both the energy consumption of the process and the control of $NH_3$ emissions within the $CO_2$ stream; in order to minimize the number of packing sections in the $CO_2$ desorber and considering their temperature, we have chosen to feed both streams together with the hot $CO_2$-rich stream. The temperature of the FG entering the $CO_2$ absorber can be controlled by means of the liquid-to-gas flowrate ratio for the chilling water and the inlet FG to the capture process, $(L/G)^{FG-DCCh}$ [$kg\,kg^{-1}$], in combination with the temperature of the water entering the DCCh, $T_{water}^{FG-DCCh}$ [°C]. Increasing values of $(L/G)^{FG-DCCh}$ make the temperature of the FG entering the $CO_2$ absorber to approach asymptotically $T_{water}^{FG-DCCh}$. Therefore, we have set the value of $(L/G)^{FG-DCCh}$ to 2.0 $kg\,kg^{-1}$ so that further increments do not have any effect on the FG temperature. Subsequently, $T_{water}^{FG-DCCh}$ is set to the maximum value that avoids the accumulation of water in the solvent circulating between the $CO_2$ absorber and the $CO_2$ desorber, thus leading to a flowrate of purged solvent, $F_{purge}$ [$kg\,t^{-1}_{CO_2,captured}$], that is equal to zero. As for the chilling considered in the FG-WW column, the minimum temperature achievable has been set to 1.5 °C. Then, the performance of the configuration without appendix stripper is assessed by analysing the impact on the energy needs of the process and on the consumption of aqueous $NH_3$ solution.

**Configuration C2 with the IS**, whose PFD is shown in Fig. 7, integrates the $NH_3$ desorber and the appendix stripper in one single column. Such integration is possible as long as the $NH_3$ desorber and the appendix stripper have the same specifications, i.e. both columns produce: (i) a gaseous distillate at the top of the column that recovers

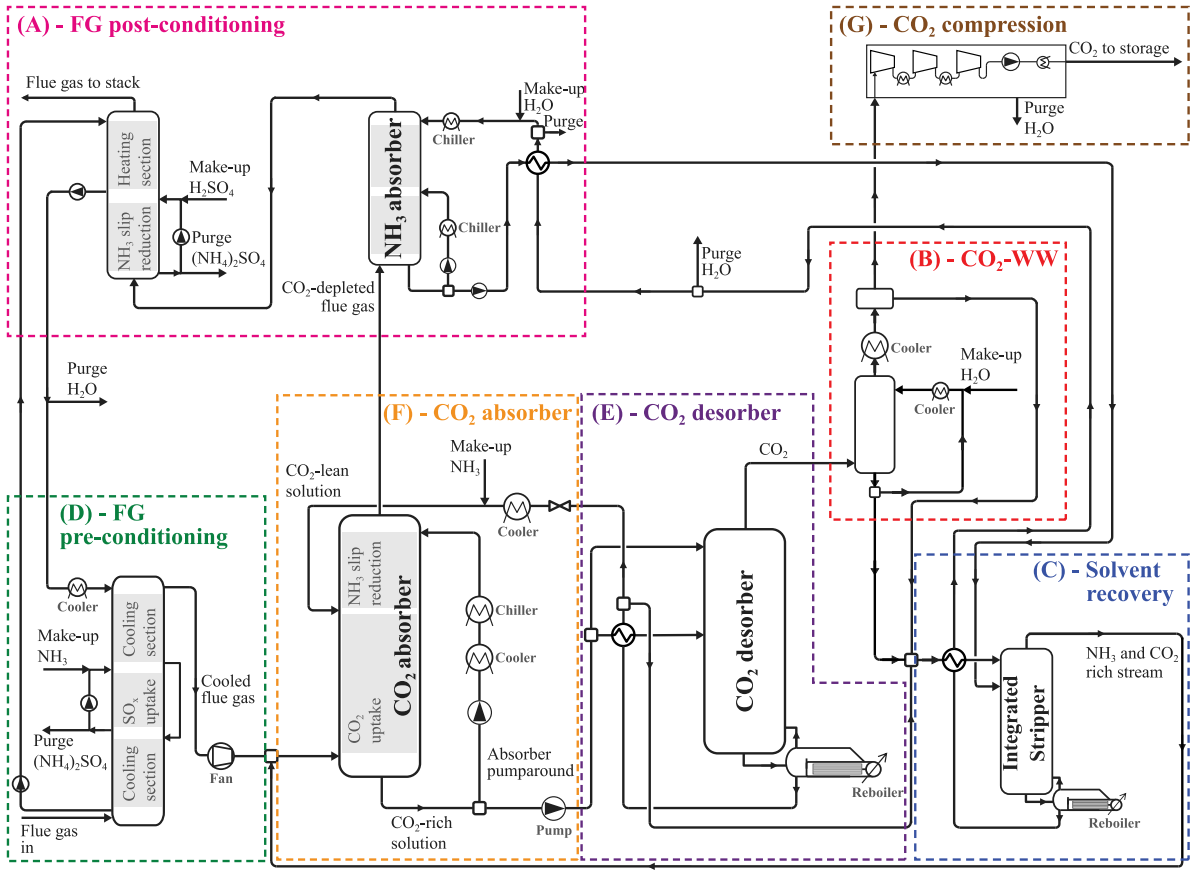


**Fig. 7.** PFD of Configuration C2 with the IS. Notice that the $NH_3$ desorber and the appendix stripper of the solvent recovery sections have been integrated in one single column, i.e. the IS. The implementation of the IS is shown in combination with the FG post-conditioning section of the reference configuration. However, the block of the latter can be exchanged for any of the advanced configurations of the FG post-conditioning section shown in Fig. 2.

most of the $NH_3$ and (almost all the) $CO_2$ contained in the column's feed stream, and (ii) an almost pure water liquid stream at the bottom of the column. While the former is always fulfilled, the latter feature is common to both columns if the apparent $NH_3$ concentration in the $NH_3$-lean stream is up to 150 $ppm_{wt}$ (equivalent to 0.0088 $mol_{NH_3}\ kg_{H_2O}^{-1}$). Although the suitability of the IS depends on the operating conditions of the FG-WW column, it is independent of the configuration of the FG-WW column and the FG post-conditioning section. Therefore, the FG post-conditioning section of the reference configuration considered in the full PFD shown in Fig. 7 can be exchanged for any of the advanced configurations of the FG post-conditioning section described in Section 4.1.1. On the one hand, the high-pressure stream resulting from the mixing of the solvent purged from the $CO_2$ absorber-$CO_2$ desorber loop, the water stream purged from the $CO_2$-WW section and the condensate of the $CO_2$ gas stream are fed to the top of the IS after exchanging heat with the bottom stream of the column, as for the appendix stripper. On the other hand, the $NH_3$-rich stream enters the IS at the top half of the column, as in the case of the $NH_3$ desorber. The process improvement introduced by the IS is based not only on the decrease of the investment costs due to the elimination of one piece of equipment with respect to the reference configuration, but also on a competitive energy performance. The latter is highly affected by the heat integration implemented upstream. The high-pressure stream fed to the top of the column flashes when entering the IS, which by default operates at atmospheric pressure, thus cooling down the top of the column and serving the purpose of the condenser of the $NH_3$ desorber. The heat of the bottom stream, which leaves the IS approximately at 100 °C (almost pure water at atmospheric pressure), is used to heat up the high-pressure stream fed to the top of the IS. The pinch point temperature in the counter-current heat exchanger is reached between the inlet hot stream (bottom stream of the IS) and the outlet cold stream (high-pressure stream fed to the top of the IS): The high pressure of the latter stream, whose flowrate is considerably lower than that of the IS bottom stream, prevents its vaporization within the heat exchanger. Then, the $NH_3$-lean hot outlet stream, still approximately at 90 °C, is able to heat up the $NH_3$-rich stream before entering the top of the FG-WW column. Aiming at minimizing the refrigeration duty associated with the chilling of the $NH_3$-lean stream, a fraction of the hot $NH_3$-lean stream is purged before entering the $NH_3$-rich/$NH_3$-lean heat exchanger. In order to also minimize the reboiler duty of the IS, the value of the aforementioned split fraction is set to equalize the heat capacity of both inlet streams to the $NH_3$-rich/$NH_3$-lean heat exchanger.

The advanced Configuration C2 with the IS is assessed by analysing its impact on the energy requirements of the process and on the consumption of water and aqueous $NH_3$ solution, with respect to the reference configuration with the appendix stripper and the $NH_3$ desorber. As far as the energy consumption associated with the IS is concerned, the column configuration is of paramount importance, i.e. the number of stages and the feed stages. On the one hand, increasing number of equilibrium stages decreases the reboiler duty of the IS towards an asymptotic minimum value. On the other hand, while the reboiler duty of the IS is always minimized when the high-pressure stream is fed to the top of the column, as mentioned above, the optimal feed stage of the $NH_3$-rich stream depends on the total number of equilibrium stages. Aiming at providing a fair assessment of the IS with respect to the reference configuration, the same number of equilibrium stages as for the $NH_3$ desorber of the reference configuration, i.e. nine including the condenser and the reboiler of the column, has been selected. Furthermore, no significant energetic improvements are found

**Table 6**
Operating conditions of the FG-WW column selected for the assessment of the IS in combination with different configurations of the FG post-conditioning section. The set of operating conditions selected for each configuration of the FG post-conditioning section corresponds to the pareto points labelled as "Opt" in Figs. 3 and 5 (see Section 4.1.2). A new "Base" set of operating conditions of the FG-WW column of the reference FG post-conditioning section has been determined for its combination with the IS in order to meet the apparent $NH_3$ concentration constraint in the purge stream (see Table 2) while minimizing the energy requirements for the same FG-WW column productivity reported in Table 3 for each $\hat{c}_{NH_3}$ case. As for the remaining process operating conditions, i.e. $CO_2$ absorber parameters and $CO_2$ desorber parameters, the values selected for the assessment of Configuration C2 with the IS are those reported in Table 3 for each $\hat{c}_{NH_3}$ case.

| Variable | Units | Configuration of the FG post-conditioning section and $\hat{c}_{NH_3}$ case | | | | | | | | | | | |
|---|---|---|---|---|---|---|---|---|---|---|---|---|---|
| | | Ref | | | | | | A1 (SNA) | | | A3 (ANA) | | |
| | | Base | | | Opt | | | Opt | | | Opt | | |
| | | low | mid | high | low | mid | high | low | mid | high | low | mid | high |
| $\hat{c}_{NH_3}^{FG-WW} \times 10^3$ | $[mol_{NH_3}\ kg_{H_2O}^{-1}]$ | 8.81 | 8.82 | 8.80 | 8.80 | 8.83 | 8.82 | 5.67 | 7.18 | 8.69 | 8.82 | 8.82 | 8.81 |
| $(L/G)^{FG-WW}$ | $[kg\ kg^{-1}]$ | 0.100 | 0.100 | 0.100 | 0.104 | 0.113 | 0.103 | 0.128 | 0.125 | 0.113 | 0.100 | 0.105 | 0.110 |
| $T_{lean}^{FG-WW}$ | [°C] | 15.7 | 16.6 | 5.7 | 7.6 | 7.9 | 8.1 | 1.6 | 1.5 | 3.9 | 7.6 | 8.1 | 1.5 |
| $h_{lean}^{FG-WW}$ | $[m\ m^{-1}]$ | 1.00 | 1.00 | 1.00 | 1.00 | 1.00 | 1.00 | 1.00 | 1.00 | 1.00 | 0.81 | 0.82 | 0.82 |
| $(L^{bot}/G)^{FG-WW}$ | $[kg\ kg^{-1}]$ | 0.195 | 0.197 | 0.126 | 2.08 | 2.25 | 2.05 | 2.57 | 2.50 | 2.26 | 2.00 | 2.10 | 2.19 |
| $T_{pa}^{FG-WW}$ | [°C] | 12.5 | 13.6 | 1.5 | 1.5 | 1.5 | 1.5 | 1.5 | 1.6 | 1.5 | 1.5 | 1.5 | 1.5 |
| $h_{pa}^{FG-WW}$ | $[m\ m^{-1}]$ | 0.53 | 0.46 | 0.58 | 0.50 | 0.53 | 0.50 | 0.20 | 0.27 | 0.25 | 0.29 | 0.28 | 0.29 |
| $(L/G)^{WW}$ | $[kg\ kg^{-1}]$ | 0 | 0 | 0 | 0 | 0 | 0 | 0 | 0 | 0 | 0.163 | 0.163 | 0.163 |

for a larger number of equilibrium stages. Therefore, the appendix stripper is effectively removed in terms of investment costs with respect to the reference configuration. For such column configuration, the optimal feed stage of the $NH_3$-rich stream to the IS that minimizes its reboiler duty is equilibrium stage 2. Additionally, the energetic performance of the IS is also affected by the operating conditions of the $CO_2$ absorber, of the $CO_2$ desorber and of the FG-WW column. The effect of the $CO_2$ absorber decision variables and of the $CO_2$ desorber decision variables on the reboiler duty of the IS is similar to their effect on the reboiler duty of the appendix stripper for the reference configuration. On the contrary, the value of the FG-WW column parameters might have to be modified with respect to the reference configuration with the $NH_3$ desorber if the apparent $NH_3$ concentration in the $NH_3$-lean stream is above the maximum allowable value, i.e. 150 $ppm_{wt}$ for this work, since a split has to be purged. Therefore, the performance of the IS has been compared with the performance of the configuration that includes both the appendix stripper and the $NH_3$ desorber for different configurations of the FG post-conditioning section. The most promising advanced configurations of the FG post-conditioning section, according to the results shown in Section 4.1.2, have been considered, namely Configuration A1 with the SNA and Configuration A3 with the ANA, as well as the reference configuration of the FG post-conditioning section with the SNA and the acid-wash column included in Fig. 1. The sets of operating conditions of the FG-WW column parameters that are used for the assessment of Configuration C2 with the IS are provided in Table 6 for each configuration of the FG post-conditioning section and $\hat{c}_{NH_3}$ case, i.e. low, mid and high. The same values of the FG-WW column parameters are considered for the corresponding processes using the same advanced configuration of the FG post-conditioning section but with both the appendix stripper and the $NH_3$ desorber. These sets correspond to the optimal operating conditions determined qualitatively from the results shown in Fig. 5 (see Section 4.1.2). As far as the reference configuration of the FG post-conditioning section is concerned, it has been combined with the IS at two different sets of operating conditions of the FG-WW column decision variables: (i) At the optimal operating conditions determined qualitatively from the results shown in Fig. 3 (see Section 4.1.2); and, (ii) at the operating conditions that allow for the minimum specific energy consumption of the process, thus at low FG-WW column productivity values. For the latter, the set of operating conditions of the FG-WW column reported in Table 3 have been used for the reference configuration with the appendix stripper and the $NH_3$ desorber; on the contrary, a new set that minimizes the energy consumption for the same productivity value has been found instead for the advanced configuration with the IS in order to constrain the apparent $NH_3$ concentration of the $NH_3$-lean stream to the maximum allowable content specified in Table 2 for liquid purge streams.

#### 4.2.2. Results and discussion

Advanced configurations falling in this category have been assessed separately. On the one hand, the configuration without the $CO_2$-WW column (Configuration B1) and the configuration without the integrated stripper (Configuration C1) have been compared to the reference configuration shown in Fig. 1 operating at the three different sets of conditions reported in Table 3. On the other hand, the advanced configuration with the IS (Configuration C2) has also been assessed in combination with the most promising advanced configurations and with the reference configuration of the FG post-conditioning section, at the operating conditions of the FG-WW column reported in Table 6.

The results of the multi-variable sensitivity analyses carried out for the assessment of **Configuration B1 without the $CO_2$-WW column** are illustrated in Fig. 8. Fig. 8(a) shows the effect of the $CO_2$ desorber variables on the energetic performance of the reference CAP configuration illustrated in Fig. 1 at the sets of operating conditions reported in Table 3 resulting from our previous process optimization work [14], while Fig. 8(b) does the same for Configuration B1 at the same sets of operating conditions. In addition to the $\omega$ isolines, Fig. 8 also includes the regions of the $CO_2$ desorber decision variables design space that are infeasible as they would not allow to meet the process constraints regarding avoidance of solid formation, maximum $NH_3$ concentration in the $CO_2$ stream entering the $CO_2$ compression section, $y_{NH_3}^{CO_2 comp,in}$, and maximum temperature of the solvent, $T_{reb,CO_2}$ (whose values are reported in Table 2). While $P_{CO_2 des}$ and $f_{cr}$ have the same effect on $\omega$ for the reference configuration [14] and for Configuration B1, the removal of the $CO_2$-WW column hinders the control of the $NH_3$ concentration in the $CO_2$ stream, thus it shrinks the feasible range of operating conditions in the $CO_2$ desorber, the more the higher the concentration of apparent $NH_3$ in the solvent is. On the one hand, the minimum $f_{cr}$ value that avoids solid formation in the condensate of the $CO_2$ stream before the $CO_2$ compression section increases with respect to the reference configuration for the same value of $P_{CO_2 des}$. On the other hand, increasing apparent $NH_3$ concentration in the solvent increases the minimum pressure of the $CO_2$ desorber at which solids might be formed. On the contrary, the removal of the $CO_2$-WW section does not affect the maximum reachable pressure in the $CO_2$ desorber that avoids violating the constraint on the maximum temperature of an aqueous $NH_3$ solution in the process, which mainly depends on the solvent composition. As a result, no feasible range of operating conditions of the $CO_2$ desorber has been found for the high $\hat{c}_{NH_3}$ case in the range of $P_{CO_2 des}$ values studied. As far as the low and the mid $\hat{c}_{NH_3}$ cases are concerned, solid formation cannot be avoided for $P_{CO_2 des}$ values below 10 and 25 bar, respectively. In the case of the low $\hat{c}_{NH_3}$ case, the shrinkage of the feasible region of operating conditions of the $CO_2$ desorber affects neither the minimum specific equivalent work of the process, nor the optimal set of operating conditions. Nevertheless, such

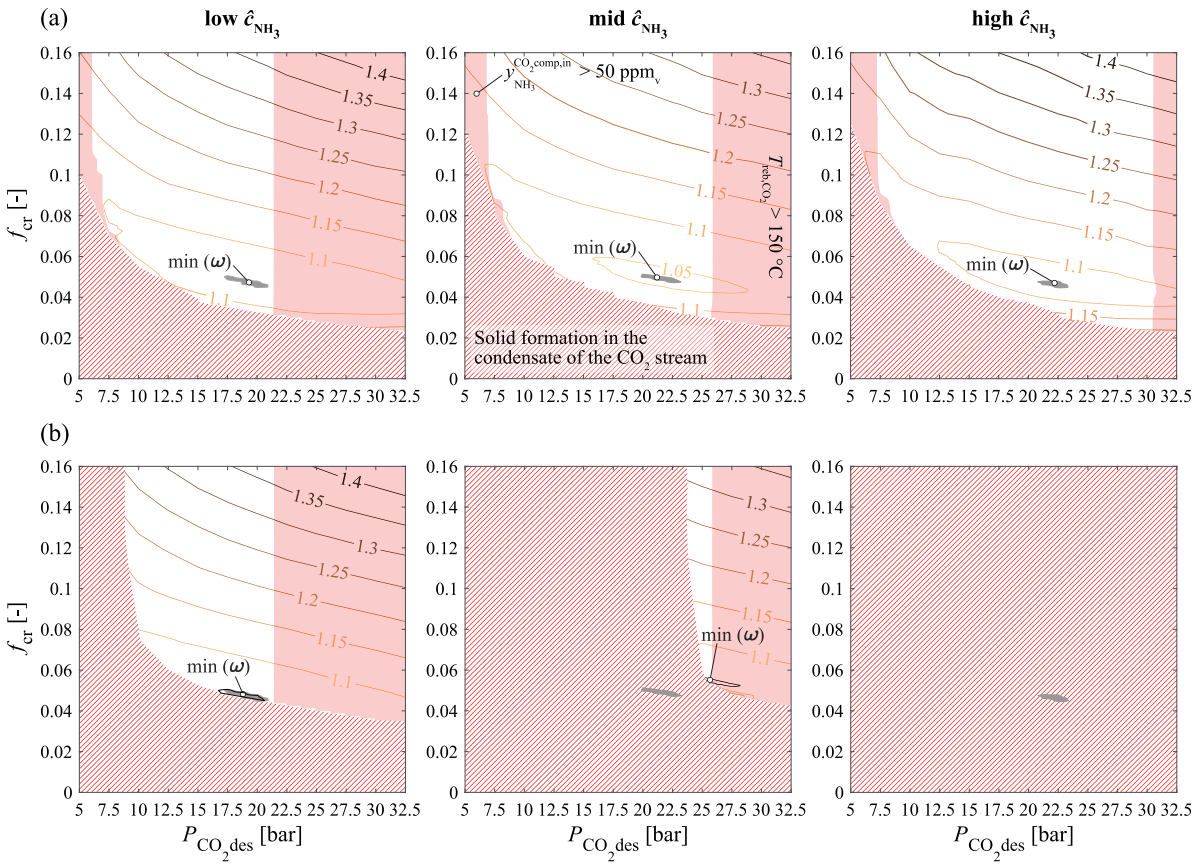


**Fig. 8.** Response surfaces showing the specific equivalent work ($\omega$ [MJ $kg^{-1}_{CO_2captured}$]) isolines in the plane cold-rich bypass split fraction vs. $CO_2$ desorber pressure when fixing the remaining process operating conditions at the values, from left to right, of the low $\hat{c}_{NH_3}$ case, the mid $\hat{c}_{NH_3}$ case and the high $\hat{c}_{NH_3}$ case, given in Table 3, for: (a) the reference configuration shown in Fig. 1; and, (b) Configuration B1 without the $CO_2$-WW column. The grey-coloured area and the black-coloured contour show the isoregion for minimum specific equivalent work for the reference configuration and for Configuration B1, respectively. For comparison purposes, both are represented in (b). The infeasible region of the process is represented by the striped area, where solids may form, and by the red shadowed regions, which define the range of $CO_2$ desorber operating conditions at which the $NH_3$ concentration in the $CO_2$ stream sent to compression, at the left, and the $CO_2$ desorber reboiler temperature, at the right, would not meet the process constraints (see Table 2). (For interpretation of the references to colour in this figure caption, the reader is referred to the web version of this article.)

shrinkage at the higher solvent $NH_3$ concentration of the mid $\hat{c}_{NH_3}$ case increases the minimum specific equivalent work of the process with respect to the reference configuration. Therefore, the advanced Configuration B1 without the $CO_2$-WW column can only be applied when the solvent contains low concentrations of $NH_3$, while removing the $CO_2$-WW column might worsen the energetic performance of the process with respect to the reference configuration, or even make the capture process infeasible, for increasing apparent $NH_3$ concentrations in the solvent.

The results that allow to carry out the performance assessment of **Configuration C1 without the appendix stripper** are shown in Fig. 9, where the overall energy consumption and the main energetic contributors of the process, as well as the consumption of aqueous $NH_3$ solution are provided for the three different sets of operating conditions given in Table 3. In addition to the results of Configuration C1, Fig. 9 also shows the performance of the reference configuration shown in Fig. 1 and of Configuration C1 without the DCCh, i.e. with the FG pre-conditioning section as in the reference configuration, for comparison purposes. As shown by the results of aqueous $NH_3$ solution consumption, the removal of the appendix stripper of the reference configuration can only be considered if it is coupled with the chilling of the FG before the $CO_2$ absorber. Otherwise, the consumption of aqueous $NH_3$ solution (25 wt%) increases from less than 1.5 $kg\,t^{-1}_{CO_2captured}$ for the reference configuration, independently of the $NH_3$ concentration in the solvent, to 19, 34 and 75 $kg\,t^{-1}_{CO_2captured}$ for the low, mid and high $\hat{c}_{NH_3}$ case, respectively. Introducing the DCCh in the FG pre-conditioning section allows to decrease the requirements of aqueous $NH_3$ solution make-up to values typical of the reference configuration, except for the high $\hat{c}_{NH_3}$ case, where the condensation of water from the FG in the DCCh operating at the minimum achievable temperature, i.e. 1.5 °C, is not low enough to avoid the accumulation of water in the solvent circulating between the $CO_2$ absorber and the $CO_2$ desorber. On the contrary, the purge of solvent from the capture loop to close the water balance is avoided for the low and for the mid $\hat{c}_{NH_3}$ cases if $T^{FG-DCCh}_{water}$ is set to 5.9 and to 1.5 °C, respectively. It is worth noting that, in order to avoid water accumulating in the solvent of the $CO_2$ absorber-$CO_2$ desorber loop, the condensation of water in the DCCh of Configuration C1 not only has to consider the water flowrate in the $CO_2$- and $NH_3$-depleted FG exiting the FG-WW column, but also has to counteract the water make-up in the $CO_2$-WW column. The water make-up to the $CO_2$-WW column, which enters the $CO_2$ absorber-$CO_2$ desorber loop in the absence of the appendix stripper, increases with higher $NH_3$ concentration in the solvent. This limits the feasibility of the $NH_3$-based capture process without the appendix stripper to scenarios where the process operates at low/mid apparent $NH_3$ concentration in the solvent, such as the low and the mid $\hat{c}_{NH_3}$ cases. As far as the energy consumption of Configuration C1 is concerned, Fig. 9 shows that the removal of the appendix stripper does not affect significantly the overall energy demand of the capture process: The increase of the chilling demand caused by the DCCh is compensated by the lower energy associated with the reboilers of the solvent recovery section due to the removal of the appendix stripper. Additionally, the specific equivalent work associated with the reboiler of the $CO_2$ desorber and with the process auxiliaries is also affected when the appendix stripper is removed and

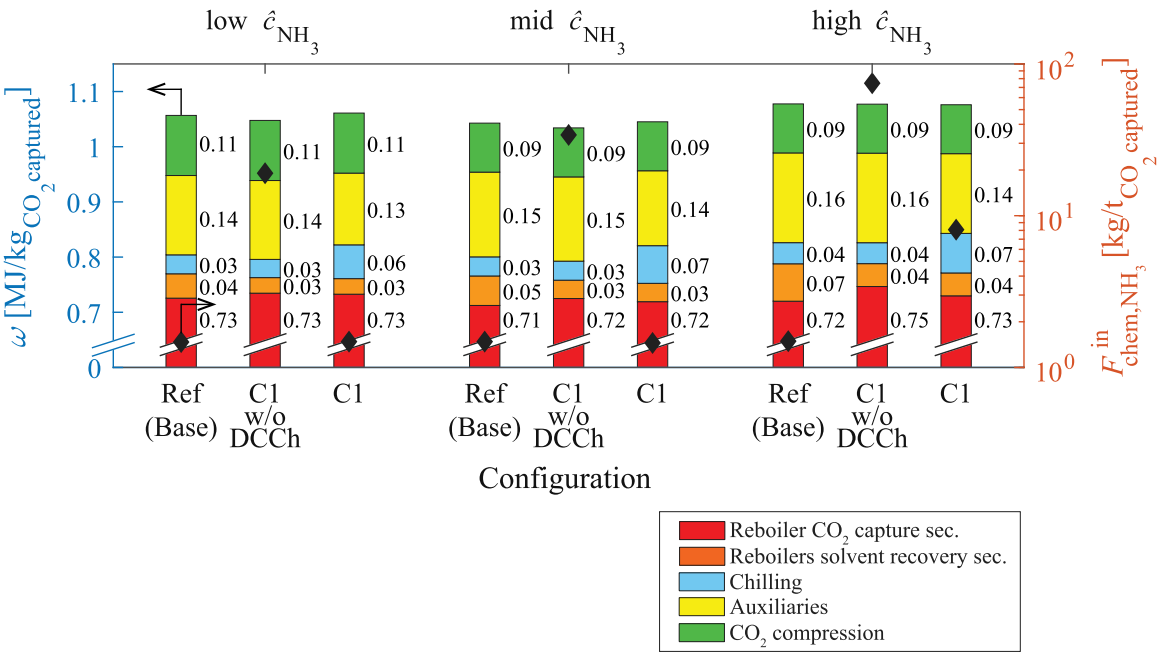


**Fig. 9.** Contribution of the key energy consumers to the specific equivalent work of the capture process (bars, left-hand y-axis) and consumption of aqueous $NH_3$ solution (25 wt%) (♦, right-hand y-axis) obtained for the reference configuration, for Configuration C1 without DCCh (FG pre-conditioning section as in the reference configuration) and for Configuration C1, at the sets of operating conditions defined by low $\hat{c}_{NH_3}$, mid $\hat{c}_{NH_3}$ and high $\hat{c}_{NH_3}$ in Table 3. The value of the specific equivalent work corresponding to each energy consumer is given by the data labels. Please, notice that the left-hand *y*-axis has been truncated for the sake of visuality. (For interpretation of the references to colour in this figure legend, the reader is referred to the web version of this article.)

the DCCh is introduced with respect to the reference configuration: The lower temperature of the FG entering the $CO_2$ absorber of Configuration C1 decreases the temperature of the cold $CO_2$-rich stream entering the rich-lean heat exchanger, thus the temperature of the other inlet and outlet streams, with respect to the reference configuration. While the lower temperature of the hot $CO_2$-rich stream entering the $CO_2$ desorber leads to a slight increase of the $CO_2$ reboiler duty, the lower temperature of the $CO_2$-lean stream exiting the rich-lean heat exchanger requires less cooling duty before entering the $CO_2$ absorber in comparison with the reference configuration, which explains the slight decrease of the specific energy associated with the auxiliaries.

The assessment of **Configuration C2 with the IS** has been carried out considering a column design that is equivalent in terms of investment costs to the $NH_3$ desorber of the reference configuration, thus removing effectively the appendix stripper. Subsequently, the energy requirements and the consumption of water and aqueous $NH_3$ solution of Configuration C2 with the IS are analysed in combination with different configurations of the FG post-conditioning section. The results obtained for Configuration C2 with the IS are reported in Fig. 10 in the form of parity plots, where the performance of the IS is compared with the performance of the same process configuration using the appendix stripper and the $NH_3$ desorber instead. Figs. 10(a) and (b) compare the energy performance, while (c) and (d) do the comparison by considering the consumption of fresh water make-up and of aqueous $NH_3$ solution, respectively, required in the process. The integration of appendix stripper and $NH_3$ desorber in a single column, i.e. the IS, does not affect significantly the required water and $NH_3$ solution make-up flowrates, while it decreases the energy consumption of the process in addition to its investment costs. The IS is able to reduce up to 40% the specific equivalent work associated with the reboilers of the columns in the solvent recovery section. Lower energetic improvements, i.e. around 25%, are achieved for the process simulated with the reference FG post-conditioning section at the base set of operating conditions of the FG-WW column, i.e. for low productivity values. The reason is that the set of operating conditions of the FG-WW column needs to be modified for the implementation of the IS (see "Base" conditions for "Ref" configuration in Table 6) in order to meet the maximum concentration of apparent $NH_3$ allowable in the purge stream, which worsens its energetic performance with respect to the base set of operating conditions of the FG-WW column provided in Table 3. The energetic advantage of the IS reveals between 1 and 3% savings of the total specific equivalent work with respect to the process using the appendix stripper and the $NH_3$ desorber.

The operation within the IS can be understood from the plots in Fig. 11, where the recovery of apparent $NH_3$, apparent $CO_2$ and apparent $H_2O$ are shown for each solvent composition case, i.e. low, mid and high $\hat{c}_{NH_3}$ cases, as well as the profiles along the column. As exemplary case, the results shown in Fig. 11 correspond to the configuration using the reference configuration of the FG post-conditioning section operating at the optimal set of operating conditions of the FG-WW column, although the conclusions of the analysis can be extended to any of the remaining cases introduced in Table 6.

Fig. 11(a) shows that the reboiler duty associated with the IS increases for greater apparent $NH_3$ concentration in the solvent. Greater apparent $NH_3$ concentration in the solvent increases the $NH_3$ (and the $CO_2$) content in all the streams entering the IS, most importantly in the $NH_3$-rich stream and in the solvent purge stream. The $NH_3$-rich stream, besides being the main carrier of $NH_3$ and $CO_2$ to be recovered in the IS, provides the IS with the vast majority of water entering the column due to the high dilution of the solvent required in the FG-WW column; while the $NH_3$ (and $CO_2$) contained in the $NH_3$-rich stream depends on the $NH_3$ concentration in the $CO_2$-depleted FG exiting the $CO_2$ absorber, the $H_2O$ flowrate is influenced by the FG-WW column operating conditions. Nevertheless, the mass flowrate of apparent $H_2O$ entering the IS does not have a significant effect on the reboiler duty of the column as a consequence of the optimal heat integration network. Fig. 11(a) also shows that the IS achieves recoveries of $CO_2$ and $NH_3$, i.e. the ratio between the component mass flowrate obtained in the distillate and the apparent component mass flowrate entering the IS, above 0.9999 and above 0.995, respectively, in all $\hat{c}_{NH_3}$ cases; the vapour distillate stream recycled to the bottom of the $CO_2$ absorber contains between 20 and 40 vol% $NH_3$ and between

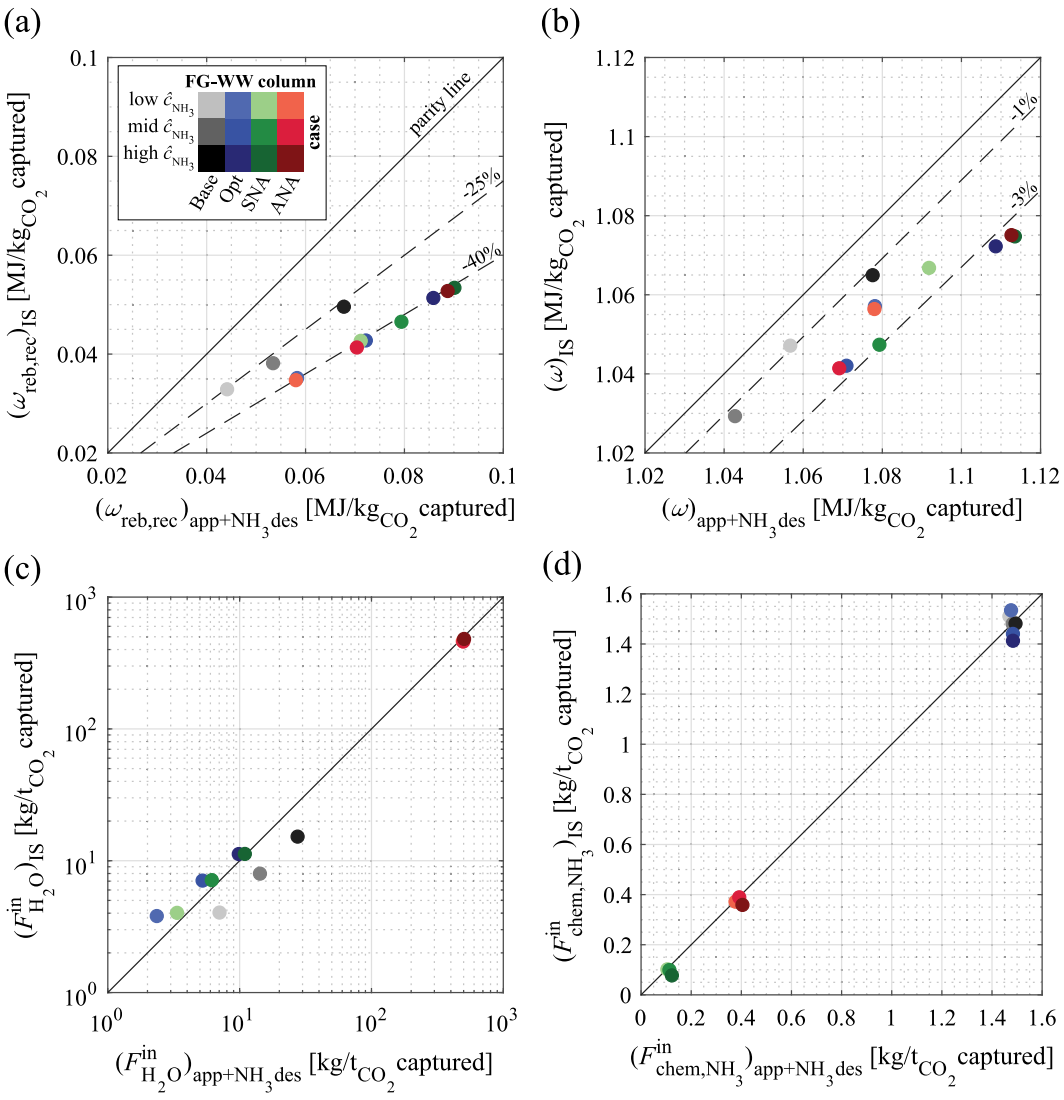


**Fig. 10.** Parity plots comparing the performance of the $NH_3$-based capture process using the IS with the performance of the same process but using the appendix stripper and the $NH_3$ desorber instead, for different performance indicators: (a) specific equivalent work associated with the reboilers of the solvent recovery sections; (b) specific equivalent work of the whole capture process; (c) consumption of process water; and, (d) consumption of aqueous $NH_3$ solution (25 wt%). Points are colour-coded depending on the configuration and operating conditions of the FG-WW column, and on the apparent $NH_3$ concentration in the solvent, as specified in Table 6. The parity line (___) and lines indicating variations with respect to the parity line (_ _) are also shown. (For interpretation of the references to colour in this figure legend, the reader is referred to the web version of this article.)

10 and 20 vol% $CO_2$, as shown in Fig. 11(b). On the contrary, recovery values between 0.08 and 0.09 are obtained for $H_2O$, as it can be inferred from Fig. 11(a). Almost pure water is obtained in the bottom stream of the IS, whose composition can be determined from Figs. 11(c) and (d). Therefore, the temperature in the reboiler of the IS equals 100 °C in all cases (see Fig. 11(e)), independently of the configuration and of the $NH_3$ concentration level in the capture solvent, since it depends on the bottom stream conditions, i.e. almost pure water at atmospheric pressure.

Besides decreasing the process complexity hence the investment costs of the capture process and improving the energetic performance with respect to the process using the appendix stripper and the $NH_3$ desorber, the feasibility of the IS is independent: (i) of the solvent composition in the range of apparent $NH_3$ concentrations studied in this work, and (ii) of the configuration of the FG post-conditioning section and operating conditions of the FG-WW column. Based on its superior performance and broad applicability, the use of the IS integrating the appendix stripper and the $NH_3$ desorber is therefore always recommended for $NH_3$-based capture processes.

### 4.3. Advanced configurations to improve the energetic performance

#### 4.3.1. Process description

As mentioned above, the main contribution to the overall energy consumption of solvent-based $CO_2$ capture processes is the thermal energy required in the $CO_2$ desorber, where $CO_2$ is stripped off with high purity and the $CO_2$-lean solvent is regenerated for re-use in the $CO_2$ absorber. In the case of $NH_3$-based capture processes applied to cement plants, steam has been reported to account approximately for 30% of the cost of $CO_2$ capture [40]. Consequently, the advanced configurations developed in this work aiming at improving the energetic performance of $NH_3$-based capture processes have focused on the reduction of the reboiler duty in the $CO_2$ desorber. One advanced configuration of the $CO_2$ desorber and one advanced configuration of the solvent recovery section specific of $NH_3$-based capture processes have been studied in detail in this work, namely the RecVC and the VIS. These have been combined with the best performing advanced configurations of the $CO_2$ desorber available in literature for solvent-based capture processes, as long as they are compatible with $NH_3$-based capture processes; namely, the LVC and the MPD have been identified

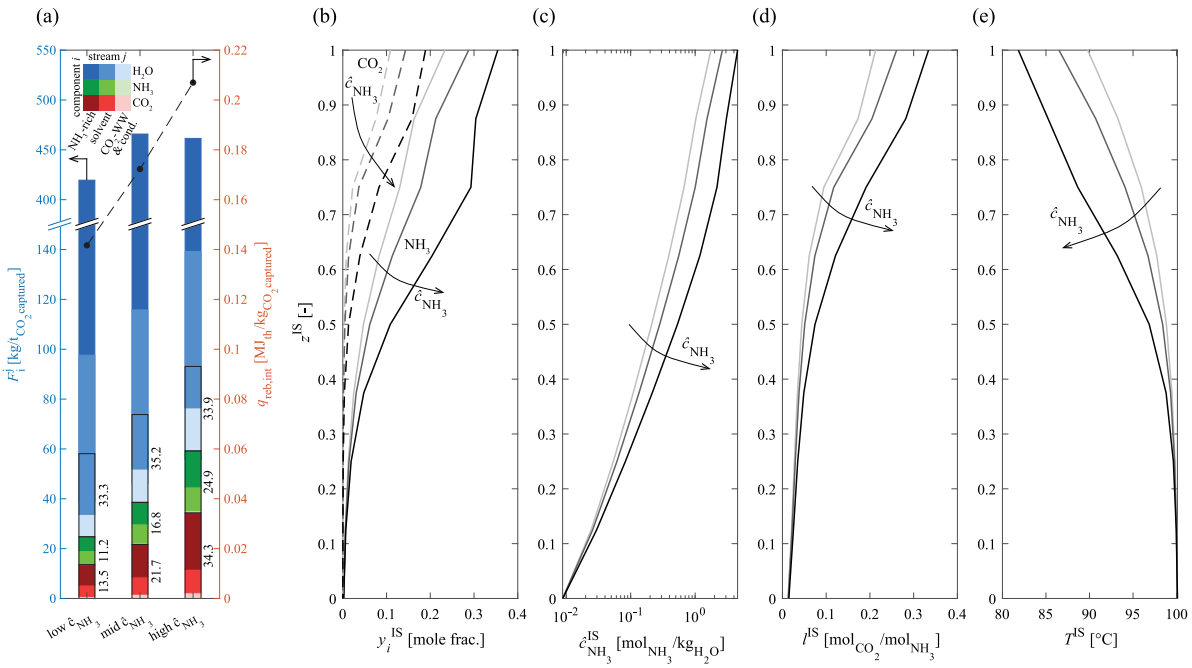


**Fig. 11.** (a) Apparent component mass flowrates in each feed stream entering the IS, colour-coded as a function of the inlet stream and of the component (coloured bars), and component mass flowrates recovered in the distillate stream leaving the top of the column (□, values given by the data labels), for the process using the reference configuration of the FG post-conditioning section operating at the optimal conditions of the FG-WW column provided in Table 6, for the three different sets of operating conditions of the $CO_2$ absorber (and the $CO_2$ desorber) provided in Table 3 (left-hand *y*-axis, which has been truncated for the sake of visuality); and corresponding reboiler duty of the IS associated with each solvent composition case (right-hand y-axis). And corresponding profiles along the relative height of the IS ($z^{IS} = 0$ at the bottom): (b) $NH_3$ and $CO_2$ mole fraction in the vapour phase, (c) apparent $NH_3$ concentration in the liquid phase, (d) apparent $CO_2$ loading in the liquid phase, and (e) temperature. (For interpretation of the references to colour in this figure legend, the reader is referred to the web version of this article.)

as the most promising advanced configurations of the $CO_2$ desorber for $NH_3$-based capture processes. As a result of the combination of different advanced concepts of the $CO_2$ desorber and of the solvent recovery section, ten different combinations of advanced configurations aiming at improving the energetic performance of $NH_3$-based $CO_2$ capture processes have been studied in detail. All of them are able to decrease the steam requirements for solvent regeneration in the $CO_2$ desorber, at the cost of increasing the electricity consumption and/or the requirements of low temperature excess heat that might be available in the $CO_2$ point source. All advanced configurations in this section have been implemented upon the process configuration shown in Fig. 7 using the IS (Configuration C2), since its performance has been proven to be superior to that of the separated $NH_3$ desorber and appendix stripper, as it has been shown in Section 4.2.2. Nevertheless, the advanced configurations presented in this section could also be implemented on processes using the separated $NH_3$ desorber and appendix stripper where the vapour distillate streams from both columns are mixed. Similarly, the different advanced configurations of the FG post-conditioning section described in Section 4.1.1 are also compatible. The different types of advanced configurations that aim at improving the energetic performance of $NH_3$-based capture are illustrated in Fig. 12, where only the relevant process sections, i.e. $CO_2$ desorber section and solvent recovery section, are shown. Each of them are described below.

**Configuration E1 with the RecVC**, where the vapour distillate stream obtained in the IS is compressed and recycled to the bottom of the $CO_2$ desorber, instead of being sent to the bottom of the $CO_2$ absorber. In terms of capital costs, recycling the distillate stream obtained in the solvent recovery section to the bottom of the $CO_2$ absorber is the most efficient solution as it does not require additional equipment. Nevertheless, the vapour distillate obtained in the IS is a concentrated stream in $CO_2$ and $NH_3$, i.e. around 30 and 25 wt%, respectively, hence the utilization of these high concentrations in the $CO_2$ desorption section would seem more appropriate than a dilution in the absorption section. Accordingly, Sutter et al. [13] proposed to mix the vapour distillate stream obtained in the $NH_3$ desorber with the $CO_2$-rich liquid stream leaving the $CO_2$ absorber, before it is pumped to the pressure of the $CO_2$ desorber, assuming that the energy demand of a direct compression of the vapour stream would be too high. However, the option of mixing a vapour with a liquid stream would require a vessel providing enough residence time to completely dissolve the vapour distillate stream into the $CO_2$-rich liquid stream, in order to avoid cavitation in the pump positioned downstream. Additionally, the positive impact on the energy performance of $NH_3$-based capture processes when mixing the vapour distillate of the IS with the $CO_2$-rich stream is expected to be negligible due to the fact that the mass flowrate of the former only represents up to 1.5% of the mass flowrate of the latter. On the contrary, the mass flowrate of the IS vapour distillate may represent up to 50% of the steam mass flowrate required for solvent regeneration in the reboiler of the $CO_2$ desorber. Considering that the compression of the vapour distillate will increase its temperature above the solvent regeneration temperature, it will deliver heat of enough quality to be used in the reboiler of the $CO_2$ desorber, thus allowing for useful heat integration and leading to a decrease of the steam requirements for solvent regeneration. Therefore, the vapour distillate of the IS is compressed up to the pressure of the $CO_2$ desorber in the case of the RecVC. A multi-stage compressor is used with isentropic efficiency of 85% and driver efficiency of 95%, as defined in literature [33,39]; four compression stages, each of them with the same compression ratio, are selected in order to make the equipment versatile for a broad range of outlet pressures, namely between 7.5 and 67.5 bar. Such multi-stage compressor configuration allows for stage-wise compression ratios ranging between 1.6 and 2.9. Inter-cooling of the vapour in between compression stages is carried out by means of the $CO_2$-rich stream leaving the rich/lean heat exchanger with the aim of maximizing heat integration before entering the $CO_2$ desorber. The temperature of the vapour has been given a lower limit in each inter-cooling stage to avoid condensation, using as a threshold the boiling point of pure water at the corresponding pressure.

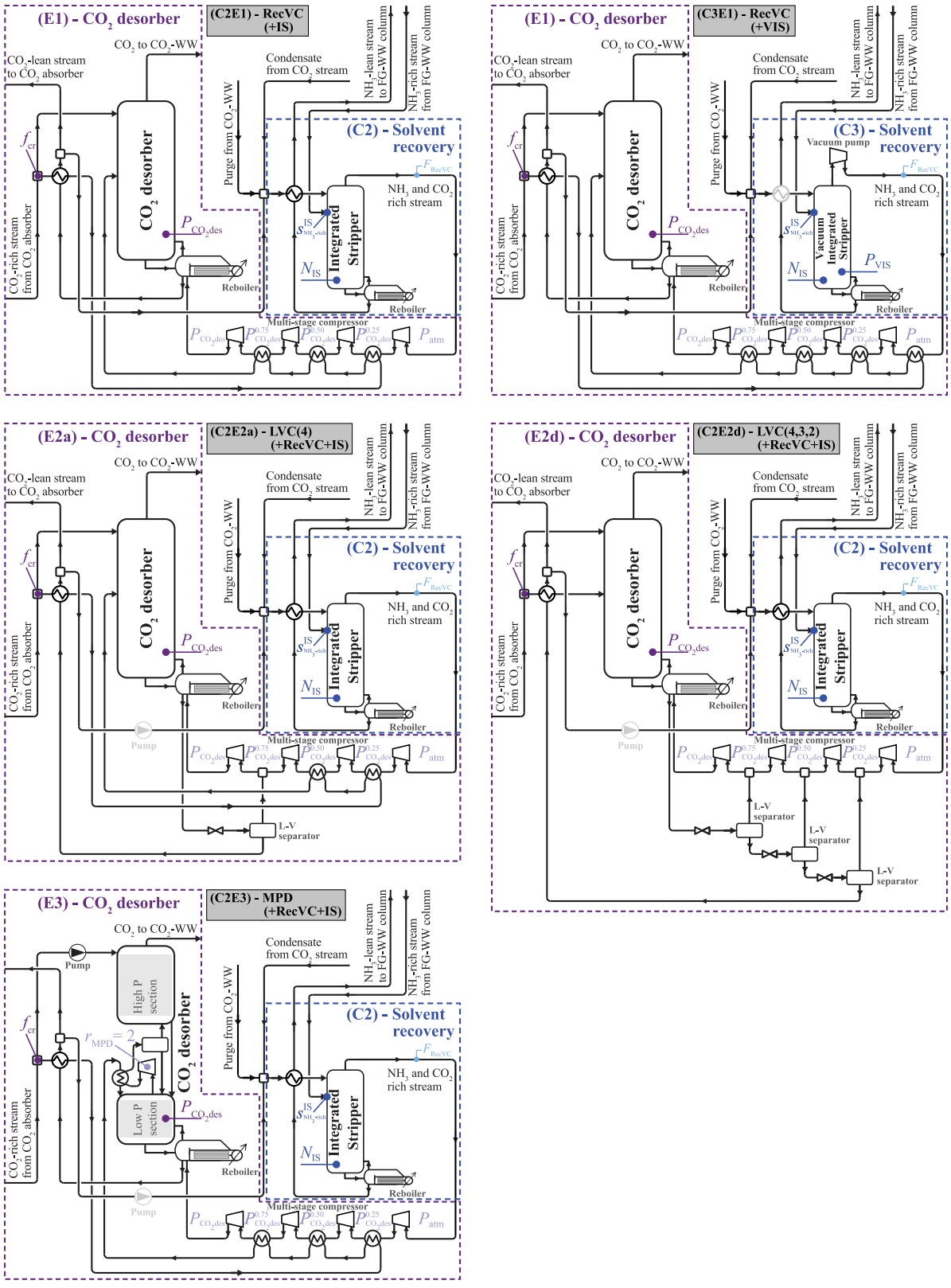


**Fig. 12.** Flow diagrams combining advanced configurations of the solvent recovery section and of the $CO_2$ desorber section. The operating variables that govern the performance of each configuration, i.e. the decision variables of the optimization problem, have been colour-coded in blue for the solvent recovery section and in violet for the $CO_2$ desorber operating conditions. Other important process variables whose values have been fixed for our simulations or depend on some of the decision variables have been introduced in lighter colours for each process section, i.e. light blue and light violet, respectively. The pump of the purge solvent stream and the heat exchanger of the solvent recovery section are represented in grey in those configurations where the piece of equipment might be required depending on the process operating conditions. (For interpretation of the references to colour in this figure caption, the reader is referred to the web version of this article.)

In addition to the influence of the operating conditions of the $CO_2$ absorber section, which affect the performance of all process sections, the energetic assessment of the RecVC depends on the operating conditions of the $CO_2$ desorber section and of the solvent recovery section. Namely, the pressure of the $CO_2$ desorber, $P_{CO_2 des}$ [bar], and the specific mass flowrate of vapour distillate recycled from the IS to the bottom of the $CO_2$ desorber, $F_{RecVC}$ [$kg\,t^{-1}_{CO_2 captured}$], determine both the energy savings in the reboiler of the $CO_2$ desorber and the additional electric power required by the new multi-stage compressor. The mass flowrate of vapour distillate exiting the top of the IS can be modified by changing the number of equilibrium stages of the column and/or the feeding stage of the inlet streams; the stripper reboiler duty is thus determined to meet the maximum $NH_3$ concentration allowable in the bottoms stream. In addition, the optimal value of the cold-rich split fraction of the RSS, $f_{cr}$ [-], that minimizes the energy performance of the capture process depends on the pressure of the $CO_2$ desorber, as pointed out elsewhere [14].

**Configuration E2 with the LVC**, where the hot $CO_2$-lean stream leaving the reboiler of the $CO_2$ desorber is expanded to lower pressure. The resulting vapour phase is re-compressed up to the $CO_2$ desorber pressure and introduced again into the bottom of the $CO_2$ desorber, while the liquid $CO_2$-lean stream exiting the L-V separator is sent to the rich/lean heat exchanger. In order to take advantage of synergies with the RecVC, the use of the same multi-stage compressor is proposed. Therefore, different alternatives of the LVC are possible depending on the pressure to which the hot $CO_2$-lean stream is expanded. In this work, we have considered the following variations of the LVC: (i) Configuration E2a (LVC(4)) where the hot $CO_2$-lean stream is expanded to the inlet pressure of the last stage of the multi-stage compressor; (ii) Configuration E2b (LVC(3)) where it is flashed to the inlet pressure of the second-to-last stage of the compressor; (iii) Configuration E2c (LVC(4,3)) where the hot $CO_2$-lean stream is expanded in two steps, first to the inlet pressure of the last stage of the multi-stage compressor, and then to the inlet pressure of the second-to-last compression stage; and (iv) Configuration E2d (LVC(4,3,2)) where it is flashed in three steps down to the inlet pressure to the second stage of the multi-stage compressor. The vapour streams resulting from the saturated liquid expansion are mixed with the vapour distillate from the IS being compressed in the multi-stage compressor (the same concept would apply in the case of using independent $NH_3$ desorber and appendix stripper). Due to the lower temperature level of the vapour resulting from the expansion of the lean stream, no additional cooling is needed. Depending on the pressure of the liquid stream exiting the last L-V separator, the split stream purged from the solvent cycle might have to be compressed up to 7 bar in order to avoid the partial vaporization of the cold stream entering the heat exchanger of the solvent recovery section, thus the possibility of a temperature crossover. For the sake of brevity, Fig. 12 only shows configurations E2a and E2d; then, configurations E2b and E2c can be easily drawn following the description provided above. Other derivations of the LVC such as one-step expansion to the inlet pressure of the second stage of the compressor or below, or four-step expansion down to atmospheric pressure have not been included in this study due to low performance; the additional demand of electrical work required for compression is far from being compensated by the energy savings in the reboiler of the $CO_2$ desorber.

**Configuration E3 with the MPD**, where the $CO_2$ desorber is divided in two different sections with the upper section operating at higher pressure than the lower section (and the reboiler). The vapour stream exiting the top of the lower section of the $CO_2$ desorber is compressed to the pressure of the upper section. A pressure ratio of 2 between the upper and the lower section of the MPD, thus in the compressor placed between the two sections of the $CO_2$ desorber, $r_{MPD}$ [-], has been selected in this work, following the guidelines provided in literature for solvent-based capture processes [29]. Before entering the bottom of the upper $CO_2$ desorber section, the compressed vapour stream transfers heat to the $CO_2$-rich stream in a counter-current heat exchanger. The latter stream enters then the top of the lower section of the $CO_2$ desorber, together with the condensate of the compressed vapour stream obtained in the L-V separator. The cold stream of this heat exchanger, i.e. the $CO_2$-rich stream, which enters as a boiling liquid, has considerably greater flowrate than the hot stream, i.e. the compressed vapour stream, so that it experiences a minor increase in temperature. Therefore, the pinch point temperature of this heat exchanger is reached at the cold-side. The upper section of the $CO_2$ desorber contains 6 equilibrium stages, while the lower section consists of 3 stages plus the reboiler; the number of equilibrium stages of the MPD and the feed stages are thus kept as in the $CO_2$ desorber of the benchmark state-of-the-art configuration.

As in the case of the RecVC, both the LVC and the MPD require finding the trade-off between additional electrical work required for vapour compression and the associated energy savings achieved in the $CO_2$ desorber. In this work, both advanced configurations have been assessed in combination with the RecVC, so that the operating conditions of the solvent recovery section will affect the performance of both the LVC and of the MPD. The MPD has not been tested in combination with the LVC because the lower pressure levels of the lower section of the MPD are expected to hinder the effect of the LVC [29].

The RecVC, the LVC and the MPD are expected to be promising advanced configurations for $NH_3$-based processes due to the broad range of solvent compositions and pressures that are allowed in the $CO_2$ desorber. Other advanced configurations of the $CO_2$ desorber available in literature that have been reported to improve significantly the energetic performance of solvent-based capture processes [29,58], such as the RVC, the IHD, the Stripper Overhead Compression (SOC) or the Multi-effect Desorber (MED), have not been considered in this study for $NH_3$-based capture processes due to four reasons: (i) worse performance when applied to $NH_3$-based capture processes; (ii) incompatibilities with the heat integration network provided by the rich/lean heat exchanger and the RSS included in the benchmark CAP configuration; (iii) incompatibilities with the control of the $NH_3$ concentration in the $CO_2$ stream exiting the top of the $CO_2$ desorber; and/or, (iv) increasing drastically the process complexity without improving significantly the energy performance.

**Configuration C3 with the VIS**, where the IS operates at sub-ambient pressures in order to decrease its reboiler temperature to values below 100 °C, which might enable the use of increasing amounts of excess heat available at the $CO_2$ point source. The heavy and the light key components in the separation carried out in the IS are $H_2O$ and $NH_3$, respectively, instead of being $NH_3$ and $CO_2$, as in the case of the separation in the $CO_2$ desorber. Therefore, while the minimum specific equivalent work associated with the solvent regeneration in the $CO_2$ desorber has been found at pressures around 20 bar and above [14], the stripping of $NH_3$ (and $CO_2$) from water has been reported to be favoured energetically under vacuum [59]. The VIS requires a vacuum pump that withdraws the vapour distillate from the stripper and guarantees pressures below atmospheric within the column, which increases the electrical work required by the capture process. Aiming at maximizing its impact on the overall energetic performance of the capture process, the VIS is implemented in combination with the RecVC, which allows for a trade-off between: (i) the high temperature steam required in the $CO_2$ desorber for solvent regeneration, (ii) the low temperature thermal energy required in the VIS for the recovery of $NH_3$ (and $CO_2$), and (iii) the electricity required in the multi-stage compressor of the RecVC and in the vacuum pump of the VIS. Contrary to operating the $CO_2$ desorber at vacuum conditions, the VIS allows to operate the $CO_2$ desorber at the optimal pressure level that minimizes the steam requirements for solvent regeneration as well as the $CO_2$ compression work.

#### 4.3.2. Optimization and implementation scenarios

The energetic optimization of each advanced configuration aiming at improving the energetic performance of $NH_3$-based capture processes has been carried out by means of a multi-variable sensitivity analysis in which the operating conditions of the capture process are modified. Namely, the operating conditions of the $CO_2$ desorber section, i.e. $P_{CO_2 des}$ and $f_{cr}$, and of the solvent recovery section, i.e. the number of equilibrium stages of the IS, $N_{IS}$ [-], and the feeding stage to the IS of the $NH_3$-rich stream, $s^{IS}_{NH_3-rich}$ [-], are varied for the three different sets of operating conditions of the $CO_2$ absorber section provided in Table 3. In addition, variations in the pressure of the VIS, $P_{VIS}$ [bar], have been included: two different $P_{VIS}$ values have been considered, namely 0.10 and 0.35 bar, which allow for temperatures at the reboiler of the stripper as low as 46 and 72 °C, respectively, in contrast to the 100 °C reached in the case of the IS operating at atmospheric pressure. At lower temperatures in the reboiler of the VIS and depending on the process operating conditions, the bottom stream of the VIS might not be able to heat up the solvent purge stream fed at the top of the column. When the VIS operates at 0.10 bar, the vacuum pump has been simulated as a two-stage compressor with intercooling and isentropic efficiencies equal to 0.600 and 0.636 for the first and the second compression stages, respectively; for $P_{VIS}$ equal to 0.35 bar, the vacuum pump has been simulated by means of a single-stage compressor with isentropic efficiency equal to 0.636 [60,61]. The mechanical efficiency of the vacuum pump has been set to 0.95 in all cases, as for pumps, fans and compressors [33,39].

The energetic assessment and the selection of the optimal set of operating conditions of the advanced configurations developed in this section have been performed aiming at the minimization of three different energy performance indicators: (i) specific equivalent work, (ii) specific electrical work demand vs. specific reboiler duty, or (iii) SPECCA index. For the last optimization problem, i.e. SPECCA index minimization, different application scenarios have been considered for the capture process, where the features of the available electricity from the grid and excess heat from the $CO_2$ point source are varied. All scenarios consider 90% $CO_2$ capture efficiency from a exhausted FG with a composition similar to the values reported in Table 1. Therefore, the results obtained in all cases can be approximated by the performance obtained when applying the capture process to the FG specified in Table 1. The specifications and constraints of the capture process reported in Table 2 are also applied to these application scenarios. The following application scenarios have been considered:

**Scenario 1.** **Cement plant** as specified in Section 3, i.e. a typical European cement plant using the BAT. The amount of excess heat from the cement plant that can be used in the reboilers of the capture process has been taken from Voldsund et al. [39] as a function of the steam temperature, i.e. $T_{reb} + 10$ °C, assuming that heat can be recovered from the cement plant's cooler exhaust air. The remaining steam required at the capture plant is produced in a Natural Gas (NG) boiler built on-site, since cement plants are normally not built integrated with or next to a power plant [39].

*Scenario 1.a.* Electricity imported from the grid considering the 2014 EU-28 average electricity mix [33,39].

*Scenario 1.b.* Electricity imported from the grid considering a hypothetical 2030 EU average electricity mix, which has been determined from the 2014 EU-28 electricity mix data [33] and from the predictions for electricity generation in the EU in 2030 according to the EUCO30 scenario [62], corrected with the new electricity generation objectives included in the EU Green Deal [63,64]. In this application scenario, 66% of electricity is assumed to be generated from renewable sources, 17% from fossil fuel sources and 17% from nuclear plants.

*Scenario 1.c.* All electricity consumed by the capture plant is generated from renewable energy sources.

**Scenario 2.** **Steel plant** in which $CO_2$ is captured from the exhausted FG streams avoiding any modification in the iron and steel manufacturing process. Overall, the exhausted flue gases contain around 20 vol% $CO_2$ [65] and account for up to 90% of the total $CO_2$ emissions of an iron and steel production facility [66]. Electricity is imported from the grid, assuming the 2014 EU-28 average electricity mix [33,39], and thermal energy required in the reboilers of the capture process that cannot be produced from the excess heat available in the industrial site is obtained in a NG boiler, as for the cement plant application scenario.

*Scenario 2.a.* Excess heat from the condenser of the CHP plant, which is generally integrated within the steelworks facility, is used as thermal energy in the reboiler of the VIS if operating at temperatures around 45 °C. A condenser operating at temperatures up to 50 °C can be assumed to have a negligible effect on the heat and electricity efficiency generation of the CHP plant.

*Scenario 2.b.* In addition to the excess heat considered in Scenario 2.a, additional excess heat is recovered from the gas flaring, the hot stove FG, the hot coke and the hot slag [66,67]. The computation of specific excess heat per unit mass of $CO_2$ captured considers: (i) the data reported by Sundqvist et al. [67] for production of steam at 130 °C, who assumed aqueous MEA as solvent in the capture plant and a steelworks site in which the blast furnace is only charged with iron ore pellets (no sinter plant); (ii) the relative increment of $CO_2$ emissions associated with the sinter plant [65]; and, (iii) a temperature dependency for steam production as that considered for the cement plant application scenarios.

**Scenario 3.** **Refinery**, in which $CO_2$ is captured from FG streams that account for 47.1% of the total $CO_2$ emissions of the site and overall contain 20.3 vol% $CO_2$, i.e. capture is applied to the FG streams exiting chimneys 3 and 4 of the refinery described by Andersson et al. [42]. Electricity is imported from the grid, assuming the 2014 EU-28 average electricity mix [33,39], while the amount of excess heat that can be recovered from the refinery has been computed from data available in literature [42]. If additional steam is required in the capture plant, it is produced in a gas boiler, as for the cement plant and the steel plant application scenarios, that burns Refinery Gas (RG) instead of NG.

The data associated with the electricity and steam generation and with the excess heat availability in each application scenario are reported in Table 7.

#### 4.3.3. Results and discussion

In total, 76,101 different combinations of operating conditions of the $CO_2$ absorber, the $CO_2$ desorber and the solvent recovery section, as described in Section 4.3.2, led to converged simulations meeting the specifications and constraints indicated in Table 2 for advanced configurations aiming at improving the energetic performance of $NH_3$-based capture processes. Firstly, such advanced configurations have been compared according to thermodynamic criteria. With that aim, Table 8 shows the operating conditions that minimize the specific equivalent work of the overall capture process, $\omega$, for the most representative advanced configurations aiming at improving the energetic performance of $NH_3$-based capture processes. The RecVC has been

**Table 7**
Assumptions on excess heat availability and on energy consumption and $CO_2$ emissions related to electricity and steam generation for each application scenario. Efficiencies of 0.33 and 1.00 $MJ_{el}\,MJ_{LHV}^{-1}$ have been assumed for nuclear and renewable electricity generation following the criteria of the International Energy Agency (IEA) [33].

| Variable | Scenario | | | | | |
|---|---|---|---|---|---|---|
| | 1.a | 1.b | 1.c | 2.a | 2.b | c |
| **Electricity generation** | | | | | | |
| Efficiency [$MJ_{el}\,MJ_{LHV}^{-1}$] | 0.459 | 0.634 | 1.0 | 0.459 | 0.459 | 0.459 |
| Specific $CO_2$ emissions [$kg_{CO_2}\,GJ_{el}^{-1}$] | 72.78 | 32.38 | 0 | 72.78 | 72.78 | 72.78 |
| **Steam generation** | | | | | | |
| Boiler efficiency (LHV basis) [$MJ_{th}\,MJ_{LHV}^{-1}$] | 0.9 | 0.9 | 0.9 | 0.9 | 0.9 | 0.9 |
| Specific $CO_2$ emissions [$kg_{CO_2}\,GJ_{LHV}^{-1}$] | 56.1 | 56.1 | 56.1 | 56.1 | 56.1 | 66.7 |
| **Specific excess heat available at the $CO_2$ point source** | | | | | | |
| $q_{rec}$ [$MJ_{th}\,kg_{CO_2\,captured}^{-1}$] | $a + bT_{steam}$ | | | $\infty, T_{reb} < 50\,°C$<br>$0, T_{reb} \geq 50\,°C$ | $\infty, T_{reb} < 50\,°C$<br>$a + bT_{steam}, T_{reb} \geq 50\,°C$ | $a + bT_{steam} +$<br>$+cT_{steam}^2 + dT_{steam}^3 +$<br>$+eT_{steam}^4 + fT_{steam}^5$ |
| Coefficients ($T_{steam}$ in °C) | | | | | | |
| $a$ | 0.3968 | | | N/A | 1.106 | 10.51 |
| $b \times 10^2$ | −0.1942 | | | N/A | −0.1942 | −4.736 |
| $c \times 10^3$ | N/A | | | N/A | N/A | −1.401 |
| $d \times 10^5$ | N/A | | | N/A | N/A | 1.561 |
| $e \times 10^8$ | N/A | | | N/A | N/A | −5.911 |
| $f \times 10^{11}$ | N/A | | | N/A | N/A | 7.789 |

included in all combinations of advanced configurations since it has shown a better performance than recycling the $NH_3$ and $CO_2$-rich stream recovered in the solvent recovery section to the $CO_2$ absorber. Subsequently, the RecVC has been combined with different designs of LVC configurations and with the MPD. Then, the VIS is always implemented in combination with the RecVC, when it is expected to be most efficient since the additional electrical work required by the vacuum pump can be compensated by reboiler duty reductions in the $CO_2$ desorber. In Table 8, the thermodynamic performance of the VIS is shown at two different working pressures in combination with the MPD and the RecVC, which is the combination that minimizes the specific equivalent work when using the IS. Configuration C2 using the IS (shown in Fig. 7) has been used as reference configuration for the assessment of advanced configurations that aim at improving the energetic performance of $NH_3$-based processes. Along with the minimum $\omega$ value achieved for each configuration and the corresponding conditions of the process parameters, Table 8 also includes the results for other performance indicators such as consumption of chemicals, reboiler duties and temperatures, and electrical demand. Moreover, Table 8 also contains the results of the heat integration performance corresponding to the rich/lean heat exchanger, the $NH_3$-rich/$NH_3$-lean heat exchanger and the rich purge/lean purge heat exchanger. Such heat integration network allows to obtain the reboiler duties indicated in Table 8 for the $CO_2$ desorber, $q_{reb,CO_2}$, and for the IS (or VIS), $q_{reb,IS}$. All liquid/liquid heat exchangers are simulated as counter-current heat exchangers in which the pinch point temperature is set to 3 °C. In the case of condensing vapour/boiling liquid heat exchangers above ambient temperature, such as the reboilers of the distillation columns and the heat exchanger introduced with the MPD, the pinch point temperature is set instead to 10 °C [33,39]. In the rich/lean heat exchanger, the hot $CO_2$-lean stream transfers heat, $q_{HTX,rich/lean}$, to the cold $CO_2$-rich stream, which amounts from two to four times the reboiler duty of the $CO_2$ desorber, depending on the process configuration and operating conditions. The heat transferred in the $NH_3$-rich/$NH_3$-lean heat exchanger, $q_{HTX,FG-WW}$, from the hot $NH_3$-lean stream to the cold $NH_3$-rich stream, and in the rich purge/lean purge heat exchanger, $q_{HTX,IS}$, from the hot lean purge stream to the cold rich purge stream, are of the same order of magnitude of the reboiler duty of the IS (or the VIS). Therefore, the proper design and simulation of such process heat exchangers is of paramount importance to find feasible reboiler duties in the distillation columns, i.e. $CO_2$ desorber and IS (or VIS), thus to determine the optimal set of operating conditions that minimize the energy demand of the capture process.

The RecVC (Configuration C2E1) is capable of reducing by 2.3% the minimum specific equivalent work of the capture process in comparison to the reference case in which the $NH_3$ and $CO_2$-rich stream recovered at the top of the IS is recycled to the $CO_2$ absorber. Such improvement is mainly obtained due to the decrease in $q_{reb,CO_2}$ achieved by means of the heat provided by the compressed $NH_3$ and $CO_2$-rich stream, which outgrows the increase in the electrical work demand required to compress such vapour stream to the pressure of the $CO_2$ desorber. The compression of the vapour distillate from the IS acts as a so-called "heat pump", which increases its heat quality to the point of making it suitable to provide heat in the reboiler of the $CO_2$ desorber, at the cost of increasing the mechanical work of the process required for compression.

When also introducing the LVC with expansion of the $CO_2$-lean stream to the inlet pressure to the fourth (last) stage of the multi-stage compressor introduced with the RecVC (Configuration C2E2a), the minimum specific equivalent work can be further decreased up to 3.2% with respect to the reference configuration, i.e. Configuration C2. While the greater vapour flowrate to be recycled to the $CO_2$ desorber increases the electrical work demand, this is outgrown as for Configuration C2E1, with RecVC but without the LVC, by the decrease of the reboiler duty required for solvent regeneration in the $CO_2$ desorber. In the case of Configuration C2E2a, such additional reboiler duty decrease is not only achieved by the additional flowrate of hot vapour recycled to the bottom of the $CO_2$ desorber, but also by the additional equilibrium stage provided by the $CO_2$-lean stream expansion, which allows to further separate $CO_2$ from $NH_3$ (and water) thus allowing for higher $CO_2$ loadings in the liquid exiting the reboiler of the $CO_2$ desorber, thus decreasing the requirements for the thermal separation. The expansion of the liquid exiting the reboiler of the $CO_2$ desorber decreases the temperature of the hot $CO_2$-lean stream, which lowers the amount of heat exchanged in the rich/lean heat exchanger and thus leads to lower temperature profiles along the $CO_2$ desorber, including lower temperature levels in the reboiler. The lower temperature levels along the column contributes to a better control of the $NH_3$ slip in the $CO_2$ stream exiting the top of the $CO_2$ desorber, as it can be deduced from the lower cold-rich bypass split fraction required with respect to Configuration C2E1 even at lower pressures of the $CO_2$ desorber. On the contrary, the lower optimal $P_{CO_2des}$ value obtained for Configuration C2E2a has the opposite effect, which overall leads to higher $NH_3$ concentrations in the $CO_2$ stream exiting the top of the $CO_2$ desorber thus to greater water make-up flowrates as a consequence of the greater water make-up flowrate required in the $CO_2$-WW section. Such increase in $F_{H_2O}^{in}$ when introducing the LVC, which is minor if compared with the process water requirements of the advanced configurations of the FG post-conditioning section using the SNA and the ANA, is allowed because it has a negligible effect

**Table 8**
Process operating conditions and performance indicators of the advanced configurations of the $CO_2$ desorber and of the solvent recovery section that allow for optimal operation in terms of minimum specific equivalent work requirements. The optimal $CO_2$ absorber conditions and $CO_2$ absorber productivity correspond in all cases to those of the mid $\hat{c}_{NH_3}$ case shown in Table 3. All cases have been simulated considering the reference configuration of the FG post-conditioning section operating at the optimal set of operating conditions ("Opt") of the FG-WW column indicated in Table 6; the corresponding dimension of the FG-WW column can be found in Table 5. The pinch point temperature in the rich/lean, in the $NH_3$-rich/$NH_3$-lean and in the rich purge/lean purge heat exchangers has been set to 3 °C, while it has been set to 10 °C in the reboilers and in the heat exchanger introduced with the MPD.

| Variable | Configuration | | | | | | | | |
|---|---|---|---|---|---|---|---|---|---|
| | C2 | C2E1 | C2E2a | C2E2b | C2E2c | C2E2d | C2E3 | C3E3 | |
| | IS | RecVC (+IS) | LVC(4) (+RecVC+IS) | LVC(3) (+RecVC+IS) | LVC(4,3) (+RecVC+IS) | LVC(4,3,2) (+RecVC+IS) | MPD (+RecVC+IS) | VIS (+MPD+RecVC) | |
| **$CO_2$ desorber parameters** | | | | | | | | | |
| $P^{top}_{CO_2 des}$ [bar] | 19.5 | 19.5 | 17.0 | 7.0 | 9.5 | 7.0 | 32.3 | 32.3 | 32.3 |
| $P^{bot}_{CO_2 des}$ [bar] | 20.0 | 20.0 | 17.5 | 7.5 | 10.0 | 7.5 | 16.4 | 16.4 | 16.4 |
| $f_{cr}$ [-] | 0.0500 | 0.0500 | 0.0400 | 0.0600 | 0.0450 | 0.0425 | 0.0400 | 0.0400 | 0.0400 |
| **Solvent recovery section parameters** | | | | | | | | | |
| $N_{IS}$ [-] | 9 | 13 | 13 | 13 | 13 | 13 | 13 | 13 | 13 |
| $s^{IS}_{NH_3\text{-rich}}$ [-] | 2 | 3 | 3 | 3 | 3 | 3 | 3 | 3 | 3 |
| $F_{RecVC}$ [$kg\,t^{-1}_{CO_2 captured}$] | 0.0 | 62.3 | 63.4 | 63.4 | 64.2 | 65.2 | 61.4 | 64.0 | 71.8 |
| $P_{IS}$ [bar] | 1.05 | 1.05 | 1.05 | 1.05 | 1.05 | 1.05 | 1.05 | 0.35 | 0.10 |
| **Heat integration performance** | | | | | | | | | |
| $q_{HTX,rich/lean}$ [$MJ_{th}\,kg^{-1}_{CO_2 captured}$] | 8.33 | 8.42 | 6.75 | 4.60 | 4.92 | 3.81 | 8.04 | 8.04 | 8.04 |
| $\Delta T_{c,rich/lean}$ [K] | 4.1 | 4.3 | 3.5 | 4.6 | 3.7 | 3.2 | 3.5 | 3.5 | 3.6 |
| $\Delta T_{h,rich/lean}$ [K] | 11.2 | 11.2 | 4.1 | 3.0 | 3.0 | 3.0 | 11.2 | 11.2 | 11.2 |
| $x_{V,hot CO_2\text{-rich}}$ [mole frac.] | 0.013 | 0.013 | 0.002 | 0.000 | 0.000 | 0.000 | 0.013 | 0.013 | 0.013 |
| $q_{HTX,FG-WW}$ [$MJ_{th}\,kg^{-1}_{CO_2 captured}$] | 0.12 | 0.12 | 0.12 | 0.12 | 0.12 | 0.12 | 0.12 | 0.09 | 0.06 |
| $\Delta T_{c,FG-WW}$ [K] | 3.0 | 3.0 | 3.0 | 3.0 | 3.0 | 3.0 | 3.0 | 3.0 | 3.0 |
| $\Delta T_{h,FG-WW}$ [K] | 7.9 | 8.5 | 8.4 | 7.9 | 8.2 | 8.0 | 8.4 | 3.5 | 3.3 |
| $x_{V,hot NH_3\text{-rich}}$ [mole frac.] | 0.005 | 0.006 | 0.006 | 0.005 | 0.006 | 0.006 | 0.006 | 0.000 | 0.000 |
| $q_{HTX,IS}$ [$MJ_{th}\,kg^{-1}_{CO_2 captured}$] | 0.02 | 0.02 | 0.02 | 0.02 | 0.02 | 0.02 | 0.02 | 0.01 | N/A |
| $\Delta T_{c,IS}$ [K] | 39.2 | 41.9 | 39.2 | 40.9 | 38.9 | 38.2 | 45.4 | 22.7 | N/A |
| $\Delta T_{h,IS}$ [K] | 3.0 | 3.0 | 3.0 | 3.0 | 3.0 | 3.0 | 3.0 | 3.0 | N/A |
| $x_{V,hotpurge}$ [mole frac.] | 0.000 | 0.000 | 0.000 | 0.000 | 0.000 | 0.000 | 0.000 | 0.000 | N/A |
| **Consumption of chemicals** | | | | | | | | | |
| $F^{in}_{H_2O}$ [$kg\,t^{-1}_{CO_2 captured}$] | 9.14 | 7.30 | 12.41 | 14.03 | 17.28 | 22.46 | 2.86 | 2.96 | 3.03 |
| $F^{in}_{chem,NH_3}$ [$kg\,t^{-1}_{CO_2 captured}$] | 1.46 | 1.44 | 1.47 | 1.46 | 1.49 | 1.60 | 1.43 | 1.43 | 1.41 |
| **Energetic performance** | | | | | | | | | |
| $q_{reb,CO_2}$ [$MJ_{th}\,kg^{-1}_{CO_2 captured}$] | 2.19 | 2.03 | 1.94 | 1.96 | 1.91 | 1.79 | 1.86 | 1.84 | 1.81 |
| $T_{reb,CO_2}$ [°C] | 143.9 | 143.9 | 134.7 | 117.7 | 121.3 | 115.4 | 139.1 | 139.1 | 139.1 |
| $q_{reb,IS}$ [$MJ_{th}\,kg^{-1}_{CO_2 captured}$] | 0.17 | 0.15 | 0.15 | 0.15 | 0.15 | 0.15 | 0.14 | 0.14 | 0.16 |
| $T_{reb,IS}$ [°C] | 100.1 | 100.1 | 100.1 | 100.1 | 100.1 | 100.1 | 100.1 | 72.3 | 45.7 |
| $e$ [$MJ_{el}\,kg^{-1}_{CO_2 captured}$] | 0.287 | 0.321 | 0.371 | 0.483 | 0.453 | 0.557 | 0.366 | 0.386 | 0.417 |
| $\omega$ [$MJ\,kg^{-1}_{CO_2 captured}$] | 1.042 | 1.018 | 1.009 | 1.070 | 1.038 | 1.091 | 0.994 | 0.998 | 1.013 |
| $\omega$ savings [%] | N/A | 2.3 | 3.2 | −2.7 | 0.4 | −4.7 | 4.6 | 4.2 | 2.8 |

on the reboiler duty of the IS. In fact, $q_{reb,IS}$ is mainly governed by variations in the greater flowrates of the $NH_3$-rich stream and of the purge stream, and not by small variations of water flowrate from the $CO_2$-WW section, as it can be inferred from the results shown in Fig. 11(a). The trends described for Configuration C2E2a including the LVC(4) can be extended for advanced configurations in which the $CO_2$-lean stream exiting the bottom of the $CO_2$ desorber is expanded to lower pressures either in one stage, as for Configuration C2E2b with the LVC(3), or in two or three stages, as for Configuration C2E2c with the LVC(4,3) and Configuration C2E2d with the LVC(4,3,2), respectively. Nevertheless, none of the LVC configurations with expansion to lower pressures decreases the specific equivalent work of the overall capture process with respect to Configuration C2E2a. Although expanding the $CO_2$-lean stream to lower pressures further decreases $q_{reb,CO_2}$, its effect on the overall specific equivalent work is compensated or outgrown by the increase in the electrical work required to compress increasing flowrates of vapour to the pressure of the $CO_2$ desorber; while the thermal energy provided to the bottom of the $CO_2$ desorber increases, lower expansion pressures also decreases the distribution coefficient of $CO_2$ with respect to $NH_3$ in the recycled vapour stream, which approaches 1 at atmospheric pressure, thus worsening the separation of $CO_2$ from $NH_3$ (and $H_2O$) in the expansion stages of the LVC.

As far as the MPD is concerned, Configuration C2E3 decreases the specific equivalent work of the capture process by 4.6% with respect to the reference Configuration C2, which doubles the exergy savings achieved when only using the IS with the RecVC and that outperforms the energetic performance of Configuration C2E2a with the LVC(4). As for the RecVC and for the LVC, the improvement in the energetic performance of the capture process is triggered by a decrease of the reboiler duty of the $CO_2$ desorber, which reaches values as low as 1.86 $MJ_{th}\,kg^{-1}_{CO_2 captured}$ at conditions that minimize the specific equivalent work of Configuration C2E3. Similarly, such decreases in the $q_{reb,CO_2}$ values are obtained at the cost of increasing the electrical work required for the compression of the vapour exiting the top of the lower section of the $CO_2$ desorber to the higher pressure of the upper section of the column. The thermal energy gained by such compressed vapour stream is used to heat up the $CO_2$-rich stream before it enters the $CO_2$ desorber and to provide thermal energy for further $CO_2$ stripping in the upper section of the $CO_2$ desorber. At minimal specific equivalent work, the compressed vapour of the MPD adds 0.20 $MJ_{th}\,kg^{-1}_{CO_2 captured}$ to the $CO_2$-rich stream and still enters the upper section of the $CO_2$ desorber at 137.9 °C. In addition, the partial condensation of the compressed vapour stream before entering the bottom of the $CO_2$ desorber upper section also allows for an additional equilibrium stage for the separation of $CO_2$ from $NH_3$ (and $H_2O$). The higher pressure in the upper section of the $CO_2$ desorber facilitates the removal of $NH_3$ from the $CO_2$ stream and allows to decouple the reboiler duty minimization from the control of the $NH_3$ slip in the exiting $CO_2$ stream. Therefore, the optimal $f_{cr}$ value in this case maximizes the heat exchanged in the rich/lean heat exchanger without increasing the $NH_3$ slip in the $CO_2$

stream thus the water make-up flowrate to the $CO_2$-WW section and the reboiler duty of the IS. These facts are confirmed by the results of Configuration C2E3 with the MPD shown in Table 8, where: (i) $q_{HTX,rich/lean}$ reaches similar values to those obtained for configurations C2 and C2E1 at lower $CO_2$ desorber reboiler pressures thus for lower temperatures of the hot $CO_2$-lean stream; (ii) the optimal value of $f_{cr}$ that minimizes the overall specific equivalent work is lower than for the same configuration without the MPD, i.e. Configuration C2E1, even when $P^{bot}_{CO_2des}$ is decreased from 20.0 to 16.4 bar—the optimal $f_{cr}$ value is the same as for Configuration C2E2a with the LVC(4) but Configuration C2E3 also operates at lower $P^{bot}_{CO_2des}$; and, (iii) $F^{in}_{H_2O}$ is decreased with respect to Configuration C2E1 without the MPD, resulting from a better control of $NH_3$ emissions in the upper section of the $CO_2$ desorber. As a consequence, the MPD achieves lower $q_{reb,CO_2}$ values than the LVC(4) at optimal process operating conditions that minimize the specific equivalent work of the full capture process. Nevertheless, when comparing the results obtained with configurations C2E2a and C2E3 shown in Table 8, one can notice that the superior energetic performance of the MPD in comparison with the LVC(4) derives also from a lower increase of the electrical work demand; in the case of the MPD, the higher pressure at which the upper section of the $CO_2$ desorber operates allows to decrease the $CO_2$ compression work.

Regarding the VIS, it mainly affects the performance of the solvent recovery section, where the reboiler temperature of the stripping column decreases from 100.1 to 72.3 and to 45.7 °C when decreasing the pressure from 1.05 to 0.35 and to 0.10 bar, respectively, without affecting significantly the reboiler duty values. The optimal process operating conditions that minimize the specific equivalent work of the capture process and the remaining performance indicators are neither affected significantly. The exception is the rich purge/lean purge heat exchanger, which cannot be implemented for the lower $P_{IS}$ value due to the fact that the rich purge stream has higher temperature than the $NH_3$-lean stream exiting the bottom of the VIS. Although low temperature excess (waste) heat might be available in the $CO_2$ point source for integration with the capture plant, the specific equivalent work computations provided in Table 8 only consider thermodynamic criteria and do not account for application scenarios. Therefore, operating the IS at vacuum conditions does not allow to decrease the specific equivalent work of the capture process since the increase in the electrical work demand driven by the vacuum pump, whose efficiency decreases for lower pressures, is not compensated by the decrease in the specific equivalent work associated with the reboiler duty of the VIS.

Something common to all advanced configurations presented in Table 8 is that they do not modify significantly the flowrate of aqueous $NH_3$ solution make-up, $F^{in}_{chem,NH_3}$, with respect to the reference Configuration C2. Therefore, the advanced configurations developed here to improve the energetic performance of the capture process do not affect the performance of the FG post-conditioning section and could also be combined equally with any of the advanced configurations of the FG post-conditioning section developed in this work.

At this point, it is worth making a clarification about the simulation of the heat exchangers in Aspen Plus. As aforementioned, the proper simulation and design of such heat exchangers is of paramount importance to obtain optimal, at the same time feasible, reboiler duties thus energetic performances of the capture process. As far as the energetic performance of the capture process is concerned, the most critical heat exchanger is the rich/lean heat exchanger, which strongly affects the $CO_2$ desorber reboiler duty, the main energy consumer of the capture process. When the RSS is in place, the flowrate of the $CO_2$-rich stream flowing through the rich/lean heat exchanger, i.e. the cold stream, might be smaller than the flowrate of the $CO_2$-lean stream, i.e. the hot stream. As a consequence, the heat capacity of the former stream might be smaller than the heat capacity of the latter, so that the pinch point temperature might be reached at the hot side of the heat exchanger, instead of at the cold side as in the case of a configuration without RSS. Nevertheless, the higher $CO_2$ concentration in the $CO_2$-rich stream may lead to partial vaporization before leaving the rich/lean heat exchanger when approaching the temperature of the hot $CO_2$-lean stream, as confirmed by the results of molar vapour fraction of the hot $CO_2$-rich stream exiting the rich/lean heat exchanger, $x_{V,hotCO_2-rich}$, given in Table 8. Consequently, the heat transferred to the $CO_2$-rich stream towards the exit of the rich/lean heat exchanger is used as latent heat and not as sensible heat to increase the temperature of the fluid. Therefore, the pinch point temperature in the rich/lean heat exchanger when using the RSS might be reached internally, instead of being reached at the cold or at the hot side as the values shown in Table 8 for $\Delta T_{c,rich/lean}$ and $\Delta T_{h,rich/lean}$, respectively, confirm. Therefore, the rich/lean heat exchanger has been simulated in Aspen Plus, Version 8.6, by means of a "MHeatX" exchanger block divided in zones, which allows to identify the internal pinch point temperature. On the contrary, setting the pinch point at the cold side of the rich/lean heat exchanger when the RSS has been implemented leads to infeasible heat exchanger designs and $CO_2$ desober reboiler duties, thus to misleading optimal process operating conditions and energetic performances of the capture process, as in the case of Jiang et al. [20]. Design considerations for other critical heat exchangers where the pinch point temperature has been set to 3 °C, i.e. in the $NH_3$-rich/$NH_3$-lean heat exchanger and in the rich purge/lean purge heat exchanger of the solvent recovery section, have been introduced in Section 4.2.1 when describing the advanced Configuration C2 using the IS. The heat integration performance results given in Table 8 for such heat exchangers confirm the avoidance of temperature crossovers or pinch point temperatures below 3 °C. As far as the $NH_3$-rich/$NH_3$-lean heat exchanger is concerned, it is similarly simulated by means of a "MHeatX" exchanger block in Aspen Plus with zones division in order to be able to predict the internal pinch point temperature, if needed. Nevertheless, the heat integration performance results given in Table 8 show that the pinch point temperature in the $NH_3$-rich/$NH_3$-rich heat exchanger is always reached at the cold side, i.e. $\Delta T_{c,FG-WW}$. Since the goal of the $NH_3$-rich/$NH_3$-rich heat exchanger is not only to minimize the reboiler duty in the IS (or VIS), but also the chilling demand of the $NH_3$-lean stream before entering the FG-WW column, purging a fraction of the hot $NH_3$-lean stream before entering the $NH_3$-rich/$NH_3$-lean heat exchanger aims at equalling the heat capacities of the cold and the hot stream such that the temperature difference between the hot stream and the cold stream remains constant along the counter-current heat exchanger. Nevertheless, the hot side temperature difference increases due to the vaporization of the $NH_3$-rich stream when approaching the temperature of the hot $NH_3$-lean stream, as shown by the results of $\Delta T_{h,FG-WW}$ and $x_{V,hotNH_3-rich}$ given in Table 8. Regarding the rich purge/lean purge heat exchanger in the solvent recovery section, it has been simulated in Aspen Plus by means of a "HeatX" exchanger block, setting the pinch point temperature at the hot side, $\Delta T_{h,IS}$, since the heat capacity of the rich purge stream is always smaller than that of the lean purge stream and the former stream is always at pressures equal or above 7 bar that avoid its partial vaporization within the heat exchanger thus a temperature crossover.

The potential of the advanced configurations developed in this work for the improvement of the energetic performance of $NH_3$-based capture processes can only be assessed in full perspective when considering the flexibility that they allow for the consumption of different types of energy, i.e. electricity, medium–high temperature steam or low temperature steam. With that aim, Fig. 13 shows the results obtained for the advanced configurations aiming at improving the energetic performance of $NH_3$-based capture processes in the plane specific electrical work vs. specific reboiler duty. In order to also include the differentiation between the medium–high temperature and low temperature steam demand when analysing the flexibility of the capture process with respect to different types of energy, the reboiler duty, $q_{reb}$, represented in the left-hand side plots of Fig. 13 corresponds to the results of $q_{reb,CO_2} + q_{reb,IS}$ obtained for advanced configurations using the IS, where medium temperature steam at 110.1 °C is required

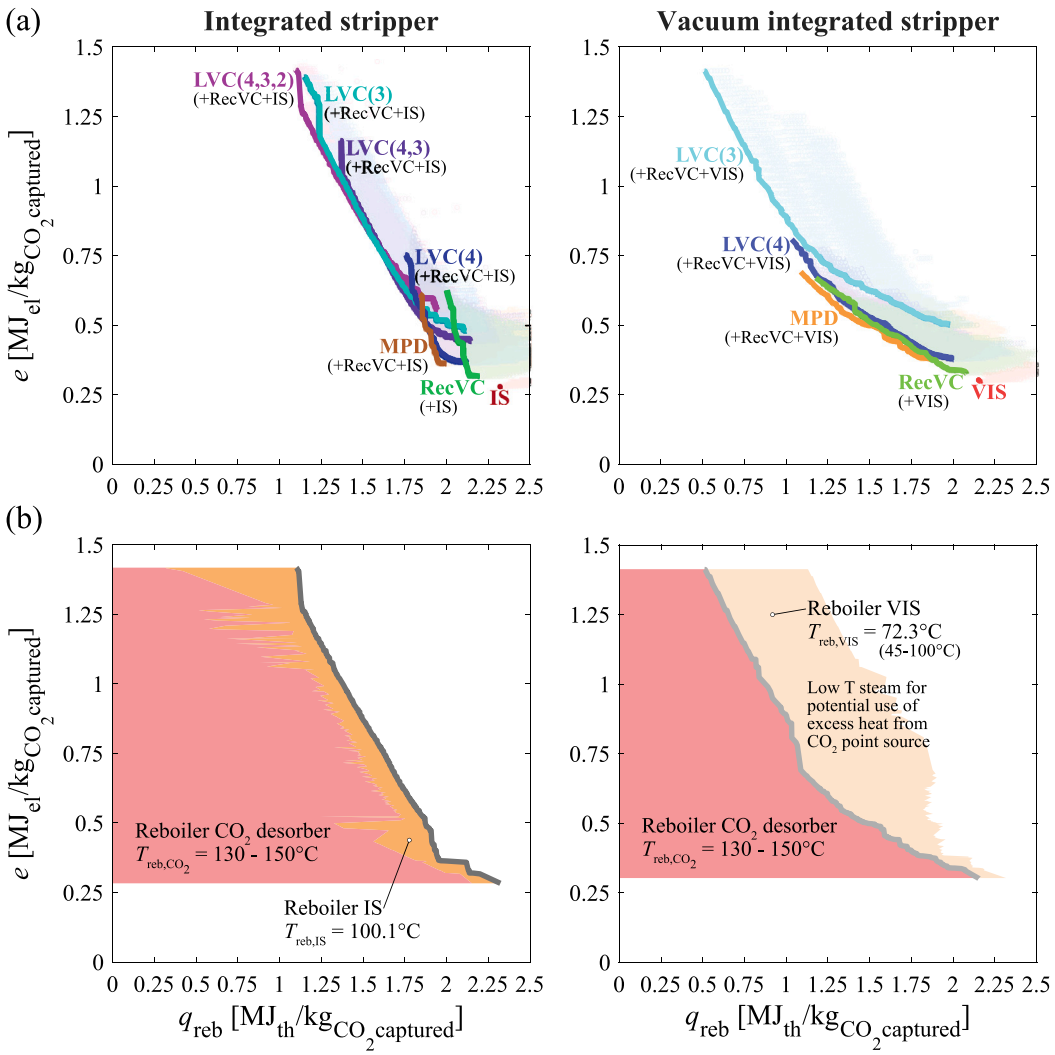


**Fig. 13.** Energetic performance of the advanced configurations of the $CO_2$ desorber in the plane specific electrical consumption vs. specific reboiler duty. The left-hand side plots have been obtained with the IS considering $q_{reb} = q_{reb,CO_2} + q_{reb,IS}$, while the right-hand side plots have been obtained with the VIS operating at 0.35 bar considering $q_{reb} = q_{reb,CO_2}$. (a) Specific electricity consumption vs. specific reboiler duty for each set of operating conditions that led to a converged simulation fulfilling specifications and constraints (○), colour-coded depending on the type of configuration; the pareto fronts (—), also colour-coded depending on the type of configuration, have been defined by the assemble of points at the frontier of each cloud. (b) Share of each reboiler duty in the overall steam demand along the overall pareto front (—) composed of the pareto fronts of all configurations in (a). (For interpretation of the references to colour in this figure legend, the reader is referred to the web version of this article.)

in addition to the high temperature steam, i.e. up to 160 °C, needed in the reboiler of the $CO_2$ desorber. On the other hand, the reboiler duty represented in the right-hand side plots of Fig. 13 corresponds only to the results of $q_{reb,CO_2}$ obtained with advanced configurations using the VIS, assuming that the low temperature steam required in the solvent recovery section, $q_{reb,IS}$, can be produced from excess heat available in the $CO_2$ point source. As an example of the latter, the results shown in the right-hand side plots of Fig. 13 have been obtained for advanced configurations using a VIS that operates at 0.35 bar thus requiring low temperature steam at 82.3 °C. Each symbol in Fig. 13(a) corresponds to a different set of operating conditions of the capture process, which has produced a converged simulation meeting specifications and constraints. Specifically, 34,366 simulations and 20,496 simulations are included in the left-hand side plot and in the right-hand side plot of Fig. 13(a), respectively, obtained at different operating conditions of the $CO_2$ absorber, solvent recovery section and $CO_2$ desorber. Specific reboiler duty minimization and specific electrical work minimization are opposing objectives, defining a frontier where the specific reboiler duty can only be decreased at the cost of increasing the specific electrical work demand (and vice-versa), the so-called "pareto front". Such pareto front is found for each advanced configuration shown in Fig. 13(a). At the same time, an overall pareto front is defined, as shown in Fig. 13(b), composed of the pareto fronts of different advanced configurations whose performance is optimal in different $q_{reb}$ ranges. In this regard, the introduction of the RecVC decreases the minimum specific reboiler duty demand but leads to higher specific electrical work requirements with respect to the reference configuration with the IS (or the VIS). Adding the LVC to the RecVC further decreases the minimum reboiler duty but also requires greater minimum specific electrical work demands. Within the LVC configurations, expanding the liquid stream exiting the reboiler of the $CO_2$ desorber to lower pressures achieves a progressive reduction of the minimum reboiler duty, along with progressive increments of the specific electrical work demand, as it can be seen in the left-hand side plot of Fig. 13(a) when comparing the LVC(4), the LVC(4,3) and the LVC(4,3,2). Moreover, expanding the $CO_2$-lean stream in one stage instead of in two stages to the same pressure level allows to reach lower minimum specific reboiler duties but with very similar energetic performance, as it can be seen when comparing the LVC(3) with the LVC(4,3) in the left-hand side plot of Fig. 13(a). As far as the advanced configurations with the MPD are concerned, they allow to achieve minimum specific reboiler duties as low as those obtained

with the LVC(4), but at lower minimum electrical work demands, which confirms the superior energetic performance of the MPD in comparison with the LVC(4) obtained in the results presented in Table 8. Similar evolution in the optimal advanced configuration that minimizes the minimal electrical work demand for decreasing values of the specific reboiler duty can be observed when considering $q_{reb,CO_2} + q_{reb,IS}$, as in the left-hand side plots for configurations using the IS, or $q_{reb,CO_2}$, as in the right-hand side plots using the VIS. Only MPD configurations are optimal for a broader range of reboiler duties when minimizing $q_{reb,CO_2}$ instead of $q_{reb,CO_2} + q_{reb,IS}$, at the cost of a narrower range of optimality for LVC configurations. For the sake of visuality, only the results obtained with the LVC(3) are represented in the right-hand side plots of Fig. 13 with the VIS, as representative of the LVC configurations with expansion of the $CO_2$-lean stream to lower pressures, since its performance is intermediate between that obtained with the LVC(4,3) and with the LVC(4,3,2), and the process operating conditions follow the same trends.

Regarding the contributors to the reboiler duty, the plots in Fig. 13(b) show that the relative contribution to the total reboiler duty is dominated by the reboiler duty of the $CO_2$ desorber independently of the type of reboiler duty minimization approach implemented, i.e. $q_{reb,CO_2} + q_{reb,IS}$ for the left-hand side plot or $q_{reb,CO_2}$ for the right-hand side plot. Also in both cases, the $q_{reb,CO_2}$ values along the overall pareto front decreases from around 2.2 $MJ_{th}\,kg^{-1}_{CO_2captured}$ to approximately 0.5 $MJ_{th}\,kg^{-1}_{CO_2captured}$. Nevertheless, the $q_{reb,CO_2}$ minimization shown in the right-hand side plot allows for a steeper decrease of the high temperature steam demand at lower-to-medium electrical work requirements, which will establish a competitive advantage in case of low temperature excess heat is available at the $CO_2$ point source to generate the steam required in the solvent recovery section.

The breakdowns of the specific electrical work demand along the overall pareto fronts shown in Fig. 13(b) are illustrated in figures included in the *Supplementary Material*. In addition, these figures also show the ranges of $q_{reb}$ for which each advanced configuration included in Fig. 13(a) is optimal, along with the evolution of the operating conditions of the solvent recovery section, of the $CO_2$ desorber and of the $CO_2$ absorber that allow to minimize the specific electrical work demand when varying the minimum reboiler duty, i.e. along the overall pareto fronts shown in Fig. 13(b). Although the effect of the process decision variables on the energetic performance of the advanced configurations shown in Fig. 13 is subject to complex interdependencies, the following qualitative trends can be inferred for the optimal process configurations and conditions:

- The decrease in the minimum specific reboiler duty is mainly achieved at the cost of increasing the electrical work required for vapour compression in the multi-stage compressor used for the configurations including the RecVC and the LVC. Such increase is mainly driven by greater flowrates of vapour recycled from the solvent recovery section to the $CO_2$ desorber, $F_{RecVC}$.
- Greater $F_{RecVC}$ are achieved by decreasing the number of equilibrium stages in the IS (or VIS), $N_{IS}$. An exception is the range of low $q_{reb,CO_2}$ values in which the LVC(3) is the optimal configuration in combination with the VIS, where the design of the latter always corresponds to the minimum value of $N_{IS}$ (and associated value of $s^{IS}_{NH_3-rich}$) that allows to maximize $F_{RecVC}$. Such increase in $F_{RecVC}$ also leads to increasing electrical work demand of the vacuum pump of the VIS when starting to decrease the minimum $q_{reb,CO_2}$ from high values.
- When LVC configurations are optimal, the increase of the minimal electrical work demand that allows to minimize the specific reboiler duty is also driven significantly by the increasing pressures required in the $CO_2$ desorber, which lead to steeper increments of the electrical work required for vapour compression in the multi-stage compressor of the RecVC and the LVC.
- Increasing pressures in the $CO_2$ desorber: (i) increase the electrical work required by the auxiliaries, which include the pumping of the $CO_2$-rich stream to the $CO_2$ desorber, and (ii) decrease the electrical work associated with the $CO_2$ compression.
- Values of $P^{bot}_{CO_2des}$ up to 67.5 bar can be reached for LVC configurations because the expansion of the liquid exiting the reboiler of the $CO_2$ desorber decreases the temperature of the hot $CO_2$-lean stream thus of the $CO_2$ desorber, including the reboiler. This allows to increase the pressure of the column without exceeding the maximum temperature allowed in the capture process for aqueous $NH_3$ solutions (see Table 2).
- The optimal value of $P^{bot}_{CO_2des}$ that allows to minimize the energy consumption of $NH_3$-based capture processes is associated with an optimal value of cold-rich bypass split fraction, $f_{cr}$.
- In the case of the $q_{reb,CO_2}$ minimization, there exists an optimal value of $P^{bot}_{CO_2des}$, which ranges between 15 and 25 bar, that allows for the best energetic performance in the plane $e$ vs. $q_{reb,CO_2}$; only the optimal value of $P^{bot}_{CO_2des}$ steadily increases from 20 to 67.5 bar to reach low $q_{reb,CO_2}$ values when the configuration using the LVC(3) is optimal. Since the steam required in the VIS is not considered in the process optimization, the corresponding optimal values of $f_{cr}$ only aim at maximizing the heat exchanged in the rich/lean heat exchanger that allows to minimize $q_{reb,CO_2}$, without considering the $NH_3$ slip to the $CO_2$ stream. Therefore, the evolution of the optimal values of $f_{cr}$ does not follow a clear trend and presents discontinuities when changing the optimal configurations along $q_{reb,CO_2}$.
- The minimization of $q_{reb,CO_2} + q_{reb,IS}$ leads to a continuous variation of the optimal $f_{cr}$ value, while the corresponding optimal $P^{bot}_{CO_2des}$ values present discontinuities when changing the optimal advanced configuration. In that case, the optimal value of $f_{cr}$ also aims at a proper control of $NH_3$ emissions from the $CO_2$ desorber that avoids excessive water make-up flowrates in the $CO_2$-WW section thus increasing values of $q_{reb,IS}$.
- The optimal apparent $NH_3$ concentration in the solvent—and associated remaining $CO_2$ absorber optimal operating conditions given in Table 3—is also influenced by the type of $q_{reb}$ minimization carried out. At low $q_{reb}$ values, while the minimization of $q_{reb,CO_2}$ requires high values of $\hat{c}_{NH_3}$, i.e. 9 $mol_{NH_3}\,kg^{-1}_{H_2O}$, the $q_{reb,CO_2} + q_{reb,IS}$ minimization leads to lower $\hat{c}_{NH_3}$ values, i.e. 5 or 7 $mol_{NH_3}\,kg^{-1}_{H_2O}$. Greater apparent $NH_3$ concentrations in the solvent increase the flowrate of vapour recycled to the bottom of the $CO_2$ desorber, which decreases $q_{reb,CO_2}$, but also leads to greater reboiler duty demands in the IS (or VIS), as shown in Fig. 11(a). At high $q_{reb}$ values, the optimal set of operating conditions of the $CO_2$ absorber found for the reference configuration is also preferred for the other advanced configurations, i.e. 7 $mol_{NH_3}\,kg^{-1}_{H_2O}$.

In order to exemplify their full potential as well as their adaptability and versatility to different types of energy, advanced configurations aiming at improving the energetic performance of $NH_3$-based capture processes have been finally assessed in terms of the minimum SPECCA index achievable for the application scenarios defined in Section 4.3.2, with the energy parameters provided in Table 7. In this regard, Table 9 shows the advanced configuration and the associated set of operating conditions that minimizes the SPECCA index of the overall capture process, $\zeta$, for each application scenario (labelled as "Best"). Additionally, Table 9 also provides, if possible for a given scenario, the advanced configuration that minimizes the SPECCA index without the requirement of producing steam from sources other than the excess heat available in the $CO_2$ point source, along with the associated set of operating conditions of the capture process (labelled as "w/o Steam"). Configuration C2 using the IS (illustrated in Fig. 7) has been used also here as reference configuration; the corresponding optimal sets of operating conditions that minimize $\zeta$ in each application scenario are also given in Table 9 (labelled as "Ref"). Along with the minimum

**Table 9**
Process operating conditions and performance indicators obtained with: (i) Configuration C2 ("Ref."), which is considered as the reference configuration in this section, (ii) the advanced configuration that allows to obtain the minimum $\zeta$ value ("Best"), and (iii) if possible, the advanced configuration with the lowest value of $\zeta$ that only uses excess heat available in the $CO_2$ point source for the reboilers of the distillation columns, thus avoiding additional steam requirements ("w/o Steam), for the scenarios defined in Section 4.3.2 with the energy parameters provided in Table 7. The optimal set of operating conditions of the $CO_2$ absorber are represented by the concentration of apparent $NH_3$ in the $CO_2$-lean stream, $\hat{c}_{NH_3}$; the remaining conditions of the $CO_2$ absorber, as well as the associated $CO_2$ absorber productivity can be found in Table 3. All cases have been simulated considering the reference configuration of the FG post-conditioning section operating at the optimal set of operating conditions of the FG-WW column indicated in Table 6; the corresponding dimension of the FG-WW column can be found in Table 5. The pinch point temperature in the rich/lean, $NH_3$-rich/$NH_3$-lean and rich purge/lean purge heat exchangers has been set to 3 °C, while it has been set to 10 °C in the reboilers and in the heat exchanger introduced with the MPD.

| | Configuration | | | | | | | | | | | | | |
|---|---|---|---|---|---|---|---|---|---|---|---|---|---|---|
| | Cement plant application | | | | | | Steel plant application | | | | | Refinery application | | |
| | Scenario 1.a | | Scenario 1.b | | Scenario 1.c | | Scenario 2.a | | Scenario 2.b | | | Scenario 3 | | |
| Variable | Ref. C2 | Best C3E3 | Ref. C2 | Best C3E3 | Ref. C2 | Best C3E2b | Ref. C2 | Best C3E3 | Ref. C2 | Best C3E3 | w/o Steam C3E2b | Ref. C2 | Best C3E3 | w/o Steam C2E2d |
| | IS | MPD +RecVC +VIS | IS | MPD +RecVC +VIS | IS | LVC(3) +RecVC +VIS | IS | MPD +RecVC +VIS | IS | MPD +RecVC +VIS | LVC(3) +RecVC +VIS | IS | MPD +RecVC +VIS | LVC(4,3,2) +RecVC +IS |
| **$CO_2$ absorber parameters** (see Table 3 for the remaining parameters) | | | | | | | | | | | | | | |
| $\hat{c}_{NH_3}$ [$mol_{NH_3}\ kg^{-1}_{H_2O}$] | 7.0 | 7.0 | 7.0 | 7.0 | 7.0 | 5.0 | 7.0 | 7.0 | 7.0 | 7.0 | 9.0 | 7.0 | 9.0 | 9.0 |
| **$CO_2$ desorber parameters** | | | | | | | | | | | | | | |
| $P^{top}_{CO_2,des}$ [bar] | 24.5 | 49.8 | 24.5 | 49.8 | 24.5 | 49.5 | 24.5 | 47.3 | 24.5 | 47.3 | 44.5 | 7.0 | 7.3 | 12.0 |
| $P^{bot}_{CO_2,des}$ [bar] | 25.0 | 25.1 | 25.0 | 25.1 | 25.0 | 50.0 | 25.0 | 23.9 | 25.0 | 23.9 | 45.0 | 7.5 | 3.9 | 12.5 |
| $f_{cr}$ [-] | 0.0475 | 0.0325 | 0.0475 | 0.0325 | 0.0475 | 0.0225 | 0.0475 | 0.0350 | 0.0475 | 0.0350 | 0.0275 | 0.0925 | 0.1100 | 0.0375 |
| **Solvent recovery section parameters** | | | | | | | | | | | | | | |
| $N_{IS}$ [-] | 9 | 13 | 9 | 6 | 9 | 5 | 9 | 4 | 9 | 4 | 4 | 9 | 4 | 4 |
| $s^{IS}_{NH_3\text{-rich}}$ [-] | 2 | 3 | 2 | 2 | 2 | 1 | 2 | 2 | 2 | 2 | 2 | 2 | 2 | 2 |
| $F_{RecVC}$ [$kg\ t^{-1}_{CO_2,captured}$] | 0.0 | 64.0 | 0.0 | 97.0 | 0.0 | 91.0 | 0.0 | 189.3 | 0.0 | 189.3 | 247.9 | 0.0 | 280.5 | 337.2 |
| $P_{IS}$ [bar] | 1.05 | 0.35 | 1.05 | 0.10 | 1.05 | 0.10 | 1.05 | 0.10 | 1.05 | 0.10 | 0.10 | 1.05 | 0.35 | 1.05 |
| **Heat integration performance** | | | | | | | | | | | | | | |
| $q_{HTX,rich/lean}$ [$MJ_{th}\ kg^{-1}_{CO_2,captured}$] | 8.89 | 9.08 | 8.89 | 9.09 | 8.89 | 7.49 | 8.89 | 8.96 | 8.89 | 8.96 | 6.69 | 6.12 | 5.32 | 4.32 |
| $\Delta T_{c,rich/lean}$ [K] | 3.9 | 3.0 | 3.9 | 3.1 | 3.9 | 3.1 | 3.9 | 3.6 | 3.9 | 3.6 | 3.0 | 6.9 | 7.5 | 3.2 |
| $\Delta T_{h,rich/lean}$ [K] | 11.3 | 11.5 | 11.3 | 11.5 | 11.3 | 3.3 | 11.3 | 11.3 | 11.3 | 11.3 | 3.0 | 10.7 | 8.5 | 3.0 |
| $q_{HTX,FG-WW}$ [$MJ_{th}\ kg^{-1}_{CO_2,captured}$] | 0.12 | 0.09 | 0.12 | 0.06 | 0.12 | 0.05 | 0.12 | 0.06 | 0.12 | 0.06 | 0.05 | 0.12 | 0.07 | 0.06 |
| $\Delta T_{c,FG-WW}$ [K] | 3.0 | 3.0 | 3.0 | 3.0 | 3.0 | 3.0 | 3.0 | 3.0 | 3.0 | 3.0 | 3.0 | 3.0 | 3.0 | 3.0 |
| $\Delta T_{h,FG-WW}$ [K] | 7.8 | 3.5 | 7.8 | 3.3 | 7.8 | 3.2 | 7.8 | 3.3 | 7.8 | 3.3 | 3.5 | 7.4 | 3.4 | 3.4 |
| $q_{HTX,IS}$ [$MJ_{th}\ kg^{-1}_{CO_2,captured}$] | 0.02 | 0.01 | 0.02 | N/A | 0.02 | N/A | 0.02 | N/A | 0.02 | N/A | N/A | 0.02 | 0.03 | 0.07 |
| $\Delta T_{c,IS}$ [K] | 43.0 | 22.3 | 43.0 | N/A | 43.0 | N/A | 43.0 | N/A | 43.0 | N/A | N/A | 33.9 | 9.5 | 10.6 |
| $\Delta T_{h,IS}$ [K] | 3.0 | 3.0 | 3.0 | N/A | 3.0 | N/A | 3.0 | N/A | 3.0 | N/A | N/A | 3.0 | 3.0 | 3.0 |
| $q_{HTX,MPD}$ [$MJ_{th}\ kg^{-1}_{CO_2,captured}$] | N/A | 0.19 | N/A | 0.19 | N/A | N/A | N/A | 0.19 | N/A | 0.19 | N/A | N/A | 0.40 | N/A |
| $\Delta T_{c,MPD}$ [K] | N/A | 10.0 | N/A | 10.0 | N/A | N/A | N/A | 10.0 | N/A | 10.0 | N/A | N/A | 10.0 | N/A |
| $\Delta T_{h,MPD}$ [K] | N/A | 75.9 | N/A | 75.9 | N/A | N/A | N/A | 75.8 | N/A | 75.8 | N/A | N/A | 69.1 | N/A |
| **Consumption of chemicals** | | | | | | | | | | | | | | |
| $F^{in}_{H_2O}$ [$kg\ t^{-1}_{CO_2,captured}$] | 3.21 | 2.71 | 3.21 | 2.90 | 3.21 | 0.14 | 3.21 | 1.62 | 3.21 | 1.62 | 1.99 | 31.63 | 21.39 | 8.91 |
| $F^{in}_{chem,NH_3}$ [$kg\ t^{-1}_{CO_2,captured}$] | 1.45 | 1.43 | 1.45 | 1.43 | 1.45 | 1.50 | 1.45 | 1.40 | 1.45 | 1.40 | 1.29 | 1.54 | 1.41 | 1.36 |
| **Energetic performance** | | | | | | | | | | | | | | |
| $q_{reb,CO_2}$ [$MJ_{th}\ kg^{-1}_{CO_2,captured}$] | 2.15 | 1.79 | 2.15 | 1.68 | 2.15 | 1.18 | 2.15 | 1.39 | 2.15 | 1.39 | 0.80 | 2.43 | 1.67 | 0.89 |
| $q_{rec,CO_2}$ [$MJ_{th}\ kg^{-1}_{CO_2,captured}$] | 0.09 | 0.09 | 0.09 | 0.09 | 0.09 | 0.09 | 0.00 | 0.00 | 0.80 | 0.80 | 0.80 | 0.95 | 1.54 | 0.89 |
| $T_{reb,CO_2}$ [°C] | 149.4 | 149.5 | 149.4 | 149.5 | 149.4 | 149.3 | 149.4 | 148.2 | 149.4 | 148.2 | 142.6 | 121.9 | 104.4 | 120.0 |
| $q_{reb,IS}$ [$MJ_{th}\ kg^{-1}_{CO_2,captured}$] | 0.17 | 0.14 | 0.17 | 0.22 | 0.17 | 0.21 | 0.17 | 0.43 | 0.17 | 0.43 | 0.55 | 0.18 | 0.64 | 0.79 |
| $q_{rec,IS}$ [$MJ_{th}\ kg^{-1}_{CO_2,captured}$] | 0.10 | 0.14 | 0.10 | 0.20 | 0.10 | 0.20 | 0.00 | 0.43 | 0.10 | 0.43 | 0.55 | 0.18 | 0.64 | 0.79 |
| $T_{reb,IS}$ [°C] | 100.1 | 72.3 | 100.1 | 45.7 | 100.1 | 45.7 | 100.1 | 45.7 | 100.1 | 45.7 | 45.7 | 100.1 | 72.3 | 100.1 |
| $e$ [$MJ_{el}\ kg^{-1}_{CO_2,captured}$] | 0.283 | 0.386 | 0.283 | 0.456 | 0.283 | 1.019 | 0.283 | 0.591 | 0.283 | 0.591 | 1.206 | 0.342 | 0.622 | 0.861 |
| $\zeta$ [$MJ_{LHV}\ kg^{-1}_{CO_2,avoided}$] | 3.539 | 3.153 | 3.293 | 2.824 | 3.070 | 2.404 | 3.831 | 3.247 | 2.479 | 2.107 | 2.880 | 2.765 | 1.592 | 2.002 |

$\zeta$ value achieved for each configuration and application scenario and the corresponding conditions of the process parameters, Table 9 also includes the results obtained for other performance indicators such as consumption of chemicals, specific electricity demand and reboiler temperatures; the total specific reboiler duties required in the $CO_2$ desorber, $q_{reb,CO_2}$, and in the IS (or VIS), $q_{reb,IS}$, and the specific reboiler duty that can be produced by heat recovered from the $CO_2$ point source for the $CO_2$ absorber, $q_{rec,CO_2}$, and for the IS (or the VIS), $q_{rec,IS}$, are also provided. Table 9 also includes the results of the heat integration performance corresponding to the rich/lean heat exchanger, to the $NH_3$-rich/$NH_3$-lean heat exchanger, to the rich purge/lean purge heat exchanger and to the heat exchanger in the MPD configuration. Furthermore, Fig. 14 provides the energy breakdown for the optimal set of operating conditions that minimizes the SPECCA index for the Ref., Best and w/o Steam configurations in each application scenario.

Besides a thermodynamic advantage, as confirmed by the results shown in Table 8, the main improvement introduced by our advanced configurations of the $CO_2$ desorber and solvent recovery section with respect to the benchmark configuration of $NH_3$-based capture processes is that the former are highly versatile towards the consumption of different types of energy. Indeed, the advanced configurations aiming at improving the energetic performance of $NH_3$-based capture processes developed in this work allow to maximize the integration of heat recovered from the $CO_2$ point source and to adapt the process operating conditions to favour the consumption of the most competitive type of energy available at the industrial site. Therefore, the performance of the advanced configurations developed in this work to decrease the energy requirements of $NH_3$-based capture processes improves with respect to the reference configuration if the assessment is carried out not only attending to a thermodynamic criterion, but also considering the specificities of the site where the capture process is applied to in terms

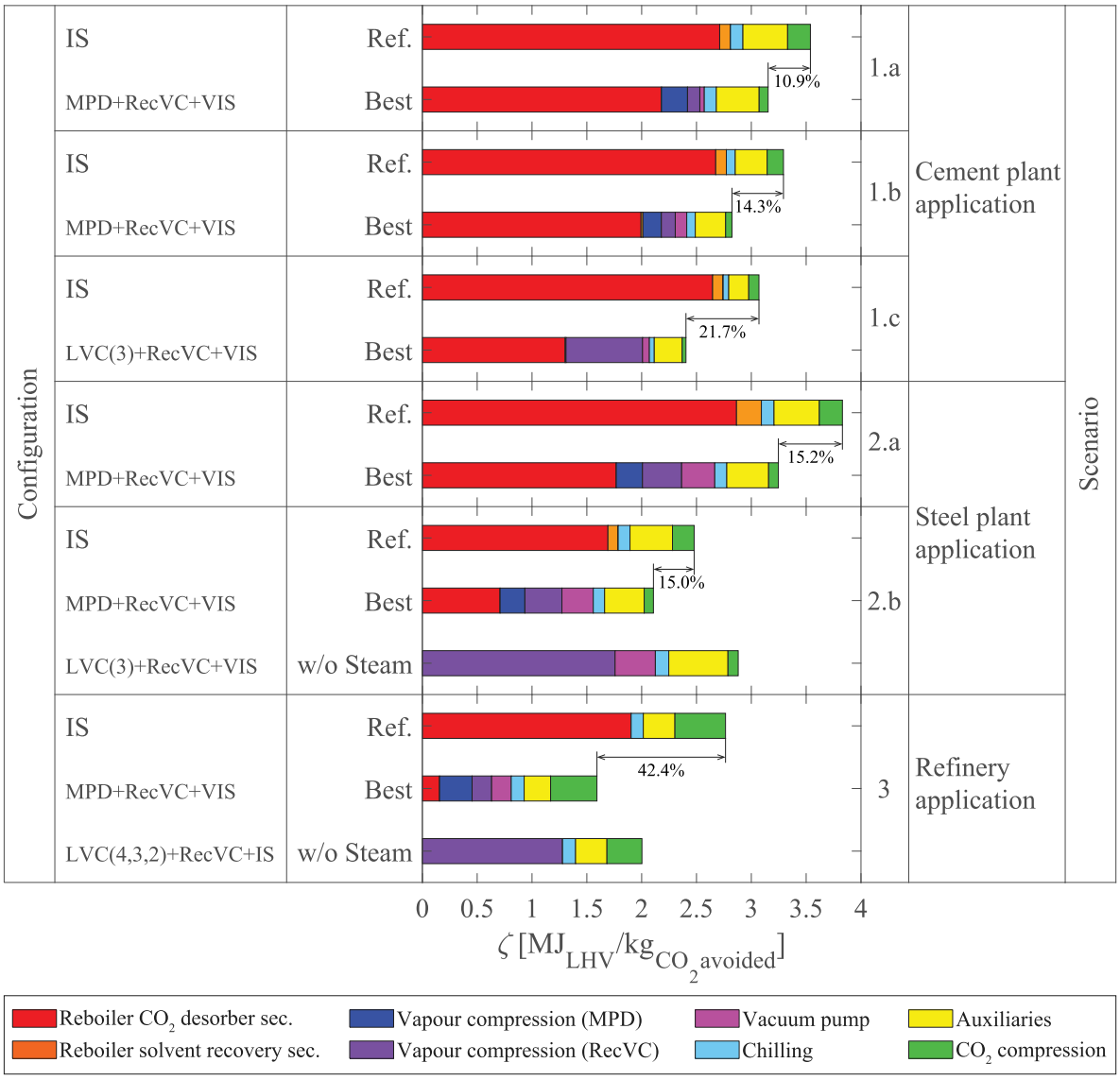


**Fig. 14.** Contributions of the key energy consumers to the minimum SPECCA value, $\zeta$, obtained with: (i) the reference configuration ("Ref."), (ii) the advanced configuration that allows to obtain the minimum $\zeta$ value ("Best"), and (iii) if possible, the advanced configuration with the lowest $\zeta$ value that only uses excess heat available in the $CO_2$ point source for the reboilers of the distillation columns avoiding additional steam requirements ("w/o Steam), for each application scenario, according to the results shown in Table 9. (For interpretation of the references to colour in this figure legend, the reader is referred to the web version of this article.)

of the type of energy available. Namely, our advanced configurations have achieved SPECCA index reductions that range between 10.9% for cement plant application scenarios and 42.9% for the refinery application scenario, with respect to the minimum $\zeta$ value achievable with the reference Configuration C2. The energetic improvements with respect to the minimum energy consumption achievable by the reference configuration increases for: (i) increasing share of renewable energy sources used in the production of the electricity consumed by the capture plant, i.e. the energy savings achieved by the advanced configuration with respect to the reference configuration increase from 10.9% in Scenario 1.a to 21.7% in Scenario 1.c; and, (ii) increasing amounts of specific excess heat available at the $CO_2$ point source, i.e. the energy savings achieved by the advanced configuration with respect to the reference configuration increase from 10.9% in Scenario 1.a to 42.9% in Scenario 3.

As for the specific equivalent work minimization, the advanced configurations including the MPD lead to the lowest SPECCA index for most of the application scenarios considered in this work, i.e. "Best" configurations in Table 9. The exception is Scenario 1.c, where the capture process is applied to a cement plant considering that the capture plant have access to electricity only produced from renewable sources. In that scenario, $\zeta$ is minimized by means of the advanced Configuration C3E2b, which uses the LVC(3). For the remaining application scenarios, even when the optimal advanced configuration that minimizes the SPECCA index always includes the MPD, different optimal set of operating conditions are found for the capture process. For example, increasing the share of renewable sources in the average electricity mix for the cement plant application scenario leads to different optimal design of the stripping column of the solvent recovery section. On the one hand, the optimal number of equilibrium stages, $N_{IS}$, decreases—the value of $s^{IS}_{NH_3-rich}$ adapts accordingly—from 13 in Scenario 1.a to 6 and 5 in Scenarios 1.b and 1.c, respectively, in order to increase the flowrate of vapour distillate recycled to the $CO_2$ desorber, $F_{RecVC}$. On the other hand, the optimal working pressure of the VIS also decreases from 0.35 bar for Scenario 1.a to 0.10 bar for Scenarios 1.b and 1.c. Another example is when modifying the features of the excess heat available in the $CO_2$ point source for integration with the capture plant, i.e. specific amount and/or temperature dependency,

for the same specifications of the electricity imported from the grid. In this regard, the cement plant application Scenario 1.a, the steel plant Scenarios 2 and the refinery Scenario 3 lead to different optimal operating conditions of the $CO_2$ absorber, of the $CO_2$ desorber and/or of the solvent recovery section: First, the optimal number of equilibrium stages of the VIS decreases from 13 in Scenario 1.a to 4 in Scenarios 2 and 3; second, the optimal pressure of the VIS in Scenarios 2 is selected in such a way that the excess heat available at the condenser of the CHP plant can be used, while higher column pressures are preferred instead in Scenarios 1.a and 3; third, aiming at decreasing the $CO_2$ desorber reboiler temperature thus at maximizing the heat recovered from the refinery for integration with the capture plant, the optimal apparent $NH_3$ concentration in the $CO_2$-lean stream increases and the optimal pressure of the lower section of the $CO_2$ desorber decreases in Scenario 3 with respect to Scenarios 1.a and 2.

The flexibility in the possible combinations of different advanced configurations and in the adaptation of the process operating conditions also allow to increase considerably the amount of $CO_2$ that can be captured from the $CO_2$ point source only using the excess heat available at the industrial site thus without additional fuel requirements for steam production. Namely, up to 81% of the $CO_2$ emissions of the steel plant could be captured under the assumptions of Scenario 2.b using electricity imported from the grid and excess heat recovered from the steel plant for the production of the steam required in the reboilers the capture process. Similarly, 42.4% of the $CO_2$ emissions of the refinery application scenario (Scenario 3) could be captured without additional fuel consumption for steam generation. Under the assumptions of Scenario 3, the advanced configuration "w/o Steam" is even able to improve the energetic performance with respect to the "Ref." configuration by 27.6%. In both "w/o Steam" cases, i.e. in Scenarios 2.b and 3, the optimal advanced configurations that minimize the energy consumption use LVC configurations in which the liquid that exits the $CO_2$ desorber is expanded in more that one step, since they allow to minimize the high temperature steam required for solvent regeneration in the $CO_2$ desorber. Also when burning additional fuel for the capture process is not required, further energy savings are expected for increasing share of renewable energy sources used in the production of the electricity consumed by the capture plant.

## 5. Conclusions

Based on the results obtained in this work we propose a new benchmark configuration for $NH_3$-based capture processes, which is shown in Fig. 15.

The new benchmark configuration proposed for $NH_3$-based capture processes is based on the Chilled Ammonia Process and includes the Recycled Vapour Compression and the Multi-pressure Desorber as advanced configuration concepts of the $CO_2$ desorber (process section E3 in Fig. 15), the Vacuum Integrated Stripper as advanced configuration concept of the solvent recovery section (C3), and uses the Standard $NH_3$ Absorber as flue gas water-wash column with the adequate specifications to avoid the use of an acid-wash column in the flue gas post-conditioning section (A1). By proper tuning of the process operating conditions, such advanced configuration allows for minimum specific energy consumption and extensive flexibility of the capture process with respect to the type and the features of the electricity and steam available at the $CO_2$ point source, at the minimum consumption of process water and chemicals, i.e. sulphuric acid and ammonia. This new benchmark configuration proposed for $NH_3$-based capture processes has been built upon a sound understanding of the $CO_2$-$NH_3$-$H_2O$ system and is able to: (i) turn the issue of the volatility of $NH_3$ and its slip to the vapour phase into an opportunity to optimize the energetic performance of the capture process avoiding solid formation; (ii) control efficiently $NH_3$ emissions; and (iii) avoid redundant unit operations thus unnecessary capital costs.

Depending on the boundary conditions and inputs of the capture plant, i.e. specific point source to which it is applied, the new benchmark configuration for $NH_3$-based capture processes proposed as a result of this work can be adapted/modified as follows to improve its performance:

- The Vacuum Integrated Stripper can be operated as an Integrated Stripper at atmospheric pressure by-passing the vacuum pump in the solvent recovery section, in order to adapt the capture process to seasonal changes of the amount and temperature of the excess heat and steam available and/or of the features of electricity.
- If the use of the acid-wash column in the flue gas post-conditioning section is economically favoured by the existence of an ammonium sulphate market, the $NH_3$-based capture process should be run with an acid-wash column in the flue gas post-conditioning section and the operating conditions and specifications of the Standard $NH_3$ Absorber adapted to minimize both the energy consumption of the process and the volume of the flue gas water-wash column.
- If there is no market for ammonium sulphate, but process water is easily available at the capture plant and the economics of waste water treatment are favourable, the energy consumption of the capture process and the volume of the flue gas water-wash column can still be decreased by substituting the Standard $NH_3$ Absorber with the Advanced $NH_3$ Absorber in the flue gas post-conditioning section.
- The removal of the $CO_2$ water-wash section (B) can be considered when applying the $NH_3$-based capture process to $CO_2$-rich flue gases. As pointed out in our previous research [14], increasing $CO_2$ concentrations in the inlet flue gas, i.e. containing around 18 vol% $CO_2$ or above, lead to lower optimal apparent $NH_3$ concentrations in the solvent, i.e. around 7 $\mathrm{mol_{NH_3}\,kg^{-1}_{H_2O}}$ or below, that allow to remove the $CO_2$ water-wash section without penalizing energetically the capture process and avoiding the formation of solids in the condensate of the $CO_2$ stream before compression.
- In the case of having access to cheap and $CO_2$ neutral electricity, or if only excess heat available at the $CO_2$ point source is to be used for the production of the steam required by the capture plant, a Lean Vapour Compression configuration might be preferred instead of the Multi-pressure Desorber, since it allows to minimize the high temperature steam requirements.

Based on the results obtained in this work, the novel advanced configuration concepts of $NH_3$-based processes here proposed should be validated by means of pilot/demo plant experiments, paying special attention to: (i) the heat integration in the advanced configurations of the $CO_2$ desorber; (ii) the performance of the Vacuum Integrated Stripper, where the lower temperatures, i.e. below 100 °C, resulting from the sub-atmospheric pressure at which the column may operate might lead to mass transfer limitations; and, (iii) the control of $NH_3$ emissions in the flue gas water-wash column of the flue gas post-conditioning section.

## CRediT authorship contribution statement

**José-Francisco Pérez-Calvo:** Conceptualization, Methodology, Software, Validation, Formal analysis, Writing - original draft, Writing - review & editing, Visualization. **Daniel Sutter:** Conceptualization, Methodology, Writing - review & editing. **Matteo Gazzani:** Conceptualization, Methodology, Software, Writing - review & editing, Visualization. **Marco Mazzotti:** Conceptualization, Writing - review & editing, Supervision, Project administration, Funding acquisition.

## Declaration of competing interest

The authors declare that they have no known competing financial interests or personal relationships that could have appeared to influence the work reported in this paper.

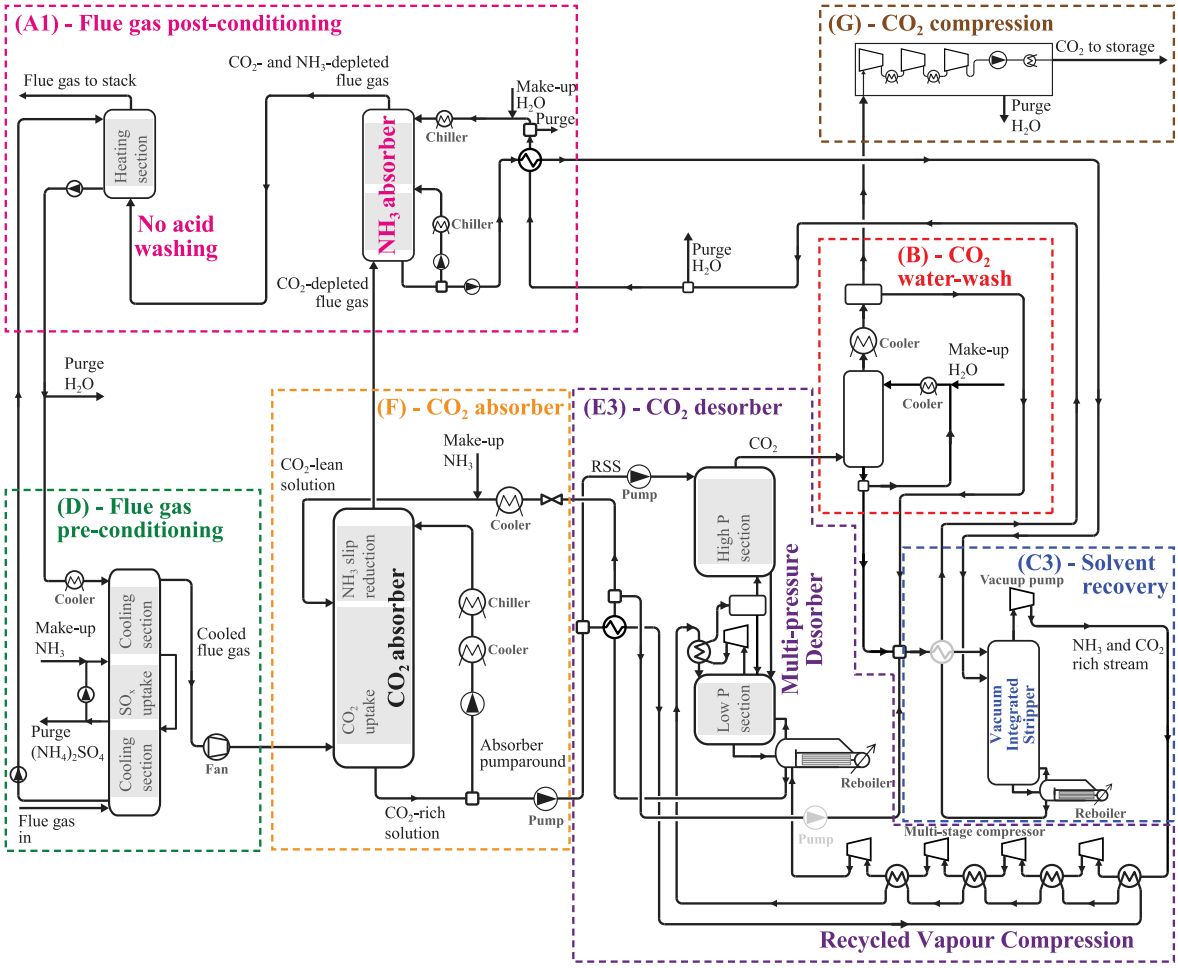


**Fig. 15.** Process flow diagram of the proposed new benchmark configuration for $NH_3$-based capture processes including the Recycled Vapour Compression, the Multi-pressure Desorber, the Vacuum Integrated Stripper and the Standard $NH_3$ Absorber without acid-wash column.

## Acknowledgements

This project has been partially funded through the European Union's Horizon 2020 research and innovation programme under grant agreement no. 641185. This work was partially supported by the Swiss State Secretariat for Education, Research and Innovation (SERI) under contract number 15.0160.

The authors would like to thank Kaj Thomsen (Department of Chemical and Biochemical Engineering, Technical University of Denmark) for making the thermodynamic model available, and for providing the relevant software.

## Appendix A. Supplementary data

Supplementary material related to this article can be found online at https://doi.org/10.1016/j.seppur.2021.118959.

## References

[1] N. Yang, H. Yu, L. Li, D. Xu, W. Han, P. Feron, Aqueous ammonia (NH3) based post combustion $CO_2$ capture: A review, Oil Gas Sci. Technol. 69 (5) (2014) 931–945, http://dx.doi.org/10.2516/ogst/2013160.

[2] K. Li, H. Yu, P. Feron, M. Tade, L. Wardhaugh, Technical and energy performance of an advanced, aqueous ammonia-based $CO_2$ capture technology for a 500 MW coal-fired power station, Environ. Sci. Technol. 49 (16) (2015) 10243–10252, http://dx.doi.org/10.1021/acs.est.5b02258.

[3] D. Sutter, M. Gazzani, M. Mazzotti, A low-energy chilled ammonia process exploiting controlled solid formation for post-combustion $CO_2$ capture, Faraday Discuss. 192 (2016) 59–83, http://dx.doi.org/10.1039/C6FD00044D.

[4] K. Jiang, K. Li, H. Yu, Z. Chen, L. Wardhaugh, P. Feron, Advancement of ammonia based post-combustion $CO_2$ capture using the advanced flash stripper process, Appl. Energy 202 (2017) 496–506, http://dx.doi.org/10.1016/j.apenergy.2017.05.143.

[5] J. Liu, S. Wang, A. Hartono, H.F. Svendsen, C. Chen, Solubility of N 2O in and density and viscosity of aqueous solutions of piperazine, ammonia, and their mixtures from (283.15 to 323.15) K, J. Chem. Eng. Data 57 (9) (2012) 2387–2393, http://dx.doi.org/10.1021/je300102d.

[6] F. Wang, J. Zhao, H. Miao, J. Zhao, H. Zhang, J. Yuan, J. Yan, Current status and challenges of the ammonia escape inhibition technologies in ammonia-based $CO_2$ capture process, Appl. Energy 230 (2018) 734–749, http://dx.doi.org/10.1016/J.APENERGY.2018.08.116.

[7] H. Yu, P.H. Feron, Aqueous ammonia-based post-combustion $CO_2$capture, in: Absorption-Based Post-Combustion Capture of Carbon Dioxide, Woodhead Publishing, 2016, pp. 283–301, http://dx.doi.org/10.1016/B978-0-08-100514-9.00012-3.

[8] G. Busca, C. Pistarino, Abatement of ammonia and amines from waste gases: A summary, J. Loss Prev. Process Ind. 16 (2) (2003) 157–163, http://dx.doi.org/10.1016/S0950-4230(02)00093-1.

[9] G. State, L.C.T.D. for Energy, Mining, Emission limit values: Comparative tables for basic, chemicals, existing installations in the EU, Tech. Rep., Government of South Australia, 2017, URL http://www.renewablessa.sa.gov.au/about-south-australia/existing-investments.

[10] E. Gal, Ultra cleaning of combustion gas including the removal of $CO_2$, WO 2006/022885 A1, 2006.

[11] G. Lombardo, R. Agarwal, J. Askander, Chilled ammonia process at technology center mongstad-first results, in: Energy Procedia, Vol. 51, 2014, pp. 31–39, http://dx.doi.org/10.1016/j.egypro.2014.07.004.

[12] O. Augustsson, B. Baburao, S. Dube, S. Bedell, P. Strunz, M. Balfe, O. Stallmann, Chilled ammonia process scale-up and lessons learned, in: Energy Procedia, Vol. 114, Elsevier, 2017, pp. 5593–5615, http://dx.doi.org/10.1016/j.egypro.2017.03.1699.

[13] D. Sutter, M. Gazzani, M. Mazzotti, Formation of solids in ammonia-based $CO_2$ capture processes — identification of criticalities through thermodynamic analysis of the $CO_2$–NH3–H2O system, Chem. Eng. Sci. 133 (2015) 170–180, http://dx.doi.org/10.1016/j.ces.2014.12.064.

[14] J.-F. Pérez-Calvo, D. Sutter, M. Gazzani, M. Mazzotti, A methodology for the heuristic optimization of solvent-based $CO_2$ capture processes when applied to new flue gas compositions: A case study of the Chilled Ammonia Process for capture in cement plants, Chem. Eng. Sci. X 8 (2020) 100074, http://dx.doi.org/10.1016/j.cesx.2020.100074.

[15] V. Darde, B. Maribo-Mogensen, W.J. van Well, E.H. Stenby, K. Thomsen, Process simulation of $CO_2$ capture with aqueous ammonia using the extended UNIQUAC model, Int. J. Greenh. Gas Control 10 (2012) 74–87, http://dx.doi.org/10.1016/j.ijggc.2012.05.017.

[16] H. Jilvero, F. Normann, K. Andersson, F. Johnsson, Ammonia-based post combustion–The techno-economics of controlling ammonia emissions, Int. J. Greenh. Gas Control 37 (2015) 441–450, http://dx.doi.org/10.1016/j.ijggc.2015.03.039.

[17] K. Han, C.K. Ahn, M.S. Lee, C.H. Rhee, J.Y. Kim, H.D. Chun, Current status and challenges of the ammonia-based $CO_2$ capture technologies toward commercialization, Int. J. Greenh. Gas Control 14 (2013) 270–281, http://dx.doi.org/10.1016/j.ijggc.2013.01.007.

[18] K. Han, C.K. Ahn, M.S. Lee, Performance of an ammonia-based $CO_2$ capture pilot facility in iron and steel industry, Int. J. Greenh. Gas Control 27 (2014) 239–246, http://dx.doi.org/10.1016/j.ijggc.2014.05.014, URL https://www.sciencedirect.com/science/article/pii/S1750583614001534.

[19] K. Li, H. Yu, G. Qi, P. Feron, M. Tade, J. Yu, S. Wang, Rate-based modelling of combined SO2 removal and NH3 recycling integrated with an aqueous NH3-based $CO_2$ capture process, Appl. Energy 148 (2015) 66–77, http://dx.doi.org/10.1016/j.apenergy.2015.03.060.

[20] K. Jiang, H. Yu, L. Chen, M. Fang, M. Azzi, A. Cottrell, K. Li, An advanced, ammonia-based combined NOx/SOx/$CO_2$ emission control process towards a low-cost, clean coal technology, Appl. Energy 260 (2020) 114316, http://dx.doi.org/10.1016/j.apenergy.2019.114316.

[21] K. Jiang, H. Yu, J. Yu, K. Li, Advancement of ammonia-based post-combustion $CO_2$ capture technology: Process modifications, Fuel Process. Technol. 210 (2020) 106544, http://dx.doi.org/10.1016/j.fuproc.2020.106544.

[22] M. Bui, C.S. Adjiman, A. Bardow, E.J. Anthony, A. Boston, S. Brown, P.S. Fennell, S. Fuss, A. Galindo, L.A. Hackett, J.P. Hallett, H.J. Herzog, G. Jackson, J. Kemper, S. Krevor, G.C. Maitland, M. Matuszewski, I.S. Metcalfe, C. Petit, G. Puxty, J. Reimer, D.M. Reiner, E.S. Rubin, S.A. Scott, N. Shah, B. Smit, J.P.M. Trusler, P. Webley, J. Wilcox, N. Mac Dowell, Carbon capture and storage (CCS): the way forward, Energy Environ. Sci. 11 (5) (2018) 1062–1176, http://dx.doi.org/10.1039/C7EE02342A.

[23] J. Liu, Investigation of energy-saving designs for an aqueous ammonia-based carbon capture process, Ind. Eng. Chem. Res. 57 (45) (2018) 15460–15472, http://dx.doi.org/10.1021/acs.iecr.8b03658.

[24] J. Liu, D.S.H. Wong, S.S. Jang, Y.T. Shen, Energy-saving design for regeneration process in large-scale $CO_2$ capture using aqueous ammonia, J. Taiwan Inst. Chem. Eng. 73 (2017) 12–19, http://dx.doi.org/10.1016/j.jtice.2016.07.041.

[25] H. Yu, G. Qi, S. Wang, S. Morgan, A. Allport, A. Cottrell, T. Do, J. McGregor, L. Wardhaugh, P. Feron, Results from trialling aqueous ammonia-based post-combustion capture in a pilot plant at Munmorah Power Station: Gas purity and solid precipitation in the stripper, Int. J. Greenh. Gas Control 10 (2012) 15–25, http://dx.doi.org/10.1016/j.ijggc.2012.04.014.

[26] Energy Sector Planning and Analysis (ESPA) and WorleyParsons Group, Quality Guidelines for Energy System Studies: $CO_2$ Impurity Design Parameters, Tech. Rep., National Energy Technology Laboratoy, 2013, URL https://www.netl.doe.gov/projects/files/QGESSCO2ImpurityDesignParameters{_}{_}092713.pdf.

[27] J. Liu, D.S.H. Wong, D.S. Chen, Energy-saving performance of advanced stripper configurations for $CO_2$ capture by ammonia-based solvents, J. Taiwan Inst. Chem. Eng. (2020) http://dx.doi.org/10.1016/j.jtice.2020.08.024.

[28] J. Yu, S. Wang, Development of a novel process for aqueous ammonia based $CO_2$ capture, Int. J. Greenh. Gas Control 39 (2015) 129–138, http://dx.doi.org/10.1016/j.ijggc.2015.05.008.

[29] Y. Le Moullec, T. Neveux, A. Al Azki, A. Chikukwa, K.A. Hoff, Process modifications for solvent-based post-combustion $CO_2$ capture, Int. J. Greenh. Gas Control 31 (2014) 96–112, http://dx.doi.org/10.1016/j.ijggc.2014.09.024.

[30] H. Lin, Z. He, Z. Sun, J. Vu, A. Ng, M. Mohammed, J. Kniep, T.C. Merkel, T. Wu, R.C. Lambrecht, $CO_2$-selective membranes for hydrogen production and $CO_2$ capture - Part I: Membrane development, J. Memb. Sci. 457 (2014) 149–161, http://dx.doi.org/10.1016/j.memsci.2014.01.020.

[31] K. Li, H. Yu, P. Feron, L. Wardhaugh, M. Tade, Techno-economic assessment of stripping modifications in an ammonia-based post-combustion capture process, Int. J. Greenh. Gas Control 53 (2016) 319–327, http://dx.doi.org/10.1016/j.ijggc.2016.08.016.

[32] G.T. Rochelle, Conventional amine scrubbing for $CO_2$ capture, in: Absorption-Based Post-Combustion Capture of Carbon Dioxide, 2016, pp. 35–67, http://dx.doi.org/10.1016/B978-0-08-100514-9.00003-2.

[33] R. Anantharaman, D. Berstad, G. Cinti, E. De Lena, M. Gatti, M. Gazzani, H. Hoppe, I. Martinez, J.G.M.-S. Monteiro, M. Romano, S. Roussanaly, E. Schols, M. Spinelli, S. Storset, P. van Os, M. Voldsund, D3.2 CEMCAP Framework for Comparative Techno-Economic Analysis Of $CO_2$ Capture from Cement Plants, Tech. Rep., Sintef, 2017, p. 81, http://dx.doi.org/10.1111/j.1552-6909.2009.01070.x.

[34] A. Ullah, M.I. Soomro, W.S. Kim, Ammonia-based $CO_2$ capture parameters optimization and analysis of lean and rich vapor compression processes, Sep. Purif. Technol. 217 (2019) 8–16, http://dx.doi.org/10.1016/j.seppur.2019.02.002.

[35] H.L.Q. Nguyen, D.S.-H. Wong, Eliminating steam requirement of aqueous ammonia capture process by lean solution flash and vapor recompression, Process Integr. Optim. Sustain. 3 (3) (2019) 307–319, http://dx.doi.org/10.1007/s41660-018-0074-x.

[36] J. Liu, Process design of aqueous ammonia-based post-combustion $CO_2$ capture, J. Taiwan Inst. Chem. Eng. 78 (2017) 240–246, http://dx.doi.org/10.1016/j.jtice.2017.06.008.

[37] M.R. Abu-Zahra, J.P. Niederer, P.H. Feron, G.F. Versteeg, $CO_2$ capture from power plants, Int. J. Greenh. Gas Control 1 (2) (2007) 135–142, http://dx.doi.org/10.1016/s1750-5836(07)00032-1.

[38] G.T. Rochelle, Y. Wu, E. Chen, K. Akinpelumi, K.B. Fischer, T. Gao, C.-T. Liu, J.L. Selinger, Pilot plant demonstration of piperazine with the advanced flash stripper, Int. J. Greenh. Gas Control 84 (2019) 72–81, http://dx.doi.org/10.1016/j.ijggc.2019.03.014.

[39] M. Voldsund, S.O. Gardarsdottir, E. De Lena, J.-F.F. Pérez-Calvo, A. Jamali, D. Berstad, C. Fu, M. Romano, S. Roussanaly, R. Anantharaman, H. Hoppe, D. Sutter, M. Mazzotti, M. Gazzani, G. Cinti, K. Jordal, Comparison of technologies for $CO_2$ capture from cement production—Part 1: Technical evaluation, Energies 12 (3) (2019) 559, http://dx.doi.org/10.3390/en12030559.

[40] S.O. Gardarsdottir, E. De Lena, M. Romano, S. Roussanaly, M. Voldsund, J.F. Pérez-Calvo, D. Berstad, C. Fu, R. Anantharaman, D. Sutter, M. Gazzani, M. Mazzotti, G. Cinti, Comparison of technologies for $CO_2$ capture from cement production—Part 2: Cost analysis, Energies 12 (3) (2019) http://dx.doi.org/10.3390/en12030542.

[41] L.M. Bjerge, P. Brevik, $CO_2$ capture in the cement industry, norcem $CO_2$ capture project (Norway), in: Energy Procedia, Vol. 63, Elsevier Ltd, 2014, pp. 6455–6463, http://dx.doi.org/10.1016/j.egypro.2014.11.680.

[42] V. Andersson, P.Å. Franck, T. Berntsson, Techno-economic analysis of excess heat driven post-combustion CCS at an oil refinery, Int. J. Greenh. Gas Control 45 (2016) 130–138, http://dx.doi.org/10.1016/j.ijggc.2015.12.019.

[43] M.T. Ho, D.E. Wiley, Liquid absorbent-based post-combustion $CO_2$ capture inindustrial processes, in: Absorption-Based Post-Combustion Capture of Carbon Dioxide, 2016, pp. 711–756, http://dx.doi.org/10.1016/B978-0-08-100514-9.00028-7.

[44] A. Arasto, E. Tsupari, J. Kärki, E. Pisilä, L. Sorsamäki, Post-combustion capture of $CO_2$ at an integrated steel mill - Part I: Technical concept analysis, Int. J. Greenh. Gas Control 16 (2013) 271–277, http://dx.doi.org/10.1016/j.ijggc.2012.08.018.

[45] R. Bollinger, D. Muraskin, M. Hammond, F. Kozak, G. Spitznogle, M. Cage, M. Varner, B. Sherrick, M. Varner, CCS project with Alstom's chilled ammonia process at AEP's mountaineer plant, in: Air Waste Manag. Assoc. - 8th Power Plant Air Pollut. Control Mega Symp. 2010, Vol. 1, 2010, pp. 539–586.

[46] V. Telikapalli, F. Kozak, J.F. Leandri, B. Sherrick, J. Black, D. Muraskin, M. Cage, M. Hammond, G. Spitznogle, CCS with the alstom chilled ammonia process development program- field pilot results, in: Energy Procedia, Vol. 4, Elsevier, 2011, pp. 273–281, http://dx.doi.org/10.1016/j.egypro.2011.01.052.

[47] Y.L. Moullec, T. Neveux, Process modifications for $CO_2$ capture, in: Absorption-Based Post-Combustion Capture of Carbon Dioxide, Woodhead Publishing, 2016, pp. 305–340, http://dx.doi.org/10.1016/B978-0-08-100514-9.00013-5.

[48] E. Gal, I. Jayaweera, Chilled ammonia based $CO_2$ capture system with water wash system, US 2011/0048239 A1, 2011.

[49] B. Baburao, Advanced intercooling and recycling in $CO_2$ absorption, WO 2011/066042 A1, 2011.

[50] S.K. Dube, Chilled ammonia based $CO_2$ capture system with wash system and processes of use, US 2013/0092026 A1, 2013.

[51] S.K. Dube, Integrated desulfurization and carbon dioxide capture system for flue gases, EP 3 257 570 B1, 2019.

[52] H. Yu, S. Morgan, A. Allport, A. Cottrell, T. Do, J. McGregor, L. Wardhaugh, P. Feron, Results from trialling aqueous NH3 based post-combustion capture in a pilot plant at munmorah power station: Absorption, Chem. Eng. Res. Des. 89 (8) (2011) 1204–1215, http://dx.doi.org/10.1016/J.CHERD.2011.02.036.

[53] G. Manzolini, E. Macchi, M. Binotti, M. Gazzani, Integration of SEWGS for carbon capture in Natural Gas Combined Cycle. Part B: Reference case comparison, Int. J. Greenh. Gas Control 5 (2) (2011) 214–225, http://dx.doi.org/10.1016/j.ijggc.2010.08.007.

[54] European Fertilizer Manufacturers' Association (EFMA), Best available techniques for pollution prevention and control in the European fertilizer industry booklet no. 1 of 8: Production of ammonia, in: Best Available Tech. Pollut. Prev. Control Eur. Fertil. Ind., Tech. Rep., (1) 2000, p. 40.

[55] C. Tsay, R.C. Pattison, Y. Zhang, G.T. Rochelle, M. Baldea, Rate-based modeling and economic optimization of next-generation amine-based carbon capture plants, Appl. Energy 252 (2019) 113379, http://dx.doi.org/10.1016/j.apenergy.2019.113379.

[56] M. van der Spek, S. Roussanaly, E.S. Rubin, Best practices and recent advances in CCS cost engineering and economic analysis, Int. J. Greenh. Gas Control 83 (February) (2019) 91–104, http://dx.doi.org/10.1016/j.ijggc.2019.02.006.

[57] G. Qi, S. Wang, H. Yu, L. Wardhaugh, P. Feron, C. Chen, Development of a rate-based model for $CO_2$ absorption using aqueous NH3 in a packed column, Int. J. Greenh. Gas Control 17 (2013) 450–461, http://dx.doi.org/10.1016/j.ijggc.2013.05.027.

[58] H. Ahn, M. Luberti, Z. Liu, S. Brandani, Process configuration studies of the amine capture process for coal-fired power plants, Int. J. Greenh. Gas Control 16 (2013) 29–40, http://dx.doi.org/10.1016/j.ijggc.2013.03.002.

[59] M. Gazzani, T. Hartmann, J.-F. Pérez-Calvo, D. Sutter, M. Mazzotti, On the optimal design of forward osmosis desalination systems with NH3–$CO_2$–H2O solutions, Environ. Sci. Water Res. Technol. 3 (5) (2017) 811–829, http://dx.doi.org/10.1039/C7EW00037E.

[60] S. Krishnamurthy, V.R. Rao, S. Guntuka, P. Sharratt, R. Haghpanah, A. Rajendran, M. Amanullah, I.A. Karimi, S. Farooq, $CO_2$ capture from dry flue gas by vacuum swing adsorption: A pilot plant study, AIChE J. 60 (5) (2014) 1830–1842, http://dx.doi.org/10.1002/aic.14435.

[61] A. Streb, M. Hefti, M. Gazzani, M. Mazzotti, Novel adsorption process for co-production of hydrogen and $CO_2$ from a multicomponent stream, Ind. Eng. Chem. Res. 58 (37) (2019) 17489–17506, http://dx.doi.org/10.1021/acs.iecr.9b02817.

[62] M. Banja, M. Jegard, Renewable Technologies in the EU Electricity Sector: Trends and Projections: Analysis in the Framework of the EU 2030 Climate and Energy Strategy, Publications Office of the European Union, 2017, http://dx.doi.org/10.2760/733769, URL https://ec.europa.eu/jrc/en/publication/eur-scientific-and-technical-research-reports/renewable-technologies-eu-electricity-sector-trends-and-projections-analysis-framework-eu.

[63] European Commission, State of the union: Q & A on the 2030 climate target plan, 2020, URL https://ec.europa.eu/commission/presscorner/detail/en/qanda_20_1598.

[64] European Commission - D.G. Climate Action, 2030 climate & energy framework - Climate Action, URL https://ec.europa.eu/clima/policies/strategies/2030{_}en{#}tab-0-0.

[65] D.E. Wiley, M.T. Ho, A. Bustamante, Assessment of opportunities for $CO_2$ capture at iron and steel mills: An Australian perspective, in: Energy Procedia, Vol. 4, Elsevier Ltd, 2011, pp. 2654–2661, http://dx.doi.org/10.1016/j.egypro.2011.02.165.

[66] M. Biermann, H. Ali, M. Sundqvist, M. Larsson, F. Normann, F. Johnsson, Excess heat-driven carbon capture at an integrated steel mill– Considerations for capture cost optimization, Int. J. Greenh. Gas Control 91 (2019) 102833, http://dx.doi.org/10.1016/j.ijggc.2019.102833.

[67] M. Sundqvist, M. Biermann, F. Normann, M. Larsson, L. Nilsson, Evaluation of low and high level integration options for carbon capture at an integrated iron and steel mill, Int. J. Greenh. Gas Control 77 (2018) 27–36, http://dx.doi.org/10.1016/j.ijggc.2018.07.008.